TRANSMISSION AND PROPAGATION PROPERTIES OF NOVEL METAMATERIALS

A THESIS SUBMITTED TO
THE GRADUATE SCHOOL OF NATURAL AND APPLIED SCIENCES
OF
MIDDLE EAST TECHNICAL UNIVERSITY

BY

LEVENT ŞAHİN

IN PARTIAL FULFILLMENT OF THE REQUIREMENTS
FOR
THE DEGREE OF MASTER OF SCIENCE
IN
ELECTRICAL AND ELECTRONICS ENGINEERING

JANUARY 2009

Approval of the thesis:

TRANSMISSION AND PROPAGATION PROPERTIES OF NOVEL METAMATERIALS

submitted by **LEVENT ŞAHİN** in partial fulfillment of the requirements for the degree of **Master of Science in Electrical and Electronics Engineering Department, Middle East Technical University** by,

Prof. Dr. Canan Özgen
Dean, Graduate School of **Natural and Applied Sciences** _____

Prof. Dr. İsmet Erkmen
Head of Department, **Electrical and Electronics Engineering** _____

Prof. Dr. Gönül Turhan Sayan
Supervisor, **Electrical and Electronics Engineering Dept., METU** _____

Examining Committee Members:

Prof. Dr. Gülbin Dural
Electrical and Electronics Engineering Dept., METU _____

Prof. Dr. Gönül Turhan Sayan
Electrical and Electronics Engineering Dept., METU _____

Prof. Dr. Mustafa Kuzuoğlu
Electrical and Electronics Engineering Dept., METU _____

Prof. Dr. Ekmel Özbay
Electrical and Electronics Engineering Dept., Bilkent Univ. _____

Hümeyra Çağlayan, M.Sc.
Physics Dept., Bilkent Univ. _____

Date: January 13, 2009

I hereby declare that all information in this document has been obtained and presented in accordance with academic rules and ethical conduct. I also declare that, as required by these rules and conduct, I have fully cited and referenced all material and results that are not original to this work.

Name, Last name : Levent ŞAHİN

Signature :

ABSTRACT

TRANSMISSION AND PROPAGATION PROPERTIES OF NOVEL METAMATERIALS

Şahin, Levent

M.Sc., Department of Electrical and Electronics Engineering

Supervisor: Prof. Dr. Gönül Turhan Sayan

January 2009, 152 pages

Metamaterials attracted significant attention in recent years due to their potential to create novel devices that exhibit specific electromagnetic properties. In this thesis, we investigated transmission and propagation properties of novel metamaterial structures. Electromagnetic properties of metamaterials are characterized and the resonance mechanism of Split Ring Resonator (SRR) structure is investigated. Furthermore, a recent left-handed metamaterial structure for microwave regime called Fishnet-type metamaterial is studied. We demonstrated the left-handed transmission and negative phase velocity in Fishnet Structures. Finally, we proposed and successfully demonstrated novel approaches that utilize the resonant

behavior of SRR structures to enhance the transmission of electromagnetic waves through sub-wavelength apertures at microwave frequency regime. We investigated the transmission enhancement of electromagnetic waves through a sub-wavelength aperture by placing SRR structures in front of the aperture and also by changing the aperture shape as SRR-shaped apertures. The incident electromagnetic wave is effectively coupled to the sub-wavelength aperture causing a strong localization of electromagnetic field in the sub-wavelength aperture. Localized electromagnetic wave gives rise to enhanced transmission from a single sub-wavelength aperture. The proposed structures are designed, simulated, fabricated and measured. The simulations and experimental results are in good agreement and shows significant enhancement of electromagnetic wave transmission through sub-wavelength apertures by utilizing proposed novel structures. Radius (r) of the sub-wavelength aperture is approximately twenty times smaller than the incident wavelength ($r/\lambda \sim 0.05$). This is the smallest aperture size to wavelength ratio in the contemporary literature according to our knowledge.

Keywords: Metamaterial, Split Ring Resonator (SRR) Structure, Fishnet Structure, Enhanced Transmission, Sub-wavelength Aperture

ÖZ

YENİ METAMALZEMELERİN GEÇİRGENLİK VE YAYILMA ÖZELLİKLERİ

Şahin, Levent

Yüksek Lisans, Elektrik ve Elektronik Mühendisliği Bölümü

Tez Yöneticisi: Prof. Dr. Gönül Turhan Sayan

Ocak 2009, 152 sayfa

Metamalzemeler, kendine has elektromanyetik özelliklere sahip yeni aygıtların tasarlanmasındaki potansiyelleri nedeniyle son yıllarda oldukça ilgi çekmişlerdir. Bu tezde, yeni metamalzeme yapılarının geçirgenlik ve yayılma özelliklerini inceledik. Metamalzemelerin elektromanyetik özellikleri tanımlandı ve Yarıklı Halka Rezonatörü yapısının rezonans mekanizması incelendi. Bunun yanında, mikrodalga frekansları için yakın zamanda önerilen solak metamalzeme yapıları olan Balıkağı şeklindeki metamalzemeler çalışıldı. Balıkağı yapılarındaki solak geçirgenlik ve negatif (ters) faz hızı gösterildi. Son olarak, elektromanyetik dalgaların mikrodalga frekanslarda dalga boyu altı aralıktan (delikten) geçişinin artırılması için yarıklı halka rezonatorünün

kullanılması esasına dayanan yeni yöntemler önerdik ve başarıyla doğruluğunu gösterdik. Elektromanyetik dalgaların dalga boyu altı aralıktan geçişinin artırılmasının; aralığın önüne yarıklı halka rezonatorü koyarak ve aralığın şeklini yarıklı halka rezonatorü şekilli aralığa dönüştürerek gerçekleştirilmesini inceledik. Gelen elektromanyetik dalganın, etkili bir biçimde dalga boyu altı aralıkla bağlaştırılması sonucu dalga boyu altı aralıkta elektromanyetik alanın güçlü toplanması (lokalizasyon) olmaktadır. Toplanan elektromanyetik dalgalar, dalga altı aralıktan artırılmış geçirgenlik olmasını sağlamaktadırlar. Önerilen yapılar tasarlandı, benzetim yapıldı, üretildi ve ölçüldü. Benzetim çalışmaları ve ölçümler benzer sonuçlar verdi ve önerilen yeni yapıların kullanılması ile dalga boyu altı aralıktan elektromanyetik geçirgenlikte önemli oranda artış gözlemlendi. Dalga boyu altı aralığın yarıçapı (r) yaklaşık olarak gelen dalganın dalga boyundan 20 kat daha küçüktür ($r/\lambda \sim 0.05$). Bu oran, bildiğimiz kadarıyla güncel literatürün en küçük aralık yarıçapının dalga boyuna oranı değeridir.

Anahtar Sözcükler: Metamalzeme, Yarıklı Halka Rezonatörü Yapısı, Balıkağı Yapısı, Artırılmış Geçirgenlik, Dalga boyu altı aralık

To my family, my greatest gift

ACKNOWLEDGEMENTS

I would like to express my sincere gratitude to my supervisor Prof. Dr. Gönül Turhan Sayan for her guidance and help throughout the thesis work. I would also like to acknowledge valuable advice and help from Prof. Dr. Ekmel Özbay. His support, guidance, encouragements and suggestions taught me much about systematically approaching to research study. I am grateful to Nanotechnology Research Center (NANOTAM) for the facilities and working environment provided for me to perform the research study. Without this support, the thesis could not be completed.

I would like to thank to the members of my thesis committee, Prof. Dr. Gülbin Dural, Prof. Dr. Mustafa Kuzuoğlu, Prof. Dr. Ekmel Özbay and Hümeyra Çağlayan, for reading the manuscript and commenting on the thesis.

I would like to express my special thanks and gratitude to Dr. Koray Aydın for his continuous support, encouragement and valuable ideas towards the realization of this thesis work. Special thanks to my friends Yusuf Öztürk and Evren Yücel for their great support during the thesis work. I would also like to express my gratitude to Nilgün and Nezih Kandemir for their support throughout my education. I would like to thank TÜBITAK - BİDEB (The Scientific and Technological Research Council of Turkey - The Department of Science Fellowships and Grant Programmes) for its support to my thesis. Also, I would like to thank SSM (Undersecreteriat for Defence Industries) for the permission to the study on the thesis by departing in work hours.

Last but not the least; I would present my special thanks to my parents, Şaziye and Sayit Şahin; and to my beloved fiancée Dr. Fatma Başıbüyük for their endless support and encouragement.

TABLE OF CONTENTS

LIST OF TABLES

LIST OF FIGURES

CHAPTER 1

INTRODUCTION

The artificially designed materials, metamaterials, have attracted a great deal of interest because of their potential to expand the range of electromagnetic properties in materials. The response of materials to an incident electromagnetic wave is determined by their constitutive macroscopic electromagnetic parameters, the dielectric permittivity (ε), and magnetic permeability (μ). Therefore, we can design artificial materials that respond to incident electromagnetic waves as we wish by changing the constitutive parameters of materials (ε, μ). Ordinary materials generally have positive ε and μ, which restrict the design of novel devices. However, new structures called metamaterials are proposed for realizing new response characteristics that do not occur in nature. The phrase "meta" means "beyond" in Greek, which refers the novel electromagnetic characteristics of metamaterials that are not available in nature. The engineered response of metamaterials has the potential to make a dramatic impact on the design of novel electromagnetic devices; as they provide the possibility to achieve novel

physical phenomena that cannot be achieved with conventional, naturally occurring materials.

Although the Russian physicist V. Veselago was the first scientist who theoretically suggested metamaterials with simultaneously negative dielectric permittivity and magnetic permeability at 1968 [24]; the increasing interest in this topic started after the seminal work of J.B. Pendry *et al.* [25] and D.R. Smith *et al.* [26]. Since metamaterials offer new physical phenomena, there is an increasing amount of interest in this topic until the end of 2000s. Therefore, a large amount of literature has been accumulated on metamaterials [1-13], and on various exciting applications such as superlenses [17, 50], enhanced magnetic resonance imaging [14], hyperlenses [15, 16], cloaking [51], and semiconductor metamaterials [52]. Moreover, metamaterials are geometrically scalable structures that can be utilized at frequency spectra ranging from RF region to optical region.

At the beginning, the research activities of metamaterials were mainly focused on obtaining artificial materials with negative permeability and negative index properties. However, new research fields for the applications of metamaterials have emerged lately. These research fields are mostly related to the transmission and propagation properties of novel structures. Fishnet structures are highly promising metamaterials that can be utilized for controlling the propagation of electromagnetic waves through planar structures.

In addition, there are wide varieties of study on metamaterials to change the transmission characteristics of several structures, which are restricted to several physical restrictions that cannot be overcome by ordinary materials. Transmission through a sub-wavelength hole is another contemporary research topic because of its applications of critical importance ranging from biomaterials to microscopy. The last century concluded with a very important discovery by Ebbesen [118]; sub-wavelength holes in a thin metal film can transmit electromagnetic waves much more strongly at certain frequencies than the Bethe's prediction [109] by utilizing hole arrays. Ebbesen's discovery (extraordinary transmission phenomenon) and new fabrication techniques opened up significant opportunities to design novel devices, such as new probes for the scanning near-field optical microscope (SNOM) [123, 124], near-field optical recording [125, 126], nano-scale lithography [127-129] tracking single molecule (fluorescence spectroscopy) [124, 130], and ultrafast miniature photodetector [131].

In the present thesis, we investigated the transmission and propagation properties of novel metamaterials. We experimentally studied and numerically verified the novel propagation characteristics of fishnet structures and the enhanced transmission through sub-wavelength aperture by utilizing split-ring resonator structures.

In Chapter 2, the basics of metamaterials are introduced and their transmission characteristics are investigated. The negative dielectric

permittivity and negative magnetic permeability phenomenon are discussed. In addition, the negative index of refraction of left-handed metamaterials is demonstrated.

Chapter 3 is about the detailed electromagnetic analysis of split ring resonator (SRR) structures. The resonance characteristic of SRR is investigated and also the effect of geometrical parameters on the magnetic resonance of SRR is discussed. Several different types of SRR are investigated in order to observe and compare their electromagnetic characteristics. Finally, the effect of SRR orientations on the resulting electromagnetic resonance mechanism is discussed.

Chapter 4 is devoted to a planar metamaterial called a Fishnet Structure, which is composed of a metallic slab and wire pairs. Transmission measurements and simulations are performed in order to observe a left-handed transmission band. Furthermore, negative-index property of Fishnet Structure is verified by using the retrieval procedure and also by observing the negative phase shift provided by the structure while adding additional structure layers in the propagation direction. Finally, the effect of several geometrical parameters on the left-handed behavior of the fishnet structure is examined. The work presented in Chapter 4 appeared as a journal article in Optics Express [104].

In Chapter 5, we proposed novel structures for increasing the transmission of electromagnetic waves through sub-wavelength

apertures. The first of these novel structures is a split ring resonator placed at the near-field of the aperture. The work on this structure was appeared as a recent journal article in Physical Review Letters [100]. The second proposed structure for enhanced transmission through a sub-wavelength aperture is an SRR-shaped aperture. The experimental and numerical results confirm a significant level of enhancement.

Finally, Chapter 6 gives a concise summary of the results achieved throughout this thesis work. Moreover, the future research directions and future work are provided in this chapter.

CHAPTER 2

METAMATERIALS

2.1 Introduction

Development of artificial dielectric media has become a remarkable research area due to its potential for creating new devices that exhibit unusual electromagnetic properties. The applications of novel dielectric media in various areas such as imaging, lensing, optical fibers, and lasers require the effective control of the transmission and propagation of electromagnetic waves.

Metamaterials are the artificial dielectric media which have unique properties that are not usually found in nature. Since the permittivity and permeability values of a metamaterial structure can be determined to a desired value, metamaterials can be used in several applications ranging from focusing without a diffraction limit to extraordinary transmission through sub-wavelength apertures.

Electromagnetic response of materials is determined by the fundamental constitutive parameters, the dielectric permittivity (ε), the magnetic

permeability (μ) and the conductivity (σ). The combined effect of permittivity and permeability determine the response of a lossless material to an incident electromagnetic field. Most of the natural structures have positive permittivity and permeability. Due to the absence of magnetic charges, it is rather difficult to have negative permeability structures, while negative permittivity is obtained below the plasma frequency of periodic sub-wavelength metallic wires at microwave frequencies as shown theoretically [21, 22] and experimentally [23]. The phenomenon of negative refraction of electromagnetic wave in media with negative permittivity and permeability was first suggested by Veselago in 1968 [24]. A material that has both negative permittivity and permeability was predicted to have negative refractive index, the reversal of Doppler Effect [24, 33] and Cerenkov radiation [24, 34]. Materials with negative index of refraction ($n<0$) demonstrate the unusual behavior that the propagation direction of electromagnetic wave is opposite to the direction of the energy flow. In other words, the phase velocity and group velocity are antiparallel, which is an extraordinary behavior of left-handed materials that may open up significant opportunities to develop novel electromagnetic devices.

Negative permittivity is demonstrated by utilizing periodic metallic wire arrangements at the microwave regime [21-23]. Dielectric permittivity is negative below the plasma frequency of a metallic wire array and no electromagnetic wave can propagate at the negative permittivity spectrum as long as the permeability remains positive. No material with

negative permeability was suggested until the seminal work of Pendry *et al.* [25], where a periodic arrangement of novel resonator structures called Split Ring Resonators (SRRs) was employed to obtain negative permeability around the resonance frequency. Afterwards, Smith *et al.* experimentally demonstrated a novel type of materials, composite metamaterials, by stacking thin wires and SRRs [26, 27] so that left-handed propagation band was observed at frequencies where both the dielectric permittivity and magnetic permeability of this composite metamaterial were both negative.

Negative index of refraction is theoretically [24, 28] and experimentally [29] verified where both permittivity and permeability are both negative. Negative index of refraction for left-handed materials has been confirmed in agreement with various other studies [30, 31, 32, 35].

In this chapter, electromagnetic transmission and propagation properties of metamaterials are investigated. The phenomena of negative dielectric permittivity and negative magnetic permeability will be discussed as well as the left-handed metamaterials having a negative index of refraction.

2.2 Transmission Properties of Metamaterials

Transmission properties of a lossless (or very low loss) material are determined by its dielectric permittivity and magnetic permeability. Therefore, we firstly investigate the phenomenon of negative permittivity. Then, the negative permeability phenomenon and negative

index metamaterials which possess both negative permittivity and negative permeability will be investigated.

The fundamental postulate for the large-scale (macroscopic) electromagnetic phenomena is described by Maxwell's Equations. Therefore, the theoretical analysis of metamaterials starts with Maxwell's Equations.

Electromagnetic field solutions at every point in space must satisfy the Maxwell's Equations which are expressed in time domain as follows:

$$\nabla \times \overline{E} = -\frac{\partial \overline{B}}{\partial t} \quad \text{(Faraday's Induction Law)} \tag{2.1}$$

$$\nabla \times \overline{H} = \frac{\partial \overline{D}}{\partial t} + \overline{J} \quad \text{(Generalized Ampere's Circuital Law)} \tag{2.2}$$

$$\nabla \bullet \overline{D} = \rho \quad \text{(Gauss' Law)} \tag{2.3}$$

$$\nabla \bullet \overline{B} = 0 \quad \text{(Conservation of Magnetic Flux)} \tag{2.4}$$

Also, the mathematical statement of "conservation of electric charge" is given by the Continuity Equation:

$$\nabla \bullet \overline{J} = -\frac{\partial \rho}{\partial t} \tag{2.5}$$

which is linearly dependent on Maxwell's Equations.

The vector and scalar quantities in Eq. 2.1 through Eq. 2.5 are functions of both space variables and time.

We considered the uniform plane wave excitation at a given angular frequency w for the simplicity of our analysis. Using the e^{+jwt} convention, the mathematical expressions for the $\overline{E}$ and $\overline{H}$ fields of a uniform plane wave in phasor domain can be given as

$$\overline{E} = \overline{E_0} e^{+j\bar{k}\bullet\bar{r}} \tag{2.6.a}$$

$$\overline{H} = \overline{H_0} e^{+j\bar{k}\bullet\bar{r}} \tag{2.6.b}$$

where $\bar{k}$ is the propagation vector, $\bar{r}$ is the position vector and the wave is assumed to propagate in a simple (linear, homogeneous and isotropic), lossless and source-free media with constitutive relations

$$\overline{B} = \mu\overline{H} \tag{2.7.a}$$

$$\overline{D} = \varepsilon\overline{E} \tag{2.7.a}$$

The reduced Maxwell's equations for monochromatic, isotropic plane wave can be derived in phasor domain as;

$$\bar{k} \times \overline{E} = -w\mu\overline{H} \tag{2.8}$$

$$\bar{k} \times \overline{H} = w\varepsilon\overline{E} \tag{2.9}$$

Moreover, the simplest dispersion relation for the isotropic, homogeneous and lossless materials can be derived as:

$$k^2 - w^2 \mu\varepsilon = 0 \tag{2.10.a}$$

$$k^2 = w^2 n^2 \tag{2.10.b}$$

where n, the refractive index of the medium, is given by

$$n = \sqrt{\mu\, \varepsilon} \tag{2.11.a}$$

or, for a composite medium with effective medium parameters μ_{eff} and ε_{eff}, given by

$$n = \sqrt{\mu_{eff}\, \varepsilon_{eff}} \tag{2.11.b}$$

The dispersion relation (Eq. 2.10.a) determines the propagation of electromagnetic wave in the specified matter. Since ε and μ are the only material properties in Eq. 2.10.a, we can state that the dielectric permittivity (ε) and magnetic permeability (μ) of a material are the characteristic parameters of the material for our lossless media. On the other hand, Eq. 2.10.b states that as both ε and μ become negative, the refractive index (n) does not change its sign; however, the Maxwell's relations show the effect of simultaneous negative dielectric permittivity and magnetic permeability. The materials with simultaneous negative ε and μ exhibit unique properties that are different from ordinary positive ε and μ materials [24].

As can be seen in Eqs. (2.8) and (2.9), $\{\overline{E}, \overline{H}, \overline{k}\}$ form a right-handed orthogonal coordinate system (see Figure 2.1.a) for materials with positive ε and μ. In case both ε and μ are negative, an interesting result arises; $\{\overline{E}, \overline{H}, -\overline{k}\}$ forms a left-handed orthogonal coordinate system (see Figure 2.1.b).

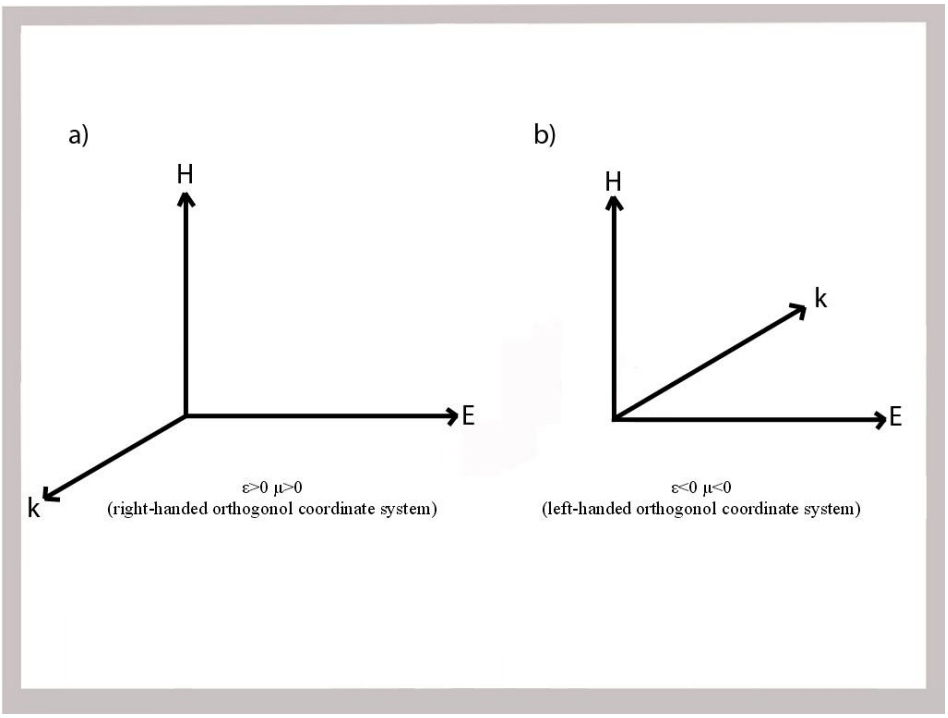

Figure 2.1: a) right-handed orthogonal coordinate system for materials with positive ε and μ. b) left-handed orthogonal coordinate system for materials with negative ε and μ.

In addition, since the sign of Poynting Vector ($\overline{P}$) is independent of the sign of ε and μ (Eq. 2.12), the direction of the energy flow does not change:

$$\overline{\mathrm{P}} = \overline{E} \times \overline{H} \tag{2.12}$$

Therefore, the direction of the power flow never changes. However, the wave propagation direction is opposite to the direction of power flow in left-handed metamaterials. In other words, this result causes the famous effect of an antiparellel phase and group velocity, the reversal of the Doppler Shift [53], and Cerenkov radiation [54].

So far, we analyzed the situation when ε and μ are both positive and negative. If the signs of ε and μ are opposite (εμ<0), then the electromagnetic waves are reflected totally and evanescent waves occur. Figure 2.2 summarizes the behavior of the materials for four different combinations of ε and μ signs.

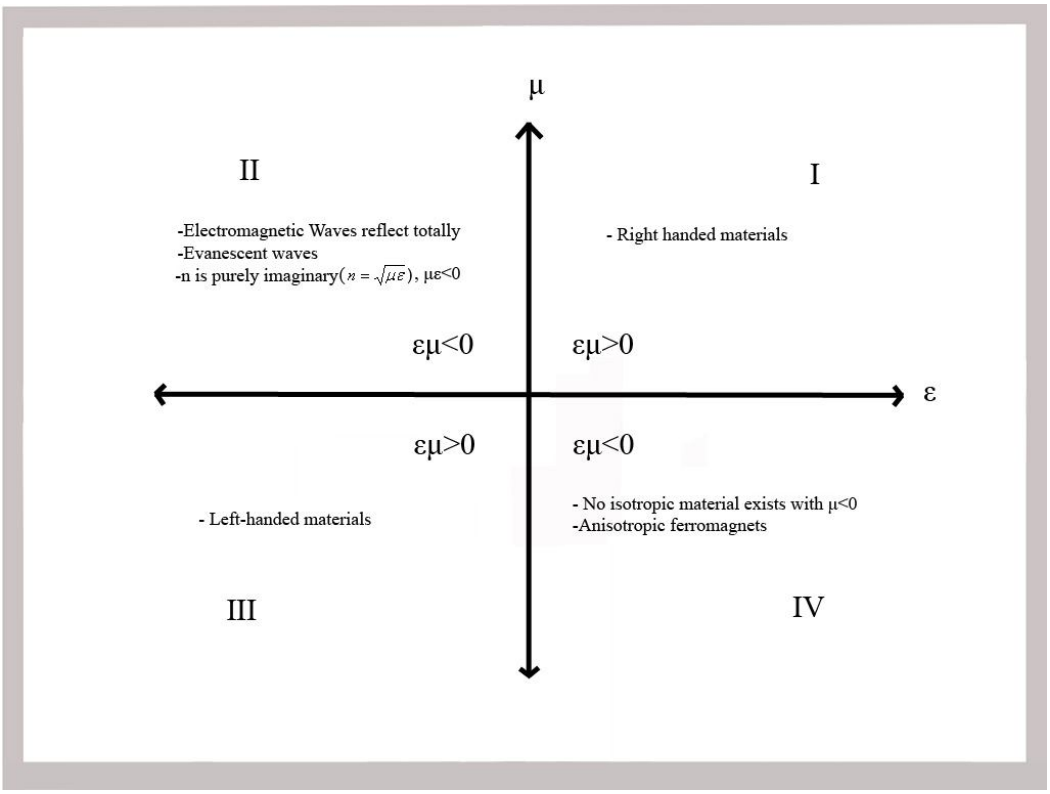

Figure 2.2: The ε-μ diagram (A simple classification).

The first quadrant of the graph (see Figure 2.2) is for ordinary materials with positive ε and μ. The second quadrant of the graph is for materials with negative ε and positive μ. Electromagnetic waves become evanescent as a result of imaginary propagation constant (k). The third quadrant is of importance as a result of abovementioned extraordinary electromagnetic characteristics. Both ε and μ are negative, but the wave can propagate as a result of $\varepsilon\mu>0$ (real propagation constant, k). Finally, the fourth quadrant is for materials with positive ε and negative μ, in which most of the materials are anisotropic ferromagnets. Electromagnetic waves become evanescent also in this quadrant.

2.2.1 Negative Permittivity

In this section, we will discuss the negative dielectric permittivity phenomena. A periodic array of metallic thin wires are commonly utilized to obtain negative permittivity ($\varepsilon<0$) in the microwave spectrum [21-23].

The real part of permittivity parameter of a plasma medium is negative permittivity under a specific frequency called plasma frequency. In visible light and ultraviolet light frequencies, negative dielectric permittivity is dominant for metals as a result of the plasma frequency of metals which is seen in optical frequencies. However, it is hard to have negative dielectric permittivity at lower frequencies, such as near infrared and the microwave regime; because, the dissipation dominates in metallic

media as a result of significant increase in the dissipation of the plasmon's energy in the system [21]. Therefore, the dielectric permittivity becomes purely imaginary. In 1996, Pendry *et al.* proposed the arrangement of periodic metal wires for the depression of the plasma frequency into the near infrared and GHz band [21]. The physical mechanism behind Pendry *et al.*'s suggestion is the confinement of electrons into thin wires for enhancing the effective electron mass through self-inductance. Therefore, the proposed structure has negative permittivity at microwave frequencies by using suitable parameters. The plasma frequency of the periodic thin wire array is given by making detailed analytical derivations as follows [21]:

$$w_p^2 = \frac{n_{eff} \cdot e^2}{\varepsilon_0 \cdot m_{eff}} = \frac{2\pi \cdot c_0^2}{a^2 \cdot \ln \frac{a}{r}} \tag{2.13}$$

where, c_0 is the speed of light, a is the lattice parameter and r is the radius of each wire (see Figure 2.3).

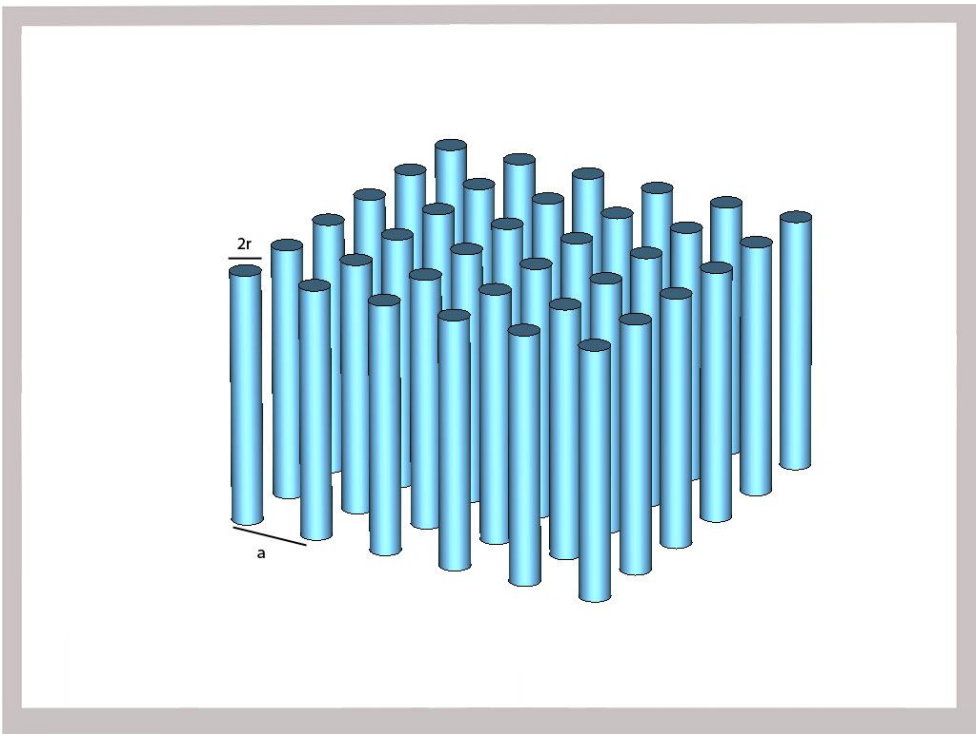

Figure 2.3: The schematic representation of a periodic metallic wire array. a is the lattice constant and r is radius of a single wire.

Eq. 2.13 states the fact that the plasma frequency can be expressed in terms of the macroscopic parameters of the array structure (a, r) instead of the microscopic quantities (effective electron mass-m_{eff}, effective electron density-n_{eff}). Moreover, the parameters of the metallic wire array lattice (a, r) are much smaller than the wavelength. When all the lattice parameters (a, r) of the thin metallic wires are much smaller than the wavelength ($a \ll \lambda$, $r \ll \lambda$), the response of the wire array can be interpreted by the effective medium theory. Therefore, an effective dielectric permittivity (ε_{eff}) can be used to define the dielectric permittivity parameter of the material/medium. In other words, the periodic array of

metallic wires appears to be an effective homogeneous material having an effective dielectric permittivity with negative real part.

We calculated the plasma frequency of various fictitious thin wire arrays and made simulations in the CST Microwave Studio in order to confirm the theoretical expectations. The analytical calculations and simulation results were in good agreement as shown in Figure 2.4 where an aluminum wire array of dimensions r=1.5 x 10^{-6} m, a=5 x 10^{-3} m was used in simulations.

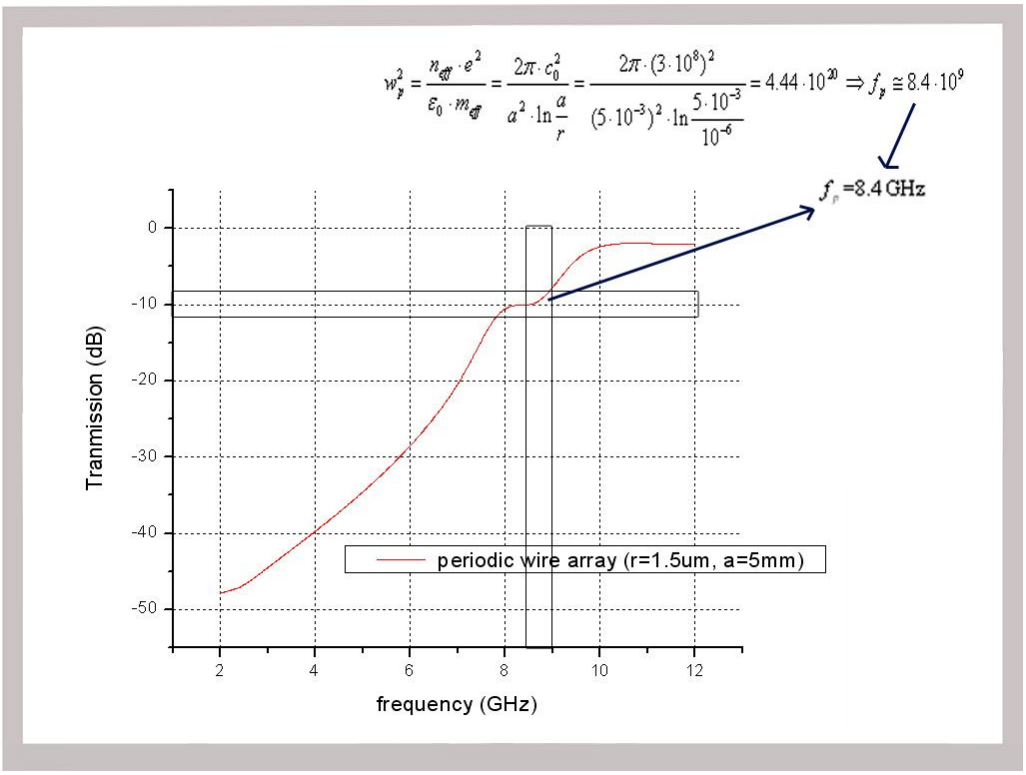

Figure 2.4: The simulation results of a thin wire array (r = 1.5 x 10^{-6} m, a = 5 x 10^{-3}) along with analytical calculations.

The model of Pendry *et al.* was further improved in various other studies [36]. Different approaches such as the one which models a periodic metallic wire array by using circuit models have been proposed [37].

2.2.2 Negative Permeability

Designing a material with negative permeability is much more difficult than designing one with negative dielectric permittivity. The lack of a magnetic charge in nature is the main reason behind the difficulty of obtaining negative permeability materials. Since the magnetic response of natural materials is not strong at microwave frequencies, the magnetic moment of atom or molecules cannot be utilized effectively. Therefore, we need to have a strong magnetic dipole moment effect obtained artificially. In 1999, Pendry *et al.* suggested several types of periodically arranged resonator structures that give strong enough magnetic response to an incident electromagnetic field [25].

The periodic thin wire array that was mentioned in the previous chapter responds to an incident electromagnetic field such that the effective dielectric permittivity of the structure becomes negative below the plasma frequency, but its permeability remains positive. Since, a magnetic dipole moment can be created by a current carrying conductor loop; a metallic ring structure provides a suitable structure to obtain a strong magnetic response. However, the rings should also have capacitive elements such as splits in order to be resonant at wavelengths much

larger than the diameter of the rings. The proposed structures of Pendry *et al.* [25] are shown in Figure 2.5:

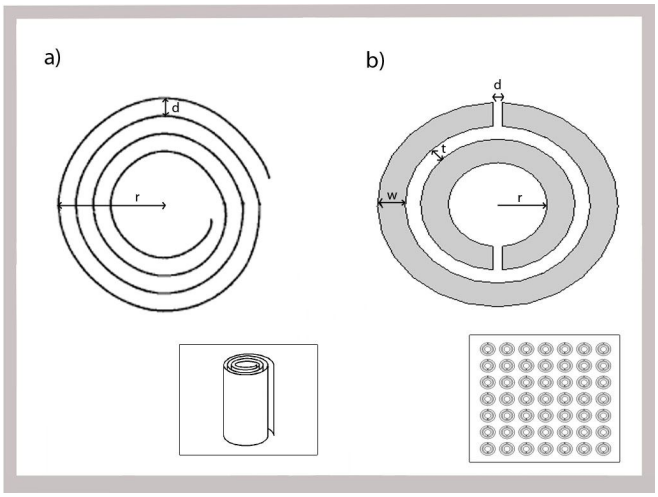

Figure 2.5: a) Swiss Roll Structure. b) Split Ring Resonator (SRR) Structure.

Note that, the structures are periodic arrangements of arrays in order to couple each other and increase the magnetic resonance. The strong magnetic resonance gives rise to negative permeability over a narrow resonance band.

The critical frequencies, such as the magnetic plasma frequency (w_{mp}) and the frequency at which μ_{eff} diverges (w_0) for the Swiss Role structure (see Figure 2.5.a) are derived as follows [25]:

$$w_{mp} = \sqrt{\frac{d \cdot c^2}{\left(1 - \frac{\pi \cdot r^2}{a^2}\right) 2\pi^2 \cdot r^3 \cdot (N-1)}} \tag{2.14}$$

$$w_0 = \sqrt{\frac{d \cdot c^2}{2\pi^2 \cdot r^3 \cdot (N-1)}} \tag{2.15}$$

where, c is the speed of light in vacuum, a is the lattice constant for a unit cell, d is the gap distance between two metallic sheets, N is the number of turns, r is the radius of the inner ring.

If the size of a single Swiss Role structure is much smaller than the excitation wavelength, the effective medium theory is valid and μ_{eff} is derived to be

$$\mu_{eff} = 1 - \frac{\frac{\pi \cdot r^2}{a^2}}{1 + \frac{2\sigma \cdot j}{wr\mu_0 (N-1)} - \frac{dc^2}{2\pi^2 r^3 (N-1) w^2}} \tag{2.16}$$

where, σ is the conductivity of the cylinder surface per unit area.

The second proposed structure for having negative permeability is a Split Ring Resonator (SRR) structure (see Figure 2.5.b) which is composed of two conducting rings with splits where the split locations are 180 degrees apart from each other. The splits are used to make the SRR resonant at wavelength much larger than the diameter of the SRR. The gap between the rings, splits, and inner split ring are all used to increase the capacitance that enables a decrease in the resonance frequency of the structure. If the largest dimension of the SRR is much smaller than the

wavelength of the resonance frequency, the response of a periodic arrangement of the SRR array can be analyzed by the effective medium theory such as we have mentioned in the case of the thin wire array. Therefore, an effective magnetic permeability (μ_{eff}) can be used to define the permeability parameter of the resulting material/medium.

The critical frequencies and effective permeability (μ_{eff}) for the SRR structure are analytically derived as [25]:

$$w_{mp} = \sqrt{\frac{3 \cdot d \cdot c^2}{\left(1 - \frac{\pi \cdot r^2}{a^2}\right)\pi^2 \cdot r^3}} \tag{2.17}$$

$$w_0 = \sqrt{\frac{3 \cdot d \cdot c^2}{\pi^2 \cdot r^3}} \tag{2.18}$$

$$\mu_{eff} = 1 - \frac{\frac{\pi \cdot r^2}{a^2}}{1 + \frac{2\sigma \cdot j}{wr\mu_0} - \frac{3dc^2}{\pi^2 r^3 w^2}} \tag{2.19}$$

where, c is the speed of light in vacuum, a is the lattice constant for a unit cell, μ_0 is the magnetic permeability constant of vacuum, r is the radius of the inner ring and σ is the conductivity of the cylinder surface per unit area.

The capacitance introduced into the system by the splits and the gap between the rings collaborates with the inductance introduced into the system by the metallic rings in order to resonate. Figure 2.6 shows the typical μ_{eff} form of a SRR as a function of angular frequency w under the assumption that the metallic rings are made of a perfect electric conductor (PEC) [25]:

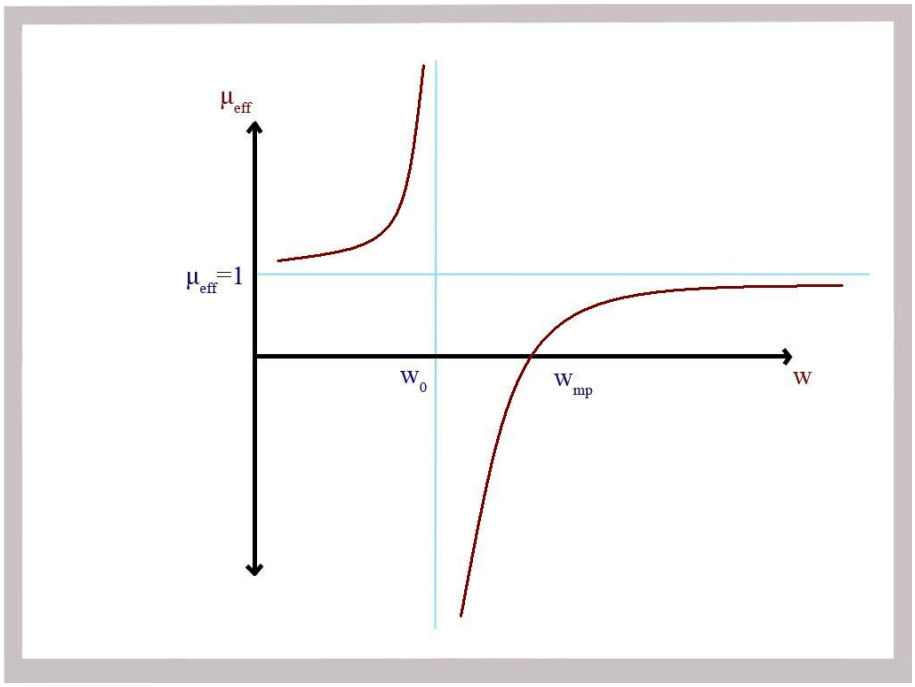

Figure 2.6: μ_{eff} -w diagram for ideal single SRR structure [25].

SRR is the most common structure that is used for the design of novel materials, such as metamaterials [38-46]. Resonator characteristics of SRRs will be used in our thesis to propose novel methods for providing enhanced (extraordinary) transmission through sub-wavelength apertures. Therefore, we need a detailed analysis of SRR, which is provided in Chapter 3.

2.2.3 Negative Index Metamaterials

The refraction phenomenon, occurring when an incident wave is transmitted from one medium to another, is governed by the well known Snell's Law of refraction which is stated as:

Snell's Law:

$$n_1 \sin \Theta_1 = n_2 \sin \Theta_2 \tag{2.20}$$

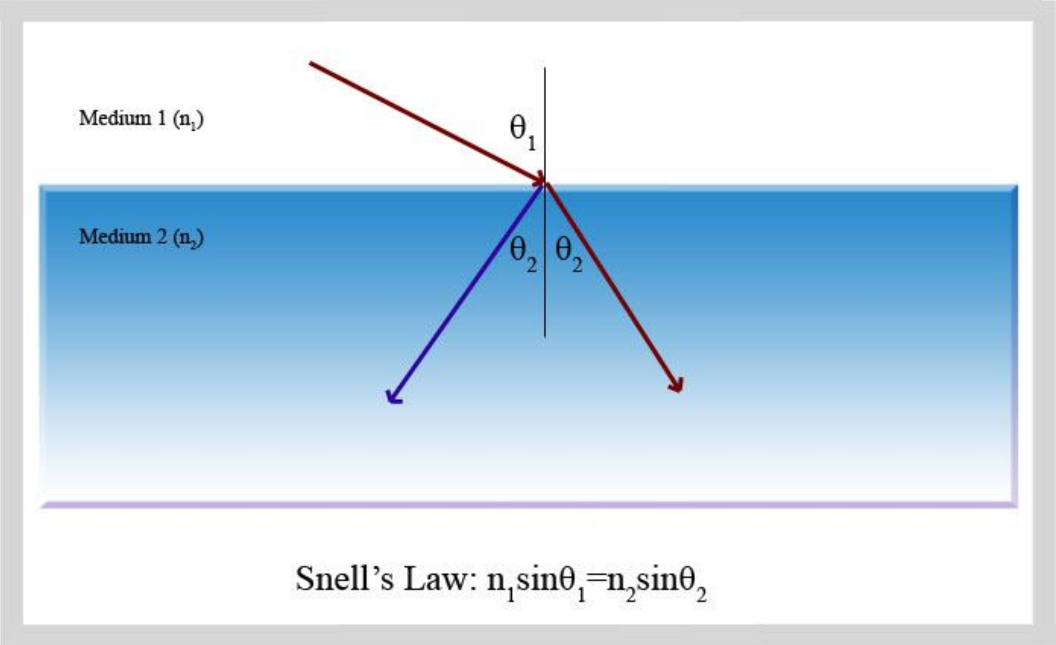

Figure 2.7: Schematic representation of refraction. Red line represents a positively refracted wave. Purple line represents a negatively refracted wave.

If both media in Figure 2.7 are filled by right-handed materials, the wave propagation vectors of the incident and transmitted wave fall into the different half spaces with respect to the surface normal [47]. However, when the incident wave is transmitted to a left-handed medium from a

right-handed medium, refraction occurs in an unusual manner as shown in Figure 2.8. Namely, when the incident waves are transmitted from a right-handed medium to a left-handed medium (negative dielectric permittivity and negative magnetic permeability), the refraction problem dictates that the wave vector of the incident wave and the transmitted wave are both on the same side with respect to surface normal [24].

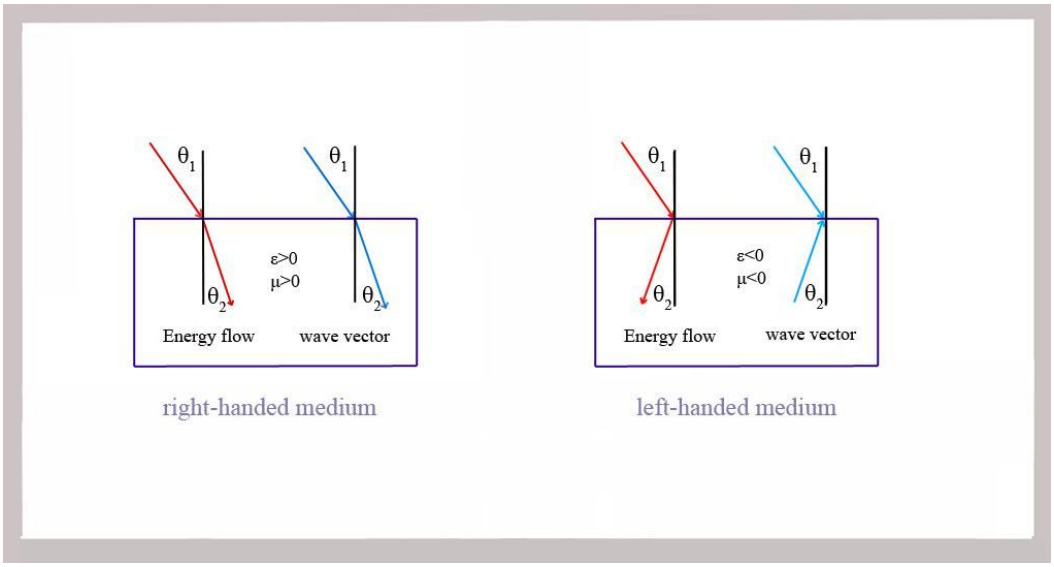

Figure 2.8: Refraction of an electromagnetic wave through right-handed and left-handed media.

Smith *et al.* have shown through an analysis of the points of a constant phase of a modulated plane wave, in which the group and phase velocities undergo negative refraction at the interface between a positive and negative index material [48].

We simulated the negative refraction through a fictitious left-handed slab material in which the Drude Dispersion model for effective dielectric

permittivity and the Lorentz Dispersion Model for the effective magnetic permeability are used.

The resonance behavior of a material is described by the so-called Lorentz Model, containing the resonance frequency w_0 and the damping factor δ:

$$\mu_{eff}(w) = \mu_{\infty} \times (1 - \frac{\frac{\mu_s}{\mu_{\infty}} \times w_m'^{\,2} - w_m'^{\,2}}{w^2 - j\delta w - w_m'^{\,2}}) \tag{2.21}$$

where, w_m' is the magnetic plasma frequency in which μ_{eff}=0.

Considering the specific plasma frequency w_p, the correspondent relative permittivity is given by the *Drude Model*:

$$\varepsilon_{eff} = \varepsilon_{\infty} - \frac{w_p^{\,2}}{w \times (w - iv_c)} \tag{2.22}$$

where, v_c is the collision frequency.

The ε_{eff} (Drude Model) [21, 64] and μ_{eff} (Lorentz Model) [21, 64] of the medium (see Figure 2.9.a) and the simulation results obtained by utilizing CST Microwave Studio are depicted (see Figure 2.9.b):

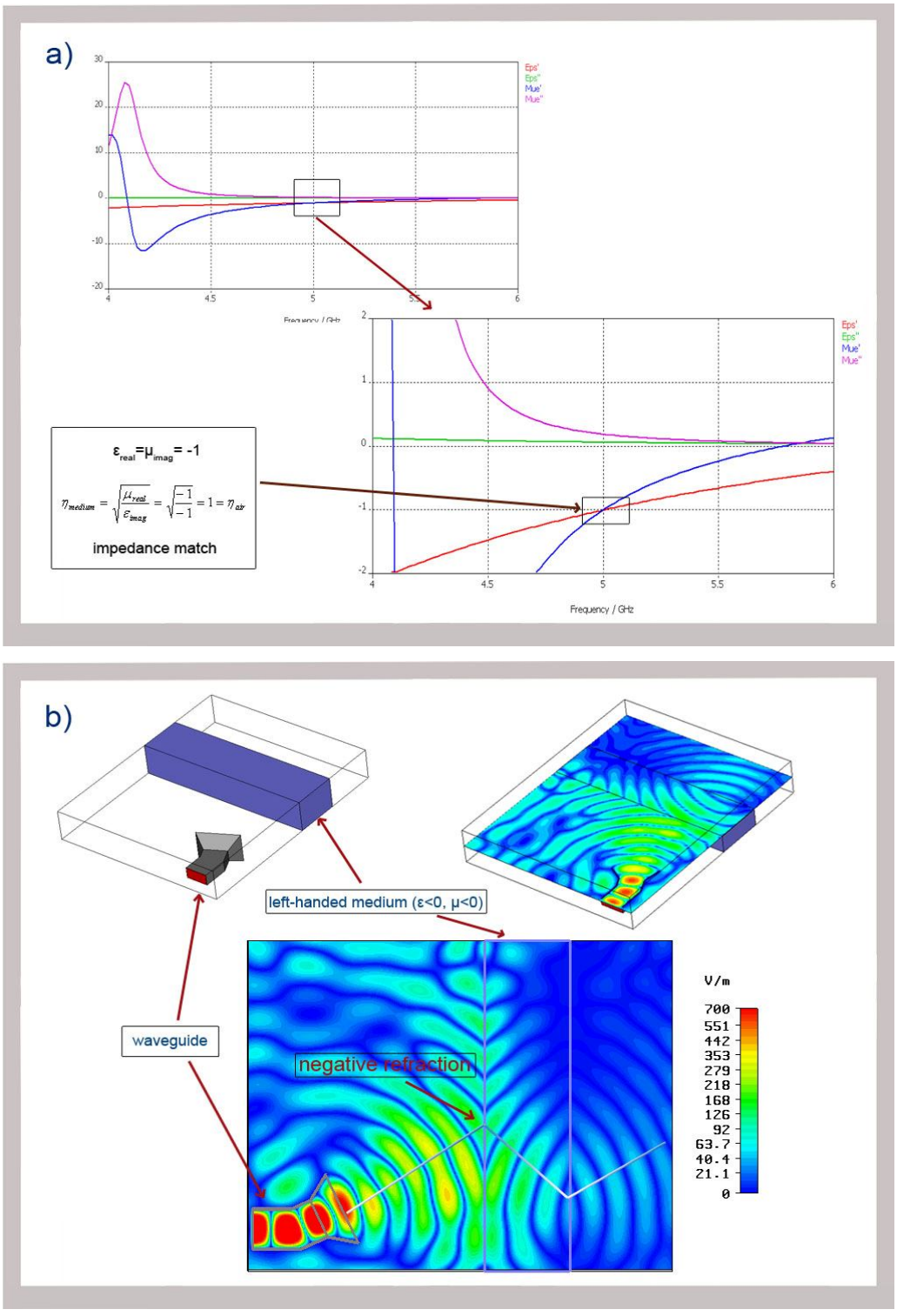

Figure 2.9: a) The ε_{eff} (Drude Dispersion Model) and μ_{eff} (Lorentz Dispersion Model) of the medium. b) Negative refraction of electromagnetic wave through a left-handed medium.

Figure 2.9.b demonstrates the opposite direction of group velocity and wave velocity. The phase fronts in the left-handed medium show that the wave propagates towards the source side (first incidence plane) which is closer to the source side, instead of propagating towards the second incidence plane.

A negative refractive index material inspires new geometrical optics devices called flat lenses. Figure 2.10 (a) shows that a rectangular slab with a negative refractive index (left-handed metamaterial) focuses the electromagnetic wave coming from a point source at locations f_1 and f_2 which is not possible with a positive refractive index material. A rectangular slab material with positive refractive index diverges the beam as shown in Figure 2.10.b. However, sub-wavelength focusing with a rectangular flat left-handed material is possible. As can be seen in Figure 2.10.a, electromagnetic waves (beam) refracts at the first incidence plane of the left-handed medium and forms a focusing point (f_1) inside the medium, and a second focusing (f_2) occurs after the second incidence plane of the left-handed medium, which is different from the case seen in positive refractive index materials.

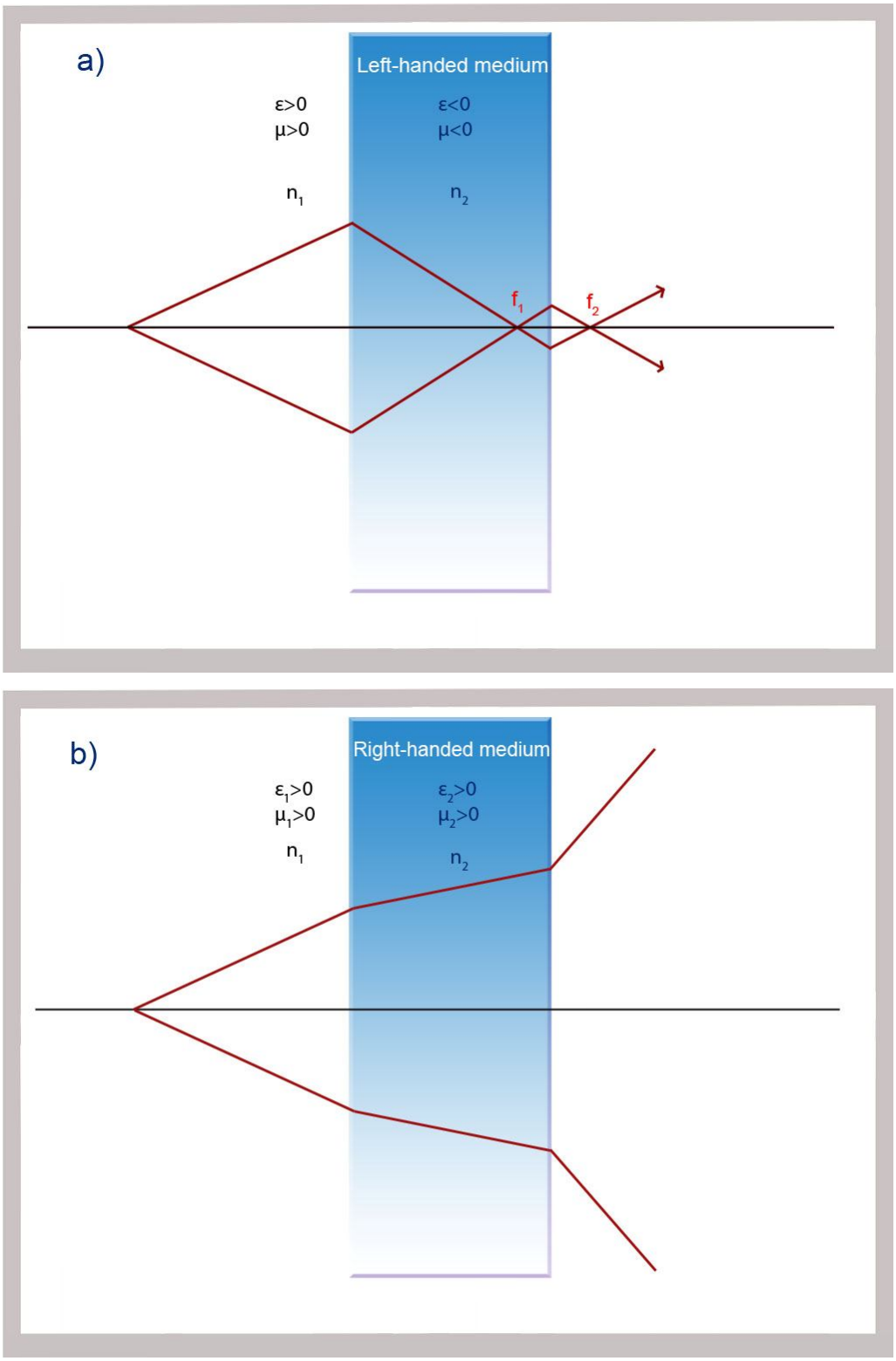

Figure 2.10: a) Focusing mechanism of a left-handed medium. b) Beam path in a right-handed medium.

The impedance match of medium-1 and medium-2 (Figure 2.10) is crucial for the design of lenses with no reflection. If the dielectric permittivity and magnetic permeability of a left-handed material medium is both equal to -1 and the source is close enough to the first incidence plane, there will be no reflection. Moreover, a perfect focus without the usual constraints imposed by wavelength can be achieved by negative refractive index materials, which are capable of restoring not only the phase of propagating waves but also the amplitude of evanescent states [49]. These new focusing devices are called "perfect lenses". Consequently, this extraordinary refraction mechanism opened up new research areas such as superlenses [50], cloaking [51], and semiconductor metamaterials [52].

CHAPTER 3

SPLIT RING RESONATOR (SRR) STRUCTURE

3.1 Introduction

The magnetic response of materials is determined by the magnetic permeability (μ), while the electric response of the materials is determined by the dielectric permittivity (ε). The combined effect of permittivity and permeability determine the response of material to incident electromagnetic field. Electric charges designate the electric response of materials. Since there is no magnetic charge in nature, it is rather difficult to have negative permeability structures, while negative permittivity is obtained below the plasma frequency of periodic sub-wavelength metallic wires at microwave frequencies. Therefore, the magnetic property of available structures should be modified to obtain artificial magnetic-like charges and create magnetic dipole moment.

In 1999, Pendry *et al.* suggested several novel resonator structures which display magnetic response to an incident electromagnetic field when arranged in a periodic array [25]. The most dominant and commonly used structure is the Split Ring Resonator (SRR) structure because of its

easier fabrication and stronger magnetic resonance. SRRs have been studied extensively in literature. There are experimental [56-58] and numerical simulation studies [67-69] on the transmission characteristics of SRRs. Analytical models are suggested to better model the resonance characteristics of SRRs [71-73]. The majority of the studies on SRR are performed in the microwave regime; but, there is an increasing amount of interest on the studies of magnetic resonance of SRRs at near infrared spectrum [74, 75].

The strong magnetic resonance of SRR is due to the additional capacitive elements such as splits and gap between the rings. Figure 3.1 demonstrates the Split Ring Resonator Structure (SRR).

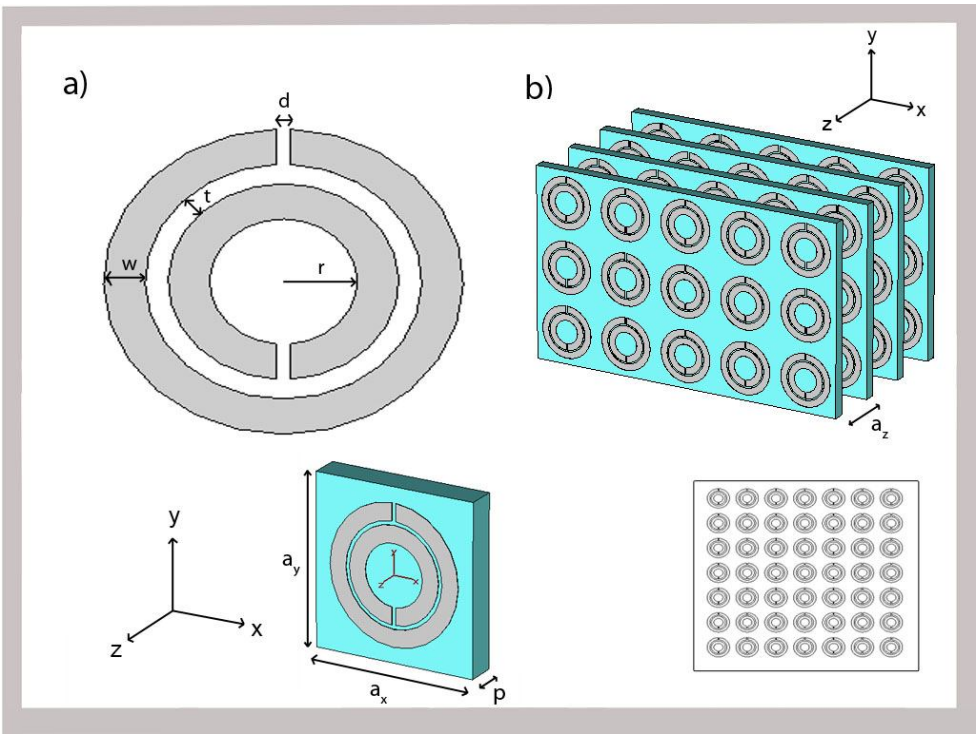

Figure 3.1: Schematics of a) single SRR b) periodic arrangement of SRR array.

Two rings with splits oriented oppositely. The capacitive elements (splits and gap) are utilized to achieve magnetic resonance at wavelengths much larger than the diameter of the rings. The second ring is actually used for increasing the capacitance of the structure. There are several split ring resonator structures such as single-split ring structures and split rings with several splits. These types of SRR structures are discussed in Chapter 3.4.

Moreover, the periodic arrangement of the SRR (Figure 3.1.b) increases the magnetic response of SRR by strong coupling between the resonators and the unique properties such as negative permeability emerges. Also, since all parameters of SRR (a, r, d, t, w, p) are much smaller than wavelength, the response of SRR array is fit to effective medium theory. Therefore, an effective magnetic permeability (μ_{eff}) and effective dielectric permittivity (ε_{eff}) can be used to define the two fundamental material parameters of the structure/medium.

3.2 Electromagnetic Resonance Mechanism of SRR

Split Ring Resonator (SRR) structures are strong magnetic resonators and they respond incident electromagnetic wave by both electrical and magnetic resonance in particular bandwidths. The magnetic resonance characteristics of SRRs are available for very narrow bandwidth [63]. Also, the SRRs respond to the magnetic component of the incident wave if the incident electromagnetic wave is excited with the appropriate

polarization [55]. Moreover, periodically arranged SRR array is shown to exhibit negative permeability ($\mu_{eff} < 0$) for frequencies close to magnetic resonance frequency (w_m) of the SRR structure [25]. In this section, we studied the mechanism of SRR structure's resonances. The SRR under investigation are comprised of concentric metallic rings on a dielectric substrate (Figure 3.2).

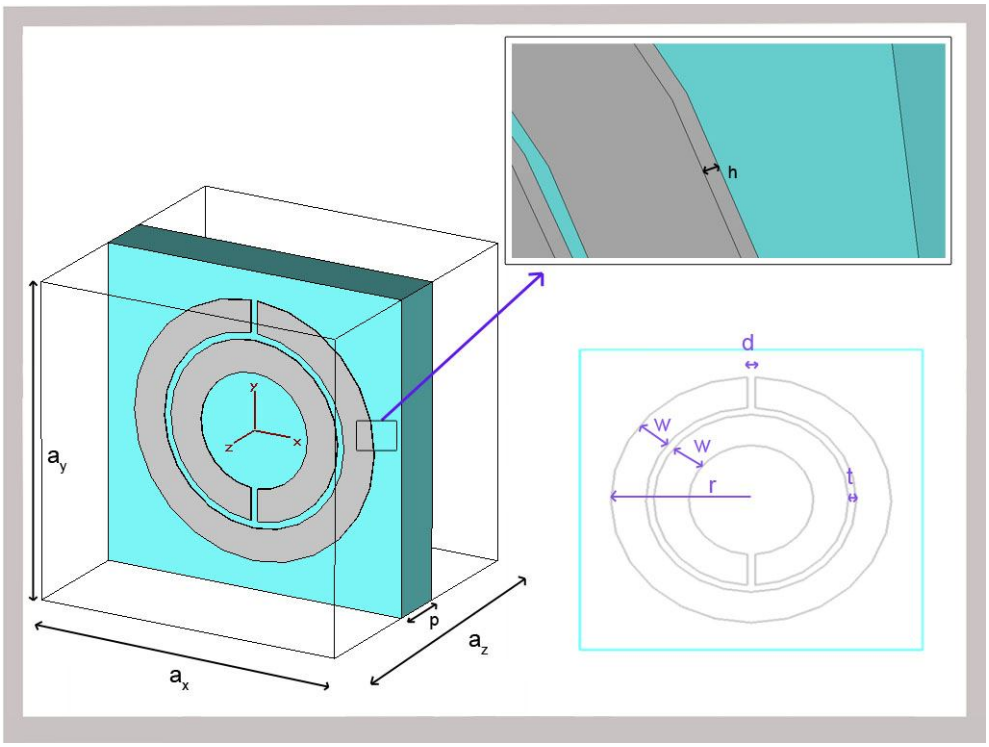

Figure 3.2: Unit cell of SRR structure which is used throughout this chapter.

The numerical simulations are done by using the commercially available software CST Microwave Studio which is a three dimensional full-wave solver employing the finite integration technique [64].

The substrate of SRR is FR-4 substrate with dielectric permittivity constant $\varepsilon = 4.0$ and tangent loss $\delta = 0.01$.

Geometrical parameters of the SRR structure are taken from a previously developed SRR structure which is designed by Aydin *et al.* [41]. The width of the splits (d) and the gap between the inner ring and the outer ring (t) is 0.2 mm, the width of metallic ring (w) is 0.9 mm, the outer radius (r) is 3.6 mm, the thickness of the deposited copper layer (h) is 30 μm and the thickness of the FR-4 substrate is 1.6 mm (p). Also, the unit cell dimensions of a single SRR structure (lattice constants) are taken to be $a_x = a_y = 8.8$ mm and $a_z = 6.5$ mm.

Since the periodic arrangement of the SRR slightly changes the magnetic response of SRR by coupling between the SRRs, the resonance behavior of a single SRR can also be observed by the frequency response of periodic arrangement of SRRs [55, 59]. Periodic arrangement of SRR arrays are utilized to investigate the magnetic response of SRRs; because the combined effect of periodic SRR array reveals the magnetic properties of SRR more clearly than a single SRR and negative permeability values can be obtained by strong magnetic response of SRR array.

Firstly, we compared the responses of periodic array of SRRs and single SRR by simulating a single SRR structure and periodic array of SRRs. The simulation methods used in periodic arrangement of SRR array is as follows: We excite the device under test (DUT) materials with a plane

wave and obtain the transmission amplitudes by an electric field probe (see Figure 3.3). The distance between the device under test and the plane wave source is 6 mm. Also, the electric field probe is placed at 50 mm away from the DUT. The distant probe location is chosen for being protected against the near-field effects due to the strong resonant nature of the devices under test. The propagation direction of plane wave is along +x and electric field vector ($\overline{E}$) of the plane wave is directed to +y. The probe is electric probe which is oriented in y-direction. Moreover, open boundary conditions are employed along the propagation direction (+x and -x). Periodic boundary conditions are used for the rest of the directions (-y, +y, -z and +z). Therefore the DUT is assumed to be periodic and infinite along the directions perpendicular to the propagation direction. The dip of the transmission data gives the electric or magnetic resonance frequency of the structure.

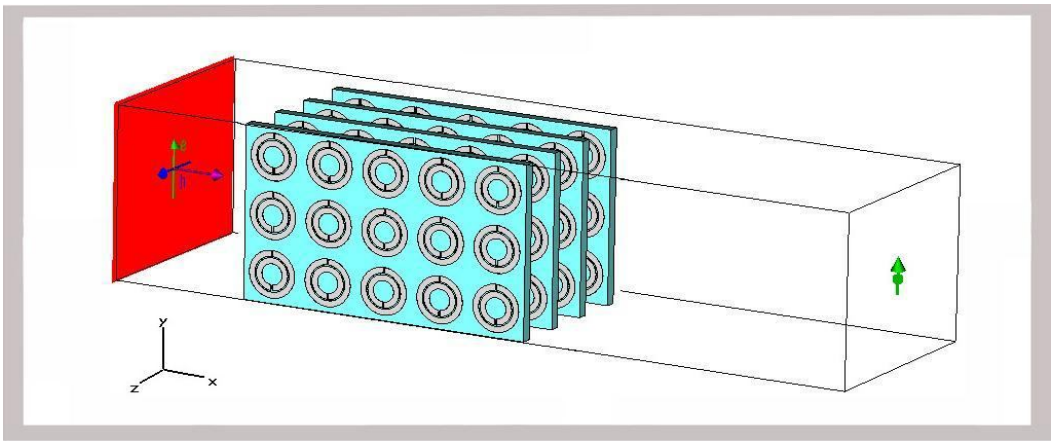

Figure 3.3: Simulation model of periodic SRR array.

The simulation of single SRR structure is done by modeling a waveguide-like structure (Figure 3.4). Namely, two waveguide ports are used to

obtain S-21 data. Open boundary conditions are employed along the propagation direction (+x and -x). Electric (E_t=0) boundary conditions are used for –y and +y direction. Also magnetic (H_t=0) boundary conditions are used for –z and +z direction.

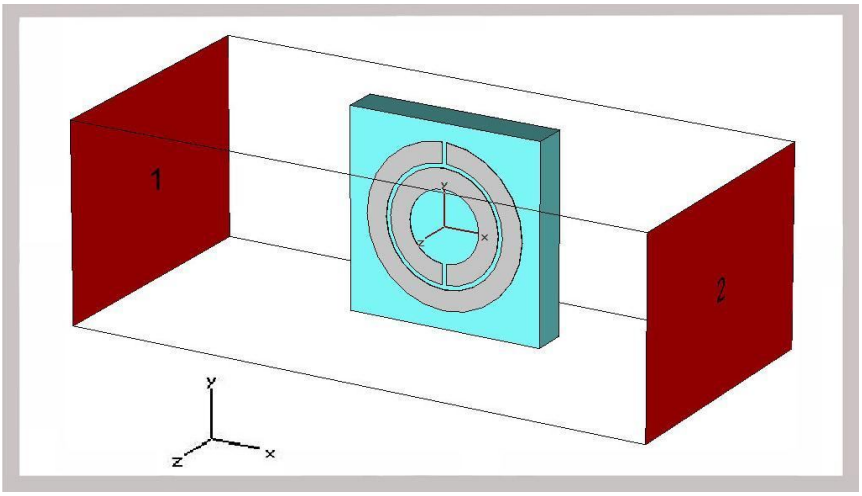

Figure 3.4: Simulation model of single SRR structure.

The simulation results for a single SRR and periodic array of SRR reveals that there is slight difference in the magnetic resonance frequency (see Figure 3.5). Therefore, we can use the results of periodic arrangement of SRRs and also a single SRR while considering the magnetic resonance frequency of SRR structure.

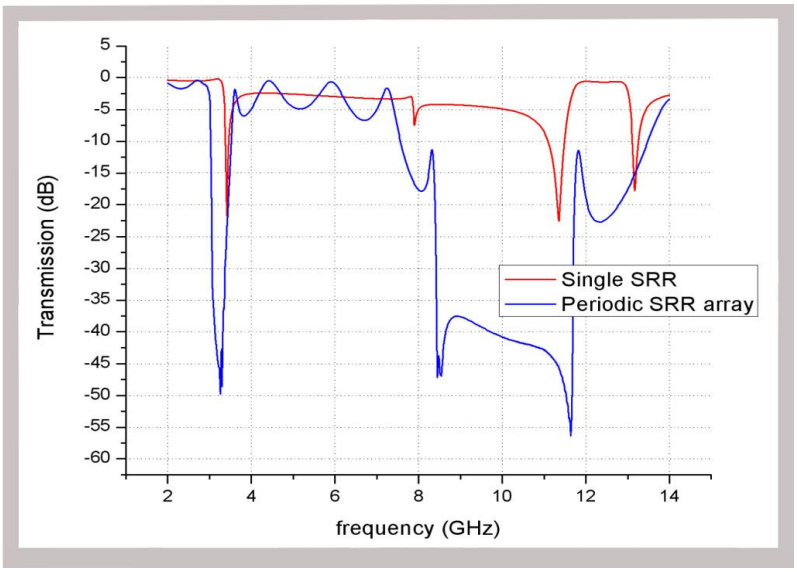

Figure 3.5: Simulation results of a single SRR structure and periodic SRR array.

The periodic arrangement of SRR suppresses the transmission of electromagnetic waves for certain frequency band which indicates resonance. The resonances of SRRs are not only the magnetic-type resonance but also the electric-type resonances. Moreover, the periodicity of SRR may cause a band gap too. Therefore, a bandgap in the transmission spectrum of periodic SRR array medium may be due to the negative permittivity or negative permeability or periodicity (Bragg gaps) [41]. The identification of negative permeability and negative permittivity regions can be done by using a closed SRR (CSRR) structure in which the splits of the SRR is closed. Since the splits of SRR play a key role in the magnetic resonance, closing the splits will annihilate the magnetic resonance but the electric resonance will still exist. We made numerical simulations by closing the splits of the structures in Figure 3.2. The simulation results for CSRR structure are demonstrated with results of SRR in Figure 3.6:

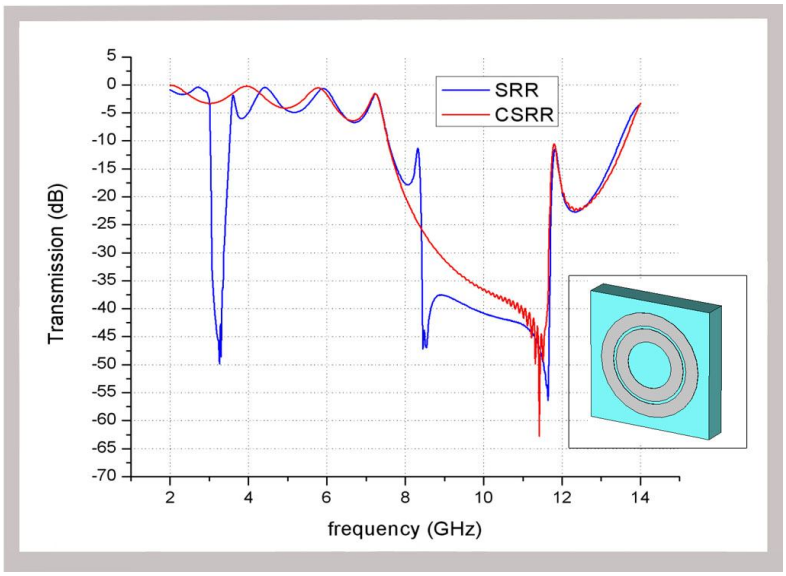

Figure 3.6: Simulation results of a SRR and CSRR structures. CSRR structure is depicted in the inset.

We observed three dips at the frequencies 3.4 GHz, 8.2 GHz and 11.4 GHz in the transmission spectrum of SRR (Figure 3.6). However, only a single dip at 11.4 GHz is observed for CSRR structure. The splits are very crucial for magnetic resonance and removing the splits of SRR prevents current to flow between the inner and the outer rings. Therefore, the magnetic resonance is destroyed. The SRR and CSRR structures act like discontinuous wires at 11.4 GHz and the bandgap of SRR coincides with the bandgap of CSRR which implies that the physical reason of this bandgap is attributed to the electric resonance of discontinuous-wire-like structures. So, the dip at 11.4 GHz is because of electric resonance. However, the dips at 3.4 GHz and 8.2 GHz are due to magnetic resonance; because, closing the splits destroys the dips at these frequencies. Since electromagnetic waves incident to an SRR array medium with the negative effective permeability can not propagate, there

exists negative permeability band gaps at 3.4 GHz and 8.2 GHz as a result SRR's magnetic resonance [41].

Note that, the diameter of the SRR (2r = 7.2mm) is less than 0.1λ for the magnetic resonance at 3.4 GHz ($\lambda \cong 88$ mm). Therefore, magnetic resonance can be achieved by SRR structures with sub-wavelength dimensions which open up significant opportunities to design novel sub-wavelength devices. So, the major reason of the increasing amount of interest on SRR is not only the ability of achieving negative permeability but also achieving resonance with sub-wavelength dimensions. The structures that we proposed in this thesis for increasing the transmission of electromagnetic waves through sub-wavelength apertures are based on novel SRR-type structures and utilize the sub-wavelength resonance mechanism of SRRs. We will discuss these novel structures in Chapter 5.

3.3 Geometrical parameters of SRR and their effect on magnetic resonance frequency

The capacitive elements of SRR are responsible for the strong magnetic and electric response of SRR. The splits are additional capacitance for the overall SRR and splits prevent current from flowing around the rings; but the mutual capacitance between the concentric rings enables the flow of current through the structure [22, 63]. Since SRR are the most prevailing resonator to achieve negative permeability, there are many research studies to understand the physical mechanism of SRR's magnetic

resonance which causes the negative magnetic permeability. One of the most common methods is to model an individual SRR with L-C circuit models [71, 72]. SRR is defined with L-C circuit structure. The total capacitance of SRR is determined by the splits of each ring and the gap between the two concentric rings. Also, the inductance of SRR originates from the metallic rings and the gap between the two concentric rings [71]. The main reason behind modeling SRR structure is to analytically define the effect of SRR parameters on resonance frequency of SRR; because defining the effect of parameters help researchers to utilize SRR structure at the desired frequency regime.

In this section, we will investigate the parameters of SRR structure (split width (d), ring width (w), gap distance (t), dielectric constant of substrate ($\varepsilon_{susbstrate}$), substrate thickness (p) on the resonance of SRR.

The simulation model of SRR structures in the following sections is same as the single SRR measurement model stated in Chapter 3.2 (Figure 3.14).

3.3.1 Effect of split width (d)

In this section, we will discuss the effect of split width (d) on the resonance frequency. SRR geometry with its main parameters is displayed on Figure 3.1.

The parameters other than the split width are kept constant. These parameters are initially set to be;

Ring width (w) = 0.9 mm

Gap distance (t) = 0.2 mm

Dielectric constant of substrate ($\varepsilon_{susbstrate}$) = 4.0

Substrate thickness (p): 1.6 mm

We span five values of split width raging from 0.1 to 0.5 while keeping other parameters constant. Figure 3.7 is the transmission result of five SRR structures with split widths of d = 0.1, 0.2, 0.3, 0.4 and 0.5 mm.

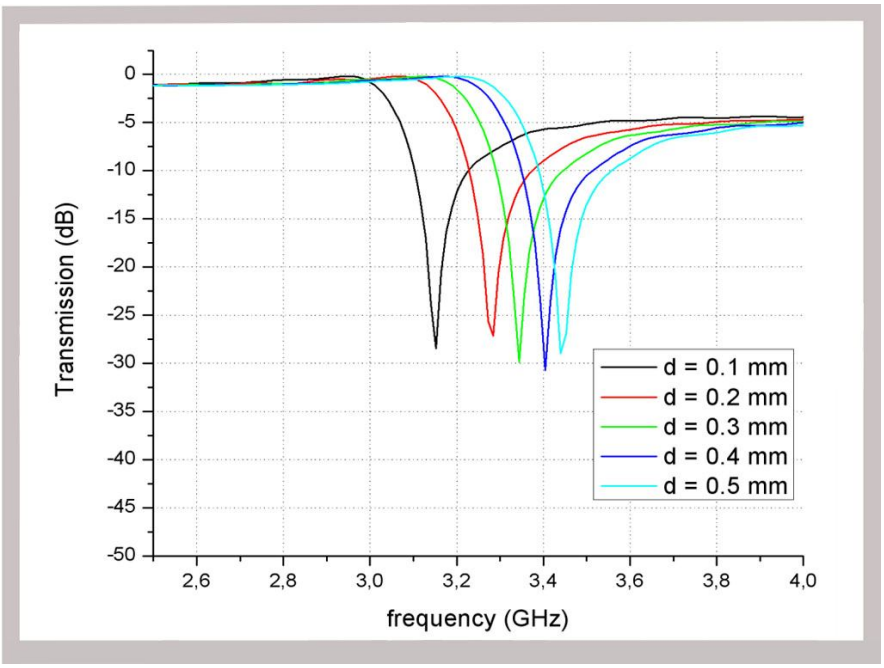

Figure 3.7: Calculated transmission spectrum of a single SRR structure with various split widths (d).

The dip frequencies of SRRs are increasing with increasing split width. The splits of rings are alike a parallel plate capacitor and as we increase the width of the splits, the capacitance due to splits decreases ($C=\frac{\varepsilon A}{d}, d \uparrow \Leftrightarrow C \downarrow$). Therefore, the L-C resonance model of SRR ($f \propto \frac{1}{\sqrt{LC}}$) dictates that as the capacitance of system decrease the resonance frequency will increase.

3.3.2 Effect of ring width (w)

The effect of ring width on the resonance frequency is discussed in this section. Ring width (w) is varied ranging from 0.1 to 0.5 mm with 0.1 mm steps while keeping other parameters constant:

Split width (d) = 0.2 mm

Gap distance (t) = 0.2 mm

Dielectric constant of substrate ($\varepsilon_{susbstrate}$) = 4.0

Substrate thickness (p): 1.6 mm

Five different values of ring width (w) raging from 0.1 to 0.5 are used to investigate the effect of ring width on magnetic resonance frequency. Figure 3.8 is the transmission results for different ring widths (w = 0.1, 0.2, 0.3, 0.4, 0.5).

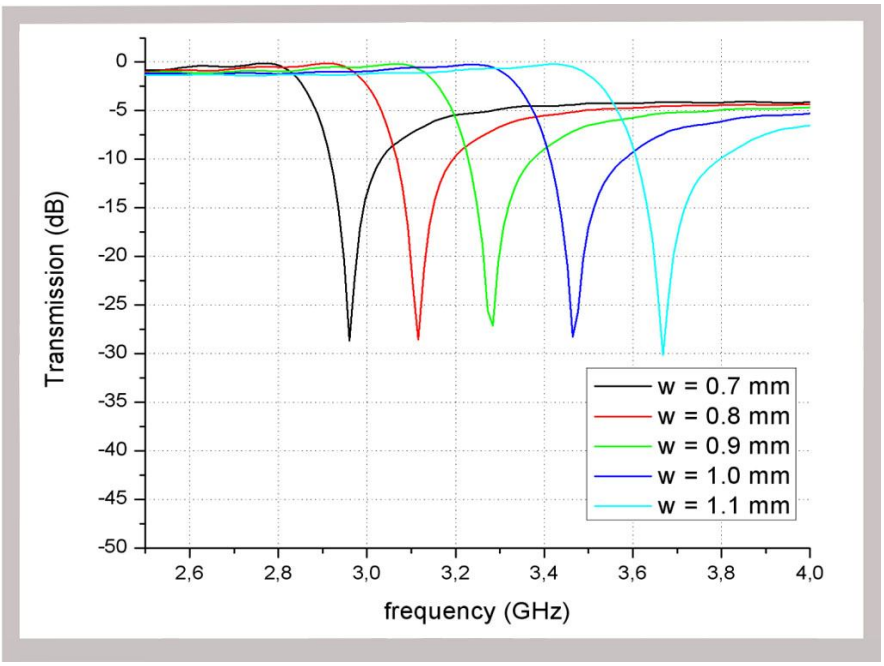

Figure 3.8: Calculated transmission spectrum of a single SRR structure with various ring widths (w).

As can be seen from Figure 3.8, the resonance frequency increases with the increasing ring width. Since the mutual inductance and capacitance of the system decreases with increasing ring width [60], the resonance frequency increases.

3.3.3 Effect of gap distance (t)

In this section, we investigated the effect of the gap distance between inner and outer concentric rings of SRR on the magnetic resonance. The gap distance is varied ranging from 0.1 to 0.5 mm with 0.1 mm steps while keeping the other parameters constant:

Ring width (w) = 0.9 mm

Split width (d) = 0.2 mm

Dielectric constant of substrate ($\varepsilon_{susbstrate}$) = 4.0

Substrate thickness (p): 1.6 mm

Moreover, the outer radius (r) of SRR is also fixed (r = 3.6 mm). Therefore, increasing the gap distance (t) will decrease the radius of inner ring. Figure 3.9 demonstrates the simulation results.

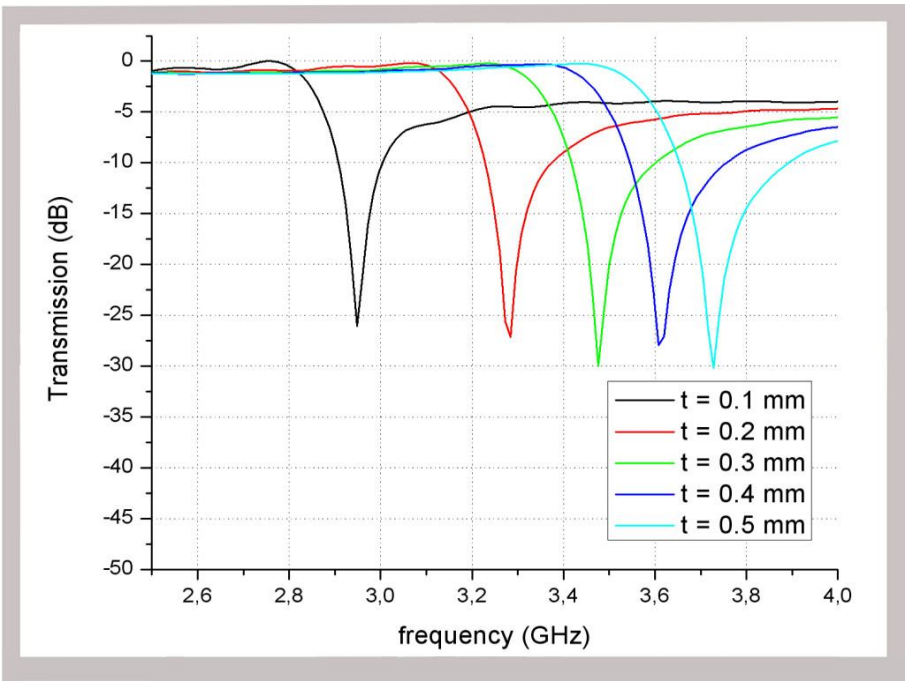

Figure 3.9: Calculated transmission spectrum of a single SRR structure with various gap distances (t).

Since the mutual capacitance due to the gap between rings decreases with increasing gap distance the magnetic resonance frequency increases. Also, the mutual inductance of the structure decreases with increasing gap distance and contributes the increase in resonance frequency [60].

3.3.4 Effect of dielectric permittivity of substrate ($\varepsilon_{substrate}$)

Dielectric permittivity of substrate ($\varepsilon_{substrate}$) is varied from 3.6 to 4.4 with 0.2 steps while keeping the other parameters constant:

Ring width (w) = 0.9 mm

Split width (d) = 0.2 mm

Gap distance (t) = 0.2 mm

Substrate thickness (p): 1.6 mm

The transmission results of changing only the dielectric permittivity of substrate is demonstrated in Figure 3.10:

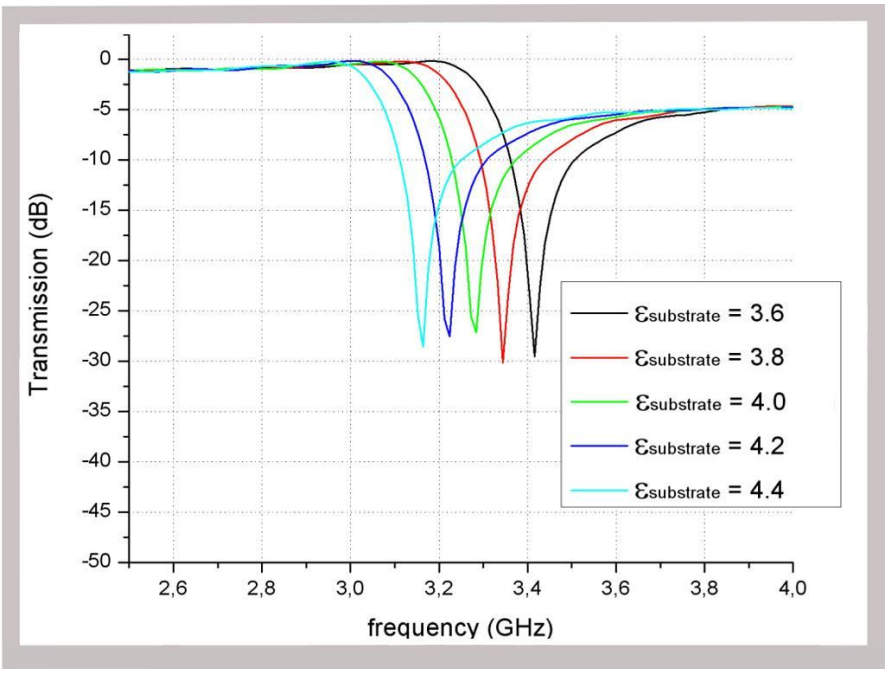

Figure 3.10: Calculated transmission spectrum of a single SRR structure with various dielectric permittivities of substrate ($\varepsilon_{substrate}$).

As we mentioned before, structures with dimensions much smaller than wavelength can be attributed as effective medium with effective permittivity and effective permeability. Therefore, the periodic arrangement of SRR array that we consider here can be considered as an effective medium with effective permittivity and effective permeability. The dielectric permittivity of the substrate contributes the value of effective dielectric permittivity of SRR array. Therefore, as the dielectric permittivity of substrate increases, the effective permittivity of SRR array medium increases; and the increase in effective permittivity causes the decrease in magnetic resonance frequency of SRR.

3.3.5 Effect of substrate thickness (p)

The effect of substrate thickness (p) on resonance frequency is investigated by varying the substrate thickness of SRR from 1.2 mm to 2 mm with 0.2 mm steps while keeping the other parameters constant:

Ring width (w) = 0.9 mm

Split width (d) = 0.2 mm

Gap distance (t) = 0.2 mm

Dielectric constant of substrate ($\varepsilon_{susbstrate}$) = 4.0

Figure 3.11 demonstrates the simulation results for varying p (p = 1.2, 1.4, 1.6, 1.8, 2.0):

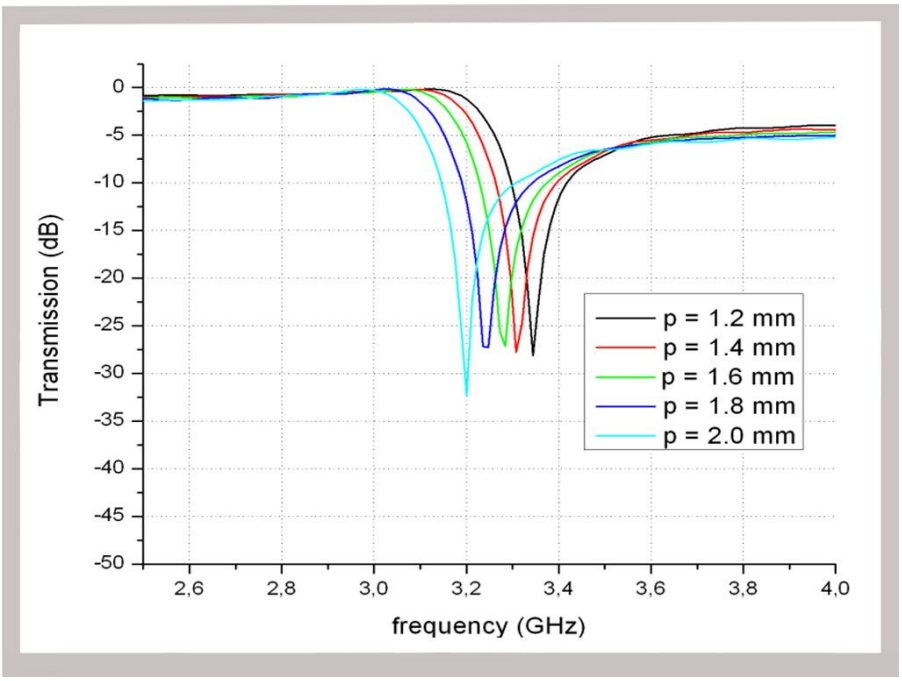

Figure 3.11: Calculated transmission spectrum of a single SRR structure with various substrate thicknesses (p).

As can be seen in Figure 3.11, the resonance frequency of SRR decreases with the increasing substrate thickness. The substrate thickness affects the mutual capacitance of the system. As substrate thickness increases the mutual capacitance of the system increases which causes the decrease in the resonance frequency.

3.4 Different Types of Split Ring Resonators

In this section, we investigated several different types of SRR structures like single-ring SRRs and SRRs with several splits. The SRR structure that we studied in previous section is composed of two concentric rings with

splits situated on the opposite side of the two concentric rings (see Figure 3.1).

The fabrication of SRRs for operating at higher frequencies is not as easy as microwave frequency range; because as the operation frequency increases the size of SRR should be decreased and the split gap dimension of SRR will be very small which is hard to fabricate. Also, the gap distance of the rings will be very small which causes to contact problems between metallic rings. Therefore, there is a tendency to manipulate the shape of conventional SRR structures to obtain resonance at higher frequencies. Namely, while conventional SRR structures can be fabricated for operating at a few THz [75], a single ring with single split is being used for resonator structure at 100 THz [74] which is easier to fabricate.

The fabrication constraint of conventional SRR is not the only reason for utilizing different SRR structure. Since the SRR structures are electrically resonant for different polarizations; 3D resonator structures can not be utilized effectively. The electrical resonance suppresses the magnetic resonance of SRR; therefore, additional splits are needed to destroy the electrical coupling to the magnetic resonance [63].

3.4.1 Single-Ring SRRs

In this section, we investigated the resonance characteristics of Single-Ring SRR structure. Conventional SRRs are composed of two concentric

rings with splits oriented opposite sides. The inner split ring of conventional SRR is utilized to increase the capacitance of the system which causes the decrease in the resonance frequency. The resonator structure with single ring, which is called Single-Ring SRR, is investigated to characterize the effect of geometrical parameters on the resonance of resonator structure. Since, enough capacitive and inductive elements are available for Single-Ring SRR structure; it is possible to obtain magnetic resonance [74].

We investigated the magnetic resonance of single-ring SRR structures by changing the split width (d), ring width (w), dielectric constant of substrate ($\varepsilon_{susbstrate}$) and substrate thickness (p). Figure 3.12 is the geometrical representation of single-ring SRR structures that we studied.

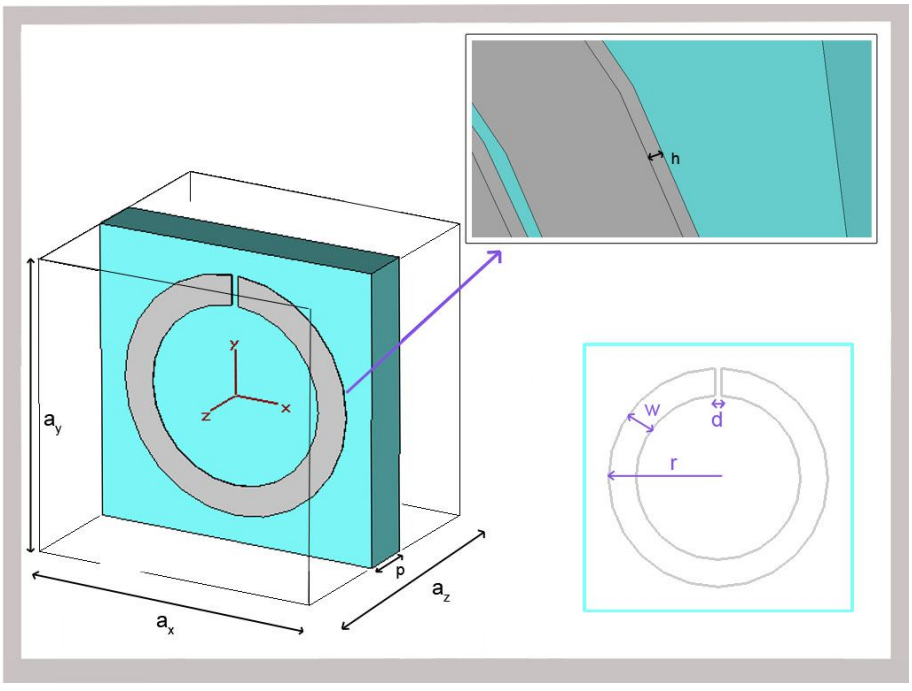

Figure 3.12: Unit cell of Single-Ring SRR structure.

The geometrical and electrical parameters of the single-ring SRR structure is derived from the parameters of conventional SRR structures that we used in previous sections. The width of the each split (d) is 0.2 mm, the width of all metallic rings (w) is 0.9 mm, the radius (r) of all rings is 3.6 mm, the thickness of the deposited copper layer (h) is 30 μm and the thickness of the FR-4 substrate is 1.6 mm (p). Also, the unit cell dimensions of a single SRR structure (lattice constants) are taken to be a_x = a_y = 8.8 mm and a_z = 6.5 mm. Finally, the substrate of SRR is FR-4 substrate with dielectric permittivity constant ε = 4.0 and tangent loss δ= 0.01. The simulation method is same as described in Chapter 3.2.

The simulation results of change in magnetic resonance with changing the split width (d = 0.1, 0.2, 0.3) are demonstrated Figure 3.13:

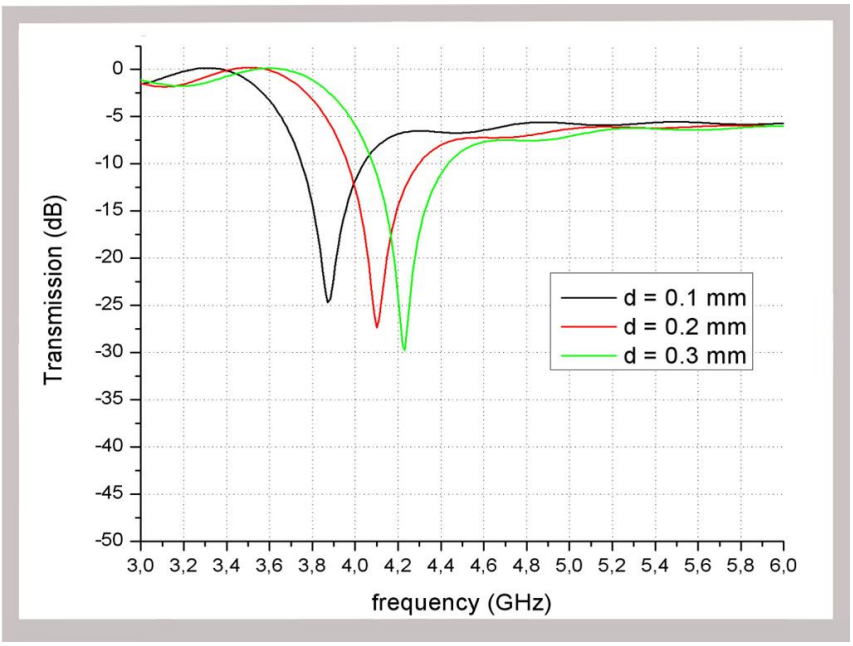

Figure 3.13: Calculated transmission spectrum of a Single-Ring SRR structure with various split widths (d = 0.1, 0.2, 0.3).

As the split width increases, the magnetic resonance of the single-ring SRR structure increases because of the decrease in total capacitance coming from the decrease in the split capacitance.

The simulation results of change in magnetic resonance with changing the ring width (w = 0.7, 0.9, 1.1) are demonstrated Figure 3.14:

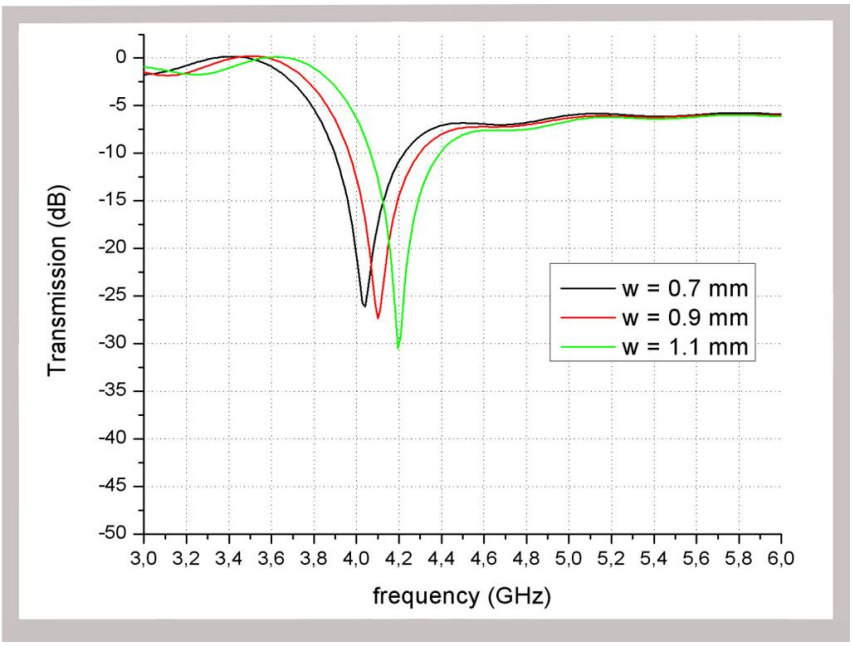

Figure 3.14: Calculated transmission spectrum of a Single-Ring SRR structure with various ring widths (w).

The magnetic resonance frequency of single-ring SRR structure increases with increasing ring width as result of decreasing capacitance of the system. The area of splits, which is similar to area of two capacitor plates, increases with increasing ring width and that phenomenon causes the decrease in capacitance of split regions.

The simulation results of change in magnetic resonance with changing the dielectric permittivity of substrate ($\varepsilon_{susbstrate}$ = 3.8, 4.0, 4.2) are demonstrated in Figure 3.15:

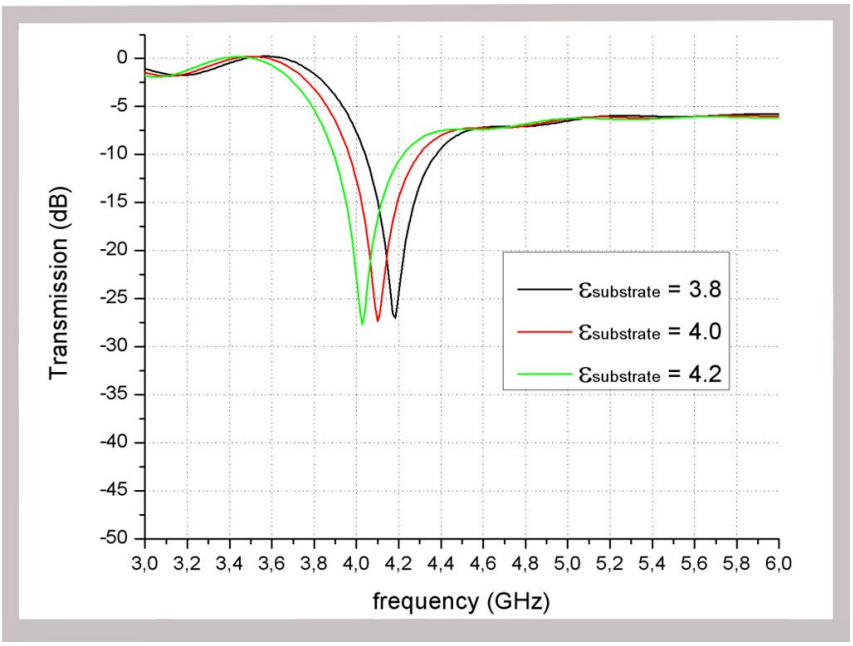

Figure 3.15: Calculated transmission spectrum of a Single-Ring SRR structure with various dielectric permittivities of substrate ($\varepsilon_{susbstrate}$).

Simulation results indicates that the magnetic resonance frequency of single-ring SRR structure decreases with increasing dielectric constant of substrate as result of increase in effective permittivity. Since the increasing permittivity causes the increase in the capacitance value of the splits, the resonance frequency decreases.

The simulation results of change in magnetic resonance with changing the substrate thickness (p = 1.2, 1.6, 2.0) are demonstrated Figure 3.16:

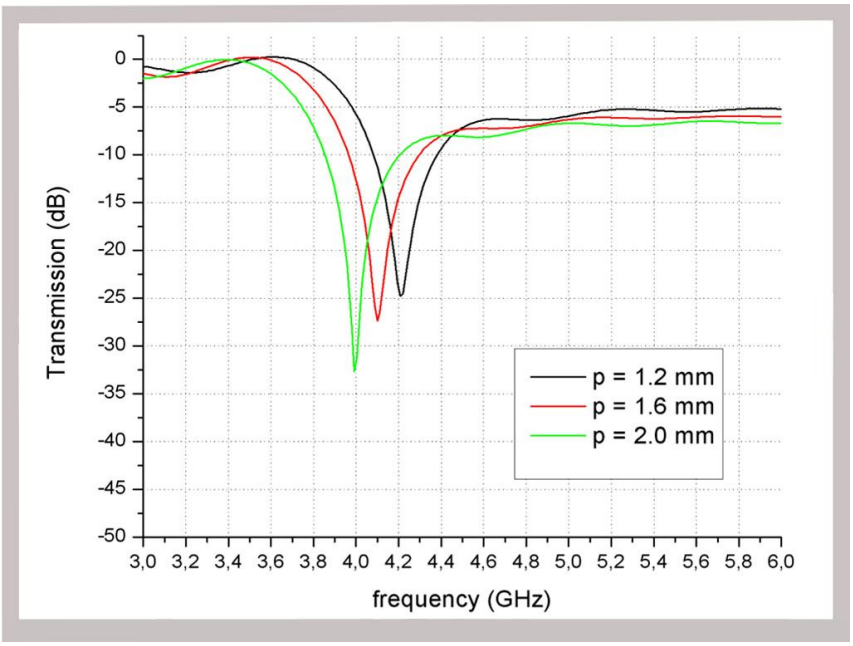

Figure 3.16: Calculated transmission spectrum of a Single-Ring SRR structure with various substrate thicknesses (p).

As can be seen in Figure 3.16, the magnetic resonance frequency of single-ring SRR structure decreases with increasing substrate thickness as a result of increase in capacitance of the system due to the increased amount of electromagnetic fields in the substrate.

Effect of geometrical parameters on the resonance of single-ring SRR structure is similar to conventional SRR structures. However, the change in resonance frequency of single-ring SRR structure and conventional SRR structure are not the same unsurprisingly; because the differences in capacitive and inductive elements of the structures causes different amount of change in total capacitance and inductance of the structures.

3.4.2 Single-Ring SRRs with several Splits

The Single-Ring Split Ring Resonator structure with several splits is investigated. Since, there are enough capacitive elements (split, mutual capacitance of wire) and inductive elements (metallic ring) for Single-Ring SRR structure; it is possible to obtain magnetic resonance with several splits [74].

We investigated the magnetic resonance of single-ring SRR structures with one, two and four splits. Figure 3.17 is the geometrical representation of single-ring SRR structures that we studied.

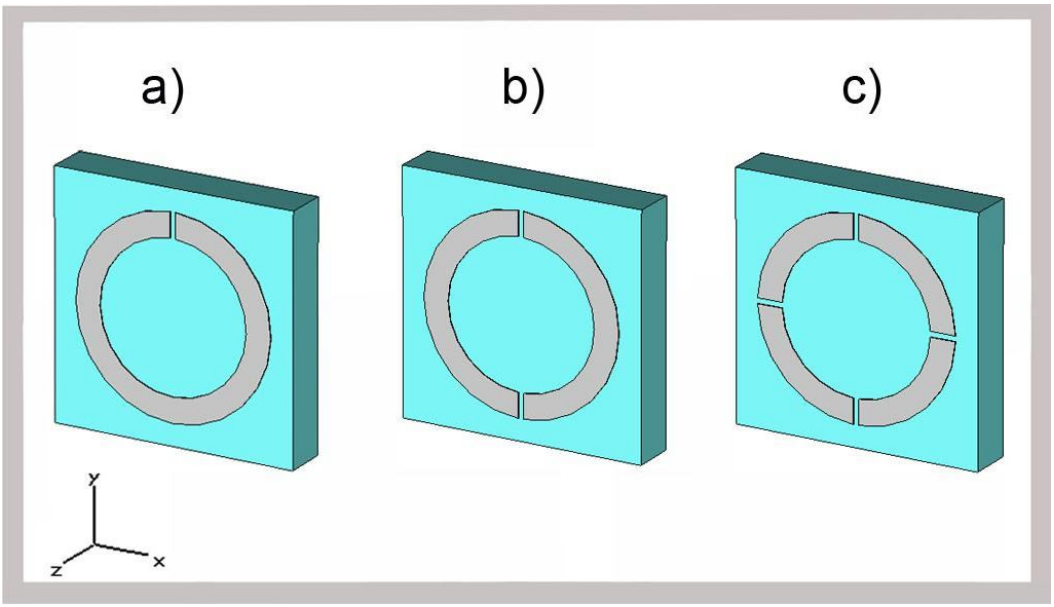

Figure 3.17: Schematics of a) Single-Ring SRR with one split. b) Single-Ring SRR with two splits. c) Single-Ring SRR with four splits.

The geometrical and electrical parameters of the single-ring SRR structure and simulation method are same as used in Section 3.4.1. The width of the

each split (d) is 0.2 mm, the width of all metallic rings (w) is 0.9 mm, the radius (r) of all rings is 3.6 mm, the thickness of the deposited copper layer (h) is 30 μm and the thickness of the FR-4 substrate is 1.6 mm (p). Also, the unit cell dimensions of a single SRR structure (lattice constants) are taken to be $a_x = a_y$ = 8.8 mm and a_z = 6.5 mm. Finally, the substrate of SRR is FR-4 substrate with dielectric permittivity constant ε = 4.0 and tangent loss δ= 0.01. The simulation results are demonstrated Figure 3.18:

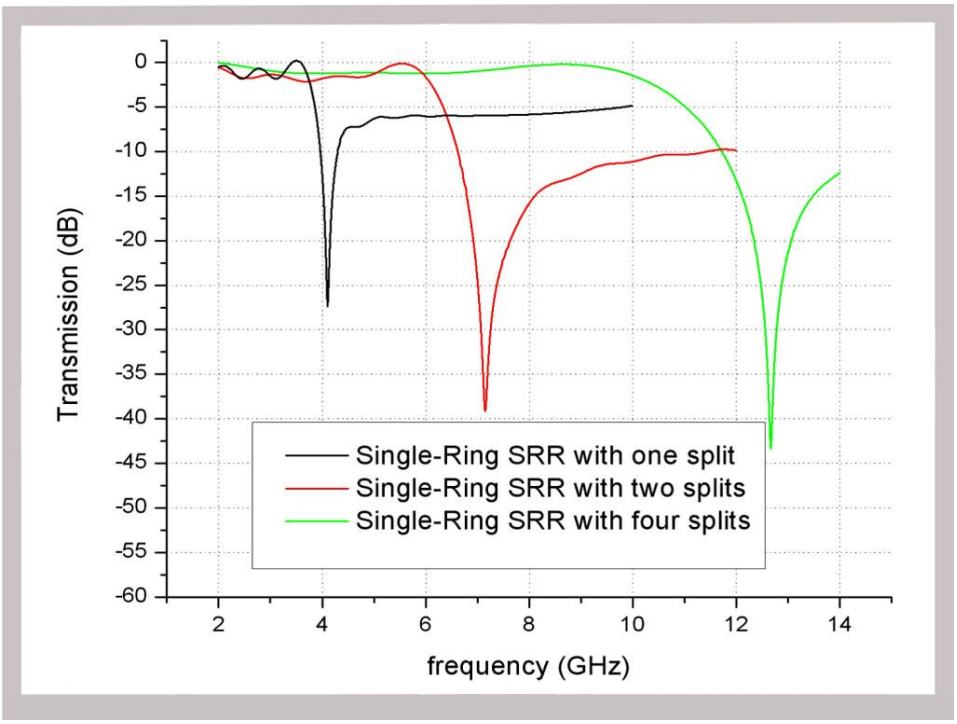

Figure 3.18: Calculated transmission spectrum of a) Single-Ring SRR with one split. b) Single-Ring SRR with two splits. c) Single-Ring SRR with four splits.

As can be seen in numerical results, the magnetic resonance frequency of single split, two split and four split structures are 4.1 GHz, 7.2 GHz and 12.8 GHz respectively.

3.4.3 Conventional SRRs with several Splits

In this section, conventional Split Ring Resonator structure with several splits is investigated. We investigated the magnetic resonance of conventional SRR structures with two, four and eight splits. Conventional SRR with two splits is the SRR structure that we investigated in Section 3.2 and 3.3.

Figure 3.19 is the geometrical representation of conventional SRRs with two, four and eight splits that we studied.

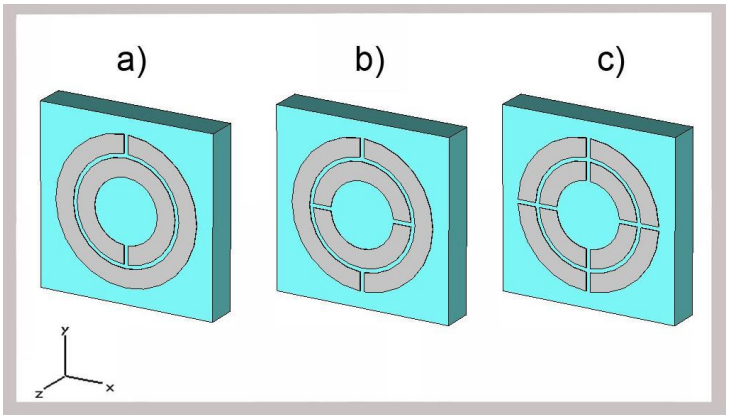

Figure 3.19: Schematics of a) Conventional SRR with two splits. b) Conventional SRR with four splits. c) Conventional SRR with eight splits.

The geometrical parameters of the models are same as stated in Section 3.2 and Section 3.3. The width of the splits (d) and the gap between the inner ring and the outer ring (t) is 0.2 mm, the width of metallic ring (w) is 0.9 mm, the outer radius (r) is 3.6 mm, the thickness of the deposited copper layer (h) is 30 μm and the thickness of the FR-4 substrate is 1.6 mm (p). Also, the unit cell dimensions of a single SRR structure (lattice

constants) are taken to be a_x = a_y = 8.8 mm and a_z = 6.5 mm. The substrate of SRR is FR-4 substrate with dielectric permittivity constant ε = 4.0 and tangent loss δ = 0.01.

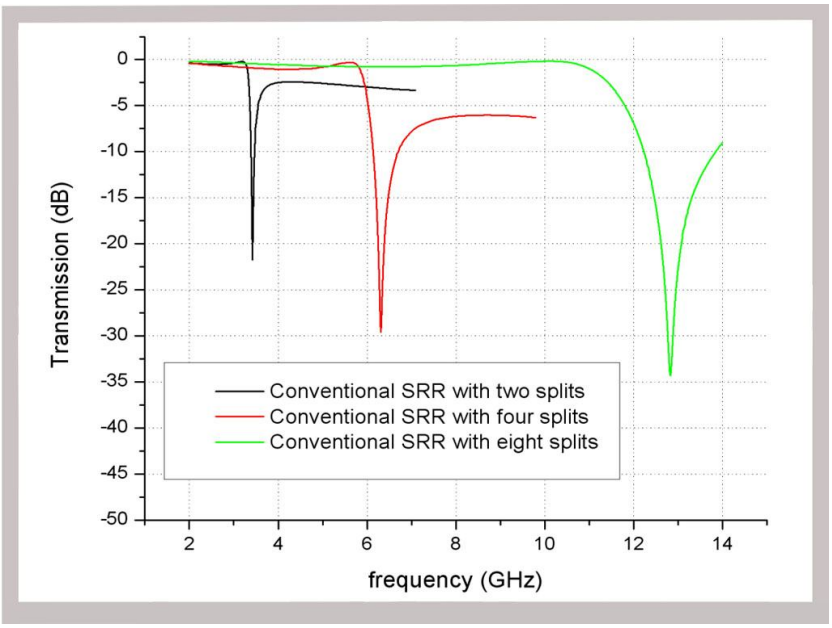

Figure 3.20: Calculated transmission spectrum of a) Conventional SRR with two splits. b) Conventional SRR with four splits. c) Conventional SRR with eight splits.

The results in Figure 3.20 point out that magnetic resonance frequency of the resonator increases with additional splits. The resonance frequencies of Split Ring Resonator structure with two, four and eight splits are found to be 3.4 GHz, 6.3 GHz and 12.8 GHz respectively.

Simulation results of Section 3.4.2 and 3.4.3 reveal that, the additional cuts increase the resonance frequency of the structure. As the additional cuts are added to the ring, total capacitance of the structure decreases; because

adding an additional cut to the ring means to connect a series additional capacitance to the total capacitance of the system which decreases the total capacitance. Therefore, the magnetic resonance increases with the decreasing total capacitance.

3.5 Effect of SRR orientations on electromagnetic resonance mechanism of SRR

In this section, the dependence of resonances of SRR on the orientation of the SRR structure is investigated. There are four possible orientations of SRR structures. These structures with excitation sources are depicted in Figure 3.21:

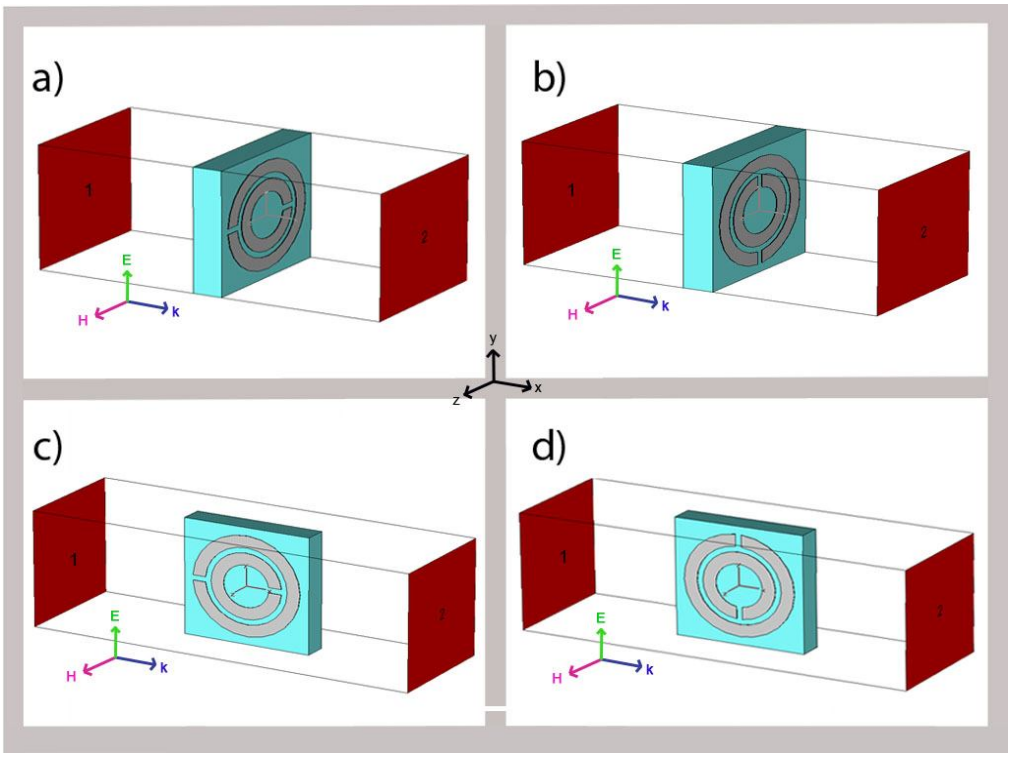

Figure 3.21: Schematics of a) SRR_A type configuration. b) SRR_B type configuration. c) SRR_C type configuration. d) SRR_D type configuration.

The resonance frequency of the SRR structures can be simply observed as the dips at the transmission spectrum. However, the type of resonance can not be observed by observing only the dips. The ways of identifying resonance type of SRR are defined in previous sections as observing the negative phase velocity and destroying the magnetic resonance by closing the splits. In this section, we will use the same SRR structures that we used in Section 3.3. Therefore, we know the electric and magnetic resonance frequencies of the SRR.

We classified the four configurations which are depicted in Figure 3.21: SRR_A and SRR_B are called "perpendicular oriented SRRs"; because the propagation direction is perpendicular to the plane of SRR. These structures can also be called as "e-coupled SRRs"; because only the electric field vector ($\overline{E}$) of the incident field is effective on the SRR structure. The magnetic field vector ($\overline{H}$) of incident field is parallel to metallic rings in which there is no magnetic excitation of SRR. On the other hand, SRR_C and SRR_D configurations are called "parallel oriented SRRs"; because the propagation direction of SRR structure is parallel to the plane of SRR. Moreover, SRR_C and SRR_D structures can also be called as "h-coupled SRRs"; the magnetic field vector (H) is perpendicular to SRR plane causing the magnetic excitation of SRR. In fact, there is also electric excitation of SRR for SRR_C and SRR_D; because, the metallic ring structure of SRR acts like discontinuous wires for incident wave and gets excited electrically for SRR_C and SRR_D [70].

The simulation of setup up of a single SRR structure is composed of two waveguide ports to obtain S-21 data and boundary conditions. Open boundary conditions are employed along the propagation direction (+x and -x). Electric (Et = 0) boundary conditions are used for –y and +y direction. Also magnetic (Ht = 0) boundary conditions are used for –z and +z direction (Figure 3.21). The simulated transmission spectrums of the four SRR orientations are plotted in Figure 3.22:

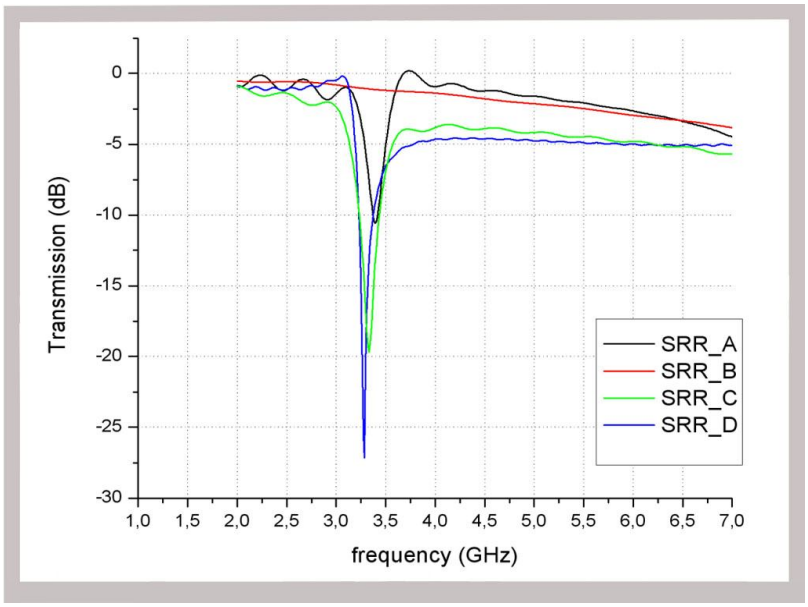

Figure 3.22: Calculated transmission spectrum of a) SRR_A type configuration. b) SRR_B type configuration. c) SRR_C type configuration. d) SRR_D type configuration.

For SRR_A type orientation, the incident electric field propagates along x-direction, with electric field vector ($\overline{E}$) and magnetic field vector ($\overline{H}$) along the y and z directions respectively. For this configuration, the magnetic field is parallel to the SRR plane (located at y-z plane). Therefore, magnetic resonance of SRR_A can not be excited. There exists

electrical resonance for SRR_A structure. The resonance frequency of SRR_A type structure is 3.4 GHz.

SRR_B type orientation of SRR is the 90^0 rotated version of SRR_A type orientation. The incident electric field propagates along x- direction, with electric field vector ($\overline{E}$) and magnetic field vector ($\overline{H}$) along the y and z directions respectively. Similar to SRR_A structure, the magnetic field is parallel to the SRR plane and therefore, there is no magnetic resonance. As can be seen in Figure 3.21, the SRR_B structure is a mirror symmetric structure. The mirror symmetry of SRR_B structure prevents the electrical coupling to the resonance of SRR [70]. Therefore, there is no resonance mechanism for SRR_B structure and there is no resonance dip as Figure 3.22 demonstrates.

SRR_C type orientation is located at x-y plane. The incident electric field propagates along x-direction, with electric field vector ($\overline{E}$) and magnetic field vector ($\overline{H}$) along the y and z directions respectively. Since the magnetic field is perpendicular to SRR_C plane, magnetic resonance exists. Also, there exists electric coupling to the resonance of the SRR due to the asymmetry of SRR_C structure [70]. The resonance frequency of SRR_C type structure is 3.3 GHz.

SRR_D type orientation is 90^0 rotated version of the SRR_C type orientation and SRR_D is located at x-y plane too. The incident electric field propagates along x-direction, with electric field vector ($\overline{E}$) and magnetic field vector ($\overline{H}$) along the y and z directions respectively. Since

the magnetic field is perpendicular to SRR_D plane, magnetic resonance exists. However, the SRR_D structure is mirror symmetric which prevents the electric coupling to the resonance of the SRR [70]. Therefore, the resonance of SRR_D is not supposed to be as strong as SRR_C type orientation and therefore the dip value of SRR_C structure is supposed to have a lower dip value; but as can be seen in Figure 3.22, SRR_D type structure has a lower dip: SRR_C type structure has a dip value of -19 dB and SRR_D type structure has a dip value of -27 dB at 3.3 GHz. Since the electrical and magnetic resonances of SRR_C structure does not work constructively, SRR_C has lower magnetic response than SRR_D type structure.

SRR_C type of structure is excited both electrically and magnetically which makes it stronger resonator than SRR_A, SRR_B and SRR_D in case electrical and magnetic resonances work constructively.

The resonance types of SRR depend on the orientation of SRR. Since different resonance mechanisms play role for different orientations of an SRR, the respond of the SRR is completely different. Therefore, these results should be considered carefully while utilizing SRRs.

CHAPTER 4

PROPAGATION THROUGH SUB-WAVELENGTH METAMATERIALS: FISHNET STRUCTURES

4.1 Introduction

In the previous chapter, we investigated the characteristics of SRR structures which received an increasing amount of interest and they are widely used for constructing metamaterials at the microwave [18, 25, 32, 41], millimeter wave [19], and terahertz [75-77] frequencies. There are also several different resonator structures for achieving negative permeability, such as S-shaped [101] omega-shaped [102] and pi-shaped structures [103]. Since the magnetic field vector ($\overline{H}$) must be perpendicular to structure plane for obtaining negative magnetic permeability ($\mu<0$), incident electromagnetic wave has to be parallel to the resonator structure plane. Therefore, fabrication difficulties such as producing large number of layers for fully covering the incident beam and limits of the current nanofabrication technology are the reasons behind the search for the alternative resonators to SRR while working at optical frequencies [97]. Moreover, the magnetic response of split ring resonators starts to saturate optical frequencies [45], which makes it very difficult to achieve optical

magnetism with SRRs. However, several studies revealed that there is an alternative structure of metal-dielectric composite providing magnetic resonance at optical frequencies [78, 79]. The proposed structure consists of parallel metal slabs with a dielectric substrate in between, wherein the metal slabs provide the inductance and the dielectric spacing in turn provides the capacitance [78]. After that, metamaterials using parallel metal slabs (also known as cut-wire pairs) at microwave frequencies are realized [80-82]. A more efficient approach called Fishnet-type metamaterials are reported to exhibit a negative-index (left-handed metamaterial behavior) at optical [83-86] and microwave frequencies [87-89]. The main advantage of Fishnet-type metamaterials is that the wires providing for negative permittivity and the slab pairs providing for negative permeability are brought together to produce a combined electromagnetic response. In other words, the opposite currents flowing between the slab pairs enable the negative permeability [87], and the wires enable the negative permittivity [22]. This combination is a simple planar structure that exhibit left-handed behavior.

In this section, we demonstrate a polarization independent negative-index metamaterial (fishnet structure) operating at microwave frequencies. We made several transmission measurements and simulations; and observed a left-handed transmission band with negative permittivity and negative permeability over a common frequency range. Moreover, negative refractive index is verified by using the retrieval procedure and also by observing the negative phase shift of structure

while adding additional structure layers in the propagation direction. Finally, we examine the effect of several geometrical parameters on the left-handed behavior of the fishnet structure. Most of the works in this section are based on a paper that we published in 2008 [104].

4.2 Electromagnetic wave propagation through a fishnet type metamaterial

The fishnet type structures were suggested to be possible candidates for planar negative index metamaterials (NIM) [83-89, 99]. In this section, we performed the transmission measurements and numerical simulations of a fishnet structure operating at microwave frequencies, attempting to understand the characteristics of the fishnet structure.

A fishnet unit cell is demonstrated in Figure 4.1.a. The structure is printed on a 1-mm-thick Teflon dielectric substrate with 20-μm-thick copper. The unit cell is repeated along the x and y directions with a periodicity of $a_x = a_y$ =14 mm. Measurements of the structure have been performed on a single fishnet layer with N_x=10 unit cells along the x-direction and N_y=10 unit cells along the y-direction (Figure 4.1.c).

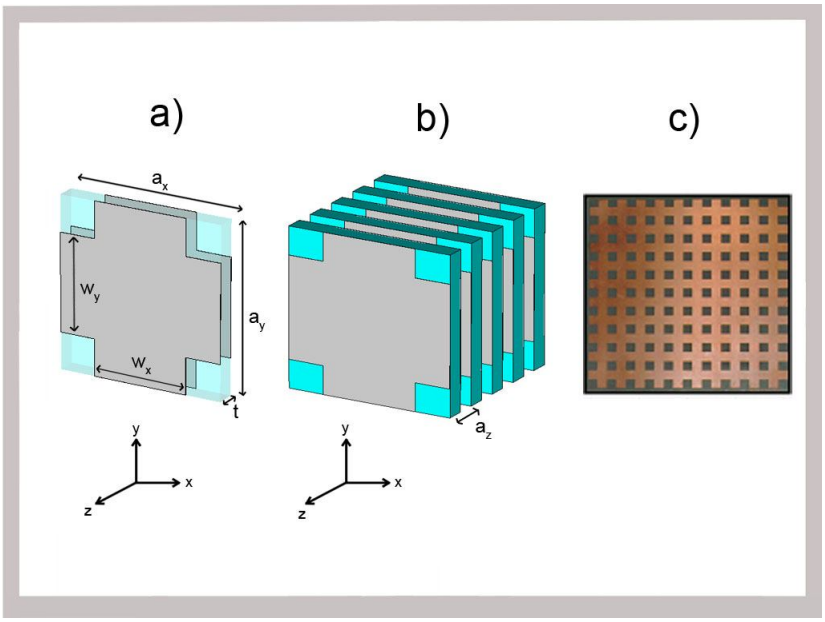

Figure 4.1: a) Schematics drawing of single fishnet unit cell. b) Schematics drawing of multi-layer fishnet structure. c) Fabricated Fishnet structure periodic along x and y directions.

The structure can be considered as a combination of parallel metal slab pairs with the sizes $w_y \times a_x$, which provide the magnetic resonance and continuous wire pairs with the sizes $w_x \times a_y$ in turn providing the negative permittivity [87]. Here, we chose $w_x = w_y$=7 mm, and therefore the structure is symmetric in all directions. The structure will then work for TE and TM polarizations, as well as for arbitrary linear polarizations due to the symmetry of the slab and wire pairs. Therefore, the fishnet structure will be functional independent of the incident polarization and can be regarded as isotropic-like fishnet [87].

After the measurement of single layer fishnet, a multi-layer fishnet structure (Figure 4.1.b) will be considered in the following parts of the

chapter. We stacked layers with a lattice constant, a_z = 2 mm along the z direction for multi-layer fishnet structure.

We performed the transmission and phase measurements in free space by using an Agilent N5230A portable network analyzer connected to high gain microwave horn antennae. The propagation direction of incident electromagnetic wave is along the z-direction, with the E-field vector is along the y-axis and the H-field vector is along the x-axis. In these measurements, the distance between the horn antennae were kept at 35 cm. We first measured the transmission through air, and then used this data for calibration. After calibrating the system, we performed measurements.

The measured transmission result of a single layer fishnet metamaterial structure is plotted in Figure 4.2. A transmission band is observed between 14.20 GHz and 14.80 GHz. The peak value of this band is -2.4 dB at 14.38 GHz. In the flowing sections we will show that, this well resolved transmission band corresponds to the negative-index regime which is a left-handed transmission band.

We performed numerical simulations in order to confirm the experimental results. Commercially available CST Microwave Studio software is employed for the simulations. The unit cell shown in Figure 4.1.a is simulated with periodic boundary conditions along the x and y axis. Open boundary conditions are applied along the propagation

direction (-z and +z directions). The structure is excited with a plane wave with a wave-vector along the +z direction. The E-field vector of the plane wave is along the y axis and the H-field is along the x axis in the simulations. Electric probe along y-direction is used to detect electromagnetic waves. The dielectric constant of the Teflon board was taken as $\varepsilon = 2.16$ with a tangent loss of $\delta = 0.005$. The calculated transmission result of the fishnet structure is plotted in Figure 4.2. Figure 4.2 reveals that the transmission peak of the simulation result is -2.9 dB at 14.33 GHz. Therefore, we can state that, there is agreement between the experimental and simulation results.

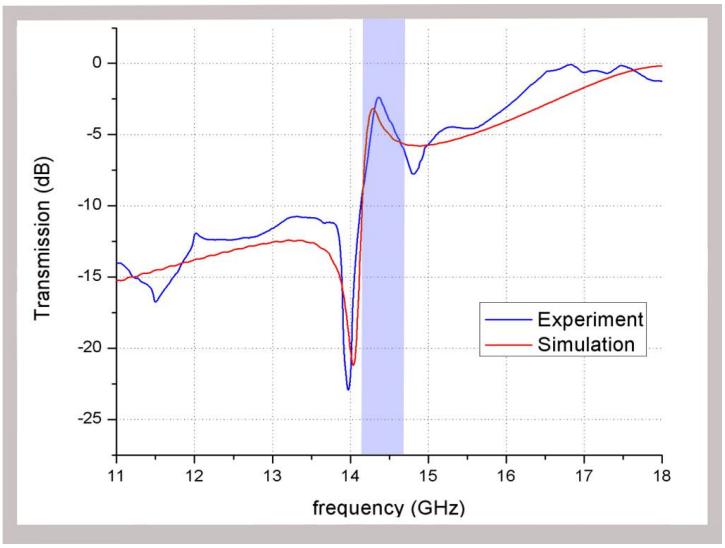

Figure 4.2: Measured and calculated transmission spectrum of a single layer fishnet structure.

Planar metamaterials, where the electromagnetic wave is normally incident to the plane of the metamaterials, were first used at optical frequencies [83-86]. The characterization of negative-index metamaterials were mainly performed by using a single layer. It is obvious that the basic

properties of metamaterial structures, such as a negative index of refraction, the negative phase velocity cannot be verified by simply using a single layer of the metamaterial [104]. Recently, there have been studies that characterize planar negative-index metamaterials with more than one layer along the propagation direction [87, 90, 91]. Here, we report the transmission measurements and simulations of a three-layer and five-layer fishnet structures for characterization of fishnet structure at microwave frequency regime. Figure 4.3.a demonstrates the measured and simulated transmission spectra of a three-layer fishnet structure. The periodicity along the propagation direction is a_z = 2 mm. There exists transmission band with a peak value of -4.5 dB at 14.39 GHz which is obtained from the measurements. The simulation results predict a transmission band similar to experimental results where the peak is at 14.38 GHz with a peak value of -3.1 dB.

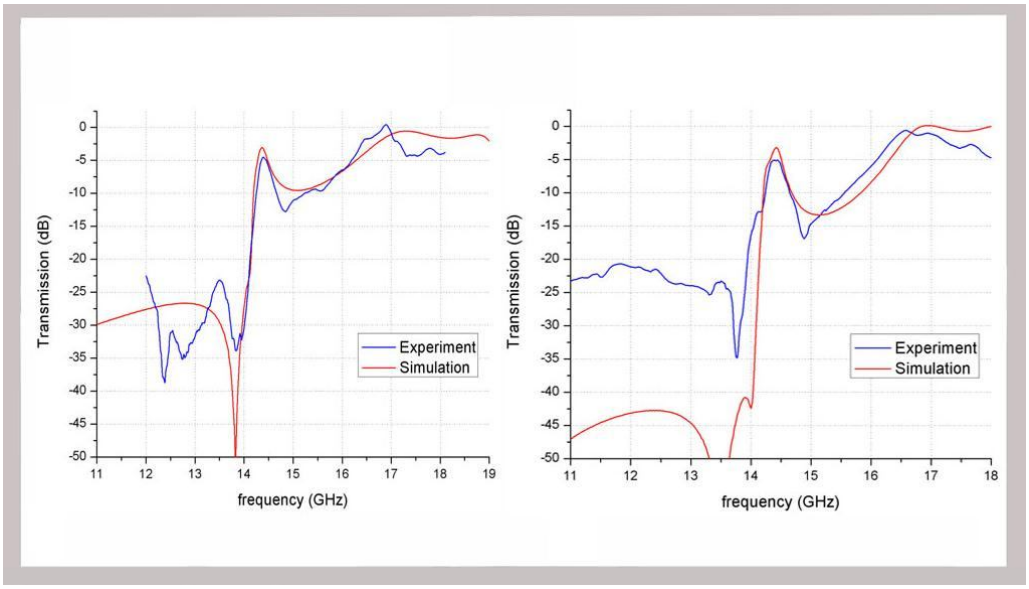

Figure 4.3: Measured and calculated transmission spectrum of a) three-layer fishnet structure and b) five-layer fishnet structure.

Experimental and simulation transmission results of the five-layer fishnet structure are shown in Figure 4.3.b. The measured transmission peak is at 14.42 GHz with a peak value of -5.0 dB while simulated peak value is -3.2 dB at 14.40 GHz. Minor differences between the simulation results and experimental results can be attributed to the deviation from the ideal material parameters and possible misalignments in the measurements that may occur during the stacking of the layers.

It is noteworthy that increasing the number of layers does not significantly change the transmission value at the left-handed transmission band. This is due to the specific choice of the substrate. Teflon is a very low loss substrate. The loss mechanism in the fishnet structure is mainly due to the substrate losses; because, the electric field concentration is almost inside the dielectric substrate (in the slab-pair-based structures) at the magnetic resonance frequency of the structure [87, 98]. In our case, the amount of metal is increased by a factor of five, from a one-layer structure to a five-layer structure. The transmission only decreased by -2.6 dB in the measurement which indicates the positive effect of using low loss substrate. The result is more significant in the simulation results (ideal case) that the transmission peak did not change from a one-layer to a five-layer fishnet structure.

4.3 Effective parameters of fishnet structure

One of the most common characterization tools for the metamaterial structures is the retrieval procedure [92-96]. The effective parameters (ε, μ) of the metamaterial are calculated by retrieval analysis. The amplitude and phase of the transmission and reflection data are used to retrieve the real and imaginary parts of the effective permittivity, permeability, and a refractive index. The retrieval approach outlined in Ref. [93] is used for the retrieval analysis in this work. The advantage of this procedure is the selection of the correct branch of the effective refractive index and effective impedance. The ambiguity in the determination of the correct branch was resolved by using an analytic continuation procedure [104].

The effective parameters of fishnet structure is retrieved by using the amplitudes and phases of transmission (S_{21}) and reflection (S_{11}) data. The S-parameters are related to refractive index and impedance by [93]:

$$S_{11} = \frac{\left(z - 1/z + 1\right)\left(1 - e^{-j2nk_0d}\right)}{1 - \left(z - 1/z + 1\right)^2 e^{j2nk_0d}} \tag{4.1}$$

$$S_{21} = \frac{\left(1 - \left(z - 1/z + 1\right)^2\right)e^{jnk_0d}}{1 - \left(z - 1/z + 1\right)^2 e^{j2nk_0d}} \tag{4.2}$$

where d is the thickness of homogenous slab of fishnet structure and k_0 is the free space propagation constant.

The refractive index (n) and impedance (z) are obtained by inverting the Eqs. (4.1) and (4.2) as [93];

$$z = \pm\sqrt{\frac{(1+S_{11})^2 - S_{21}^2}{(1-S_{11})^2 - S_{21}^2}} \tag{4.3}$$

$$e^{jnk_0 d} = X \pm j\sqrt{1-X^2} \tag{4.4}$$

where $X = \dfrac{1}{2S_{21}\left(1-S_{11}^2+S_{21}^2\right)}$.

The effective permittivity (ε_{eff}) and permeability (μ_{eff}) are obtained from the effective index and impedance by using the relations, $\varepsilon = \dfrac{n}{z}$ and $\mu = nz$.

In the retrieval procedure, a single layer of fishnet structure along the z axis is employed. The effective permittivity and permeability values were then retrieved from the transmission and reflection coefficients of a single layer of fishnet. The real and imaginary parts of the effective permittivity permeability and index of refraction for a single layer of fishnet structure (Figure 4.4) are consistent with the simulated and measured transmission spectra which we examined in Chapter 4.2.

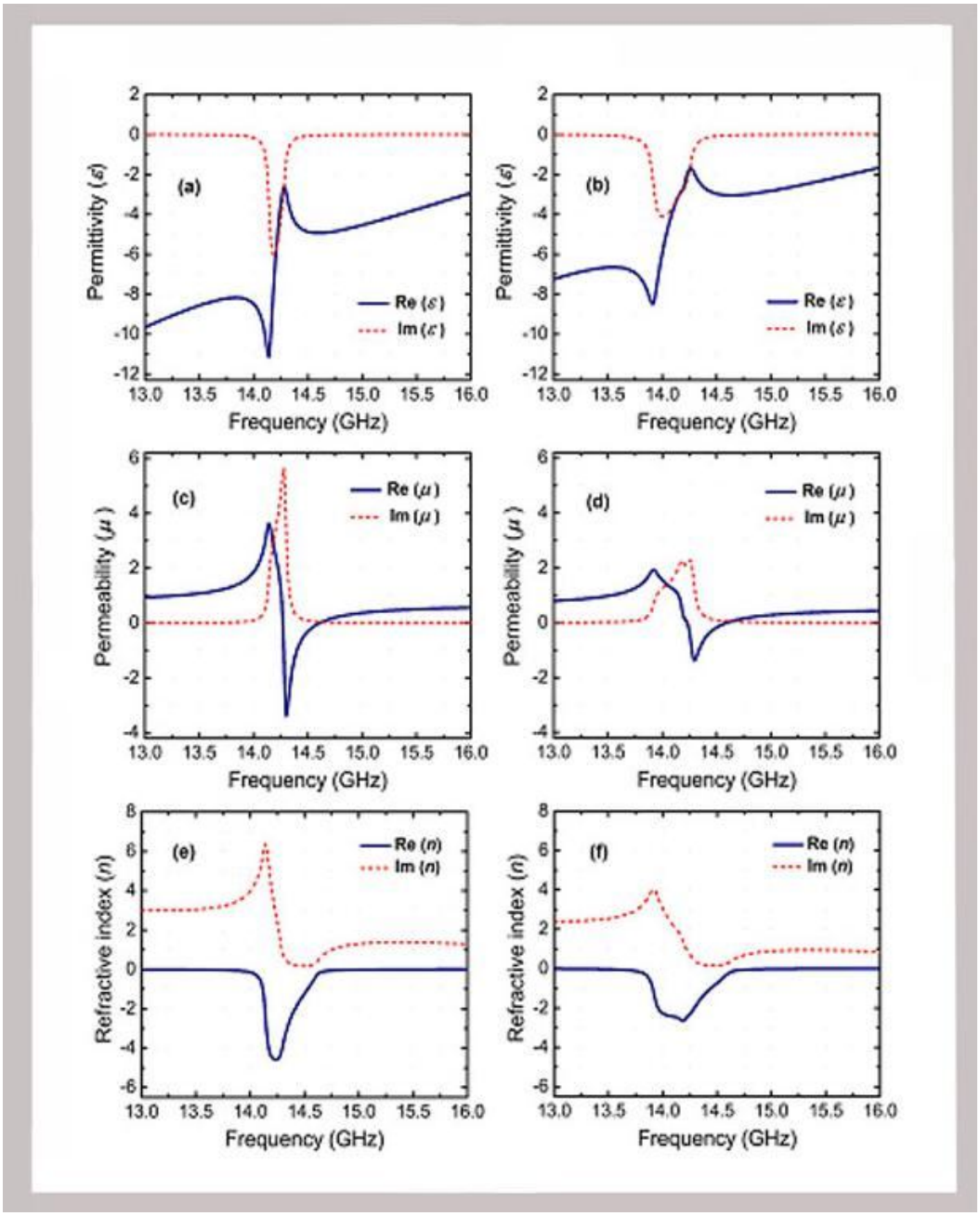

Figure 4.4: Retrieved effective parameters of one-layer and two-layer fishnet structures: a) real and imaginary parts of one-layer fishnet structure's dielectric permittivity (ε). b) real and imaginary parts of two-layer fishnet structure's dielectric permittivity (ε). c) real and imaginary parts of one-layer fishnet structure's magnetic permeability (μ). d) real and imaginary parts of two-layer fishnet structure's magnetic permeability (μ). e) real and imaginary parts of one-layer fishnet structure's refractive index (n). f) real and imaginary parts of two-layer fishnet structure's refractive index (n).

The continuous wire arrays that are the wires of fishnet along the y axis cause plasma oscillations. The plasma frequency (f_p) of the fishnet structure is around 16.50 GHz. Also, the resonance in the permittivity is at approximately 14.25 GHz which is a common characteristic of metamaterials with a negative index of refraction. As can be seen in Figure 4.4, the real part of the magnetic permeability has negative values between 14.23 and 14.65 GHz which is consistent with the results in Section 4.2. The lowest value of μ is -3.38 at 14.30 GHz for a single layer fishnet structure. Both permeability and permittivity are simultaneously negative between 14.23 and 14.65 GHz. Therefore, the fishnet structure behaves like a left handed metamaterial at this frequency range. Moreover, the refractive index of the fishnet structure is negative within the frequency range of 13.95-14.65 GHz.

Single unit cell along the propagation direction is employed to perform the retrieval analysis. However, recent studies have revealed that the geometrical size of the structure that is used to calculate the transmission and reflection coefficients of the structure affect the retrieval analysis [89, 94]. Therefore, we performed additional simulations for a two-layer fishnet structure to check this effect in our fishnet type metamaterial design. Figures 4.4.b, 4.4.d, and 4.4.f show the effective permittivity, permeability, and refractive index, respectively [104]. As can be seen in these figures, the real and imaginary parts of ε, μ, and n are different than the one-layer fishnet structures' effective parameters. The respond of a two-layer fishnet structure to the incident electromagnetic field is weaker

than the one-layer fishnet structure. Moreover, the permittivity values are higher for the two-layer fishnet NIM structure. The minimum value of permeability for a two-layer fishnet structure is -1.37 at 14.3 GHz. Throughout the frequency range of interest, we found that the absolute values of permittivity and permeability of a one-layer structure is greater than that of a two-layer NIM, i.e. $|\varepsilon_{1L}| > |\varepsilon_{2L}|$ and $|\mu_{1L}| > |\mu_{2L}|$. According to the Zhou et al's work [89], retrieved parameters converge to a value if the metamaterial length employed in the retrieval procedure is equal to the convergence length of the metamaterial. Since two unit cells are below the convergence length of a fishnet metamaterial, there is a considerable dissimilarity in the retrieved parameters of one and two layer fishnet structures. Therefore, we can state that the results reported here are consistent with Zhou *et al.*'s work, in which the authors performed a detailed analysis for the dependence of geometric size and lattice constant on the retrieved parameters of fishnet type metamaterials [89].

We also considered the effect of number of layers on refractive index. Figure 4.5.a represents real part of retrieved refractive index for one layer and two layers fishnet structures.

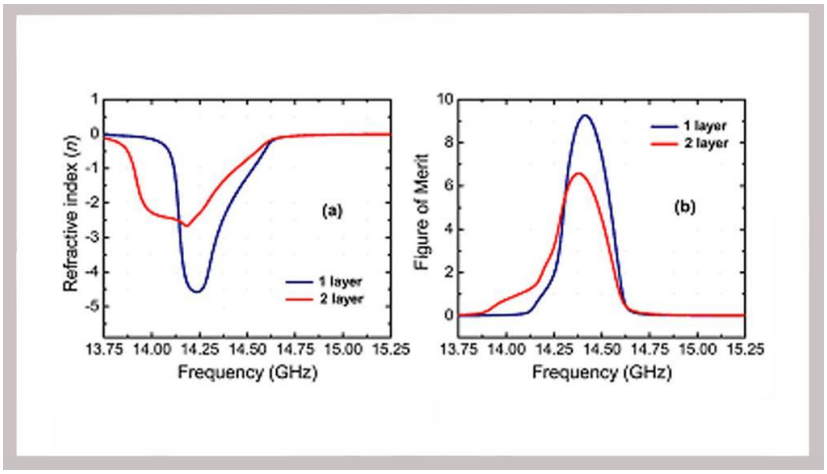

Figure 4.5: a) Retrieved refractive index of one-layer and two-layer fishnet structures. b) Figure of Merit (FOM) for one-layer and two-layer fishnet structures.

The dip values of the refractive index for one-layer fishnet structure is found to be n = -4.58 at 14.23 GHz and for two-layer fishnet structure is n = -2.66 at 14.19 GHz. As we stated before, the frequency region between 14.23-14.65 GHz is a left handed region, which means that the permeability and permittivity are both negative. By utilizing retrieval analysis, we found that the upper edge for the negative index regime is 14.65 GHz for a one and two-layer fishnet structure, where the permeability starts to take on positive values (Figure 4.5.a). However, the lower edge is not as we expected. The lower edge for the two layer fishnet structure is lower than expected. The refractive index is found negative between 13.72 and 14.23 GHz for a two-layer fishnet structure by retrieval analysis. However, the permeability is positive within this frequency range (Figure 4.4.d). Therefore, the NIM structure behaves like a single negative material [87].

Moreover, we considered the figure of merit (FOM) value for one layer and two layer fishnet structures (Figure 4.5.b). FOM for the retrieval analysis of negative-index metamaterials was defined as the ratio of the absolute value of the real part of refractive index to the imaginary part of the refractive index, FOM = $\frac{|\mathrm{Re}(n)|}{\mathrm{Im}(n)}$. As can be seen in Figure 4.5.b, the figure of merit is larger for a single layer fishnet structure. The maximum figure of merit value is 9.26 at 14.41 GHz for one-layer fishnet structure while the maximum figure of merit value of two-layer structure is 6.58 at 14.38 GHz. Therefore, Figure 4.5.b reveals that FOM decreases with the increasing number of layers due to increased losses ($loss \uparrow \Rightarrow \mathrm{Im}(n) \uparrow$).

The retrieval analysis of one-layer and two-layer fishnet structures revealed that a periodic structure cannot be characterized only by a single layer of a metamaterial unit. Additional parameters such as the lattice constant and geometric size need to be taken into account in order to make fair comparisons.

4.4 Negative phase advance and backward wave propagation

The materials with negative index of refraction (n<0) is predicted to exhibit antiparellel electromagnetic wave propagation and energy flow [24]. Therefore, negative index metamaterials inherently have a negative phase advance. In this section, we demonstrated the negative phase

advance and backward wave propagation through fishnet structure at the left-handed transmission band.

We employed a network analyzer which is capable of measuring the transmitted phase for experimental measurements. We stacked fishnet structures with a_z = 2 mm that have N_z = 2, 3, 4 and 5 layers along the propagation direction. The phase of fishnet structures were measured by using the same setup as the transmission measurements. In the measurements, the transmitted phase is calibrated with respect to the phase in free space as transmission measurements.

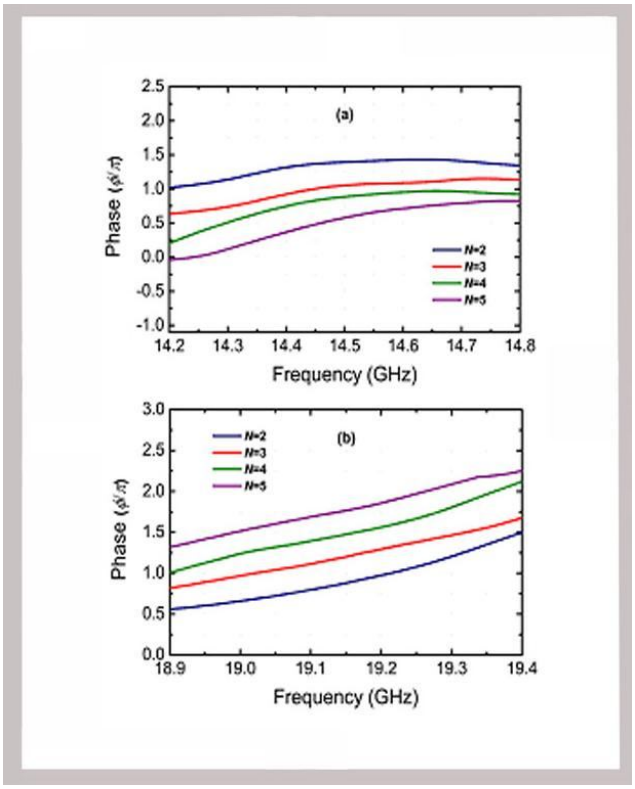

Figure 4.6: Calculated transmitted phase of fishnet structure for two, three, four, and five fishnet layers (a) at left-handed transmission regime (between 14.2 and 14.8 GHz) (b) at right-handed transmission regime (between 18.9 and 19.4 GHz).

Figure 4.6.a demonstrates the transmission phase between 14.20 and 14.80 GHz for two, three, four, and five layers of the fishnet structure. As can be seen in Figure 4.6.a, the phase decreases with the increasing number of layers along the propagation direction at the left-handed transmission band. Therefore, negative refractive index is verified by negative phase advance of structure while adding additional structure layers in the propagation direction. This is typical behavior for left-handed metamaterials with a negative phase velocity [32, 82].

We also checked the phase change of fishnet structure at a frequency band where we know that the transmission band has right handed characteristics. The phase spectra for two, three, four, and five layers of the fishnet structure are shown in Figure 4.6.b at the right-handed transmission region. As we expected, increase in the phase with the increasing number of layers along the propagation direction is observed. The negative phase advance for a NIM structure at the negative-index frequency regime means that the phase is directed towards the source. Such behavior is due to antiparellel directions of electromagnetic wave propagation and energy flow within the interested range of frequencies. Therefore, we explicitly verified the negative phase advance of planar fishnet type multi-layer metamaterials. To our knowledge, this work that we published in 2008 [104], is the first direct observation of negative phase advance for fishnet type metamaterial structures.

We simulated the electric field distribution and studied the wave propagation inside the fishnet metamaterial. Backward wave propagation

is verified at the negative refractive index band. Metamaterials with a negative phase advance are also called backward wave materials, since the wave propagation is towards the source inside the metamaterial. We performed numerical simulations in order to investigate the wave propagation inside fishnet structure. Figure 4.7.a demonstrates the fishnet structure that we simulated. We used the same geometrical parameters which we used throughout this chapter. The structure is excited with a plane wave with a wave-vector along the +z direction using CST Microwave Studio. The E-field vector is along the y-axis and the H-field vector is along the x-axis in the simulations. The structure has three unit cells along x direction and 5 unit cells along z direction.

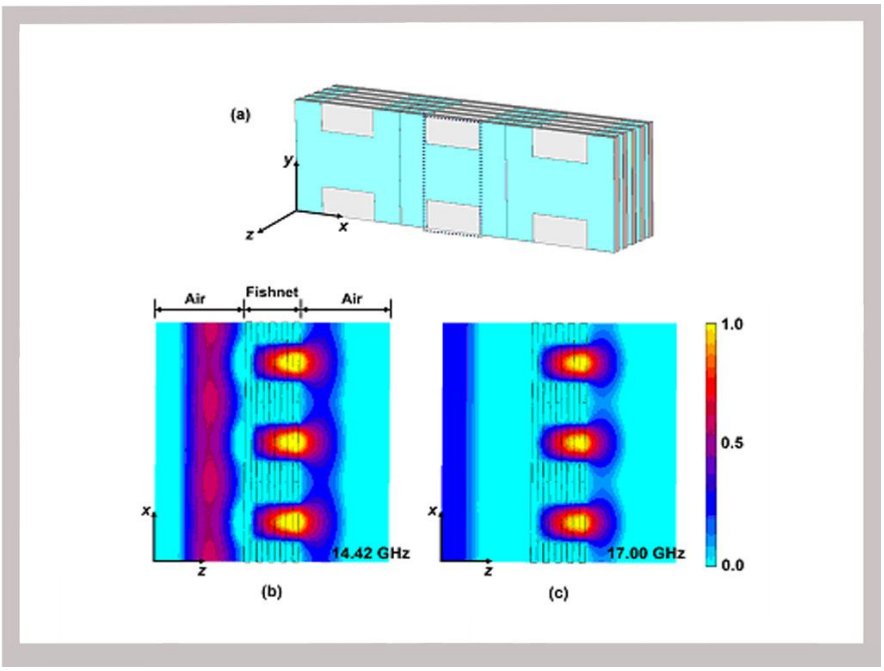

Figure 4.7: (a) Schematic drawing of a simulated fishnet structure. (b) Simulated E-field distribution at 14.42 GHz where the wave propagates along the –z direction inside the fishnet structure (see video at [105]). (c) Simulated E-field distribution at 17.00 GHz where the wave propagates along the +z direction inside the fishnet structure (see video at [106]).

The electric field distribution is calculated by placing electric field monitors along the y axis at two different frequencies, 14.42 GHz and 17.00 GHz. 14.42 GHz is the frequency of the highest transmission within the negative-index regime for a five-layer fishnet structure. Also, 17.00 GHz is chosen for right handed transmission. Figure 4.7.b shows the E-field intensity along the y direction, where the profile was calculated at the point y = 5 mm. The wave propagates along the +z direction in air. However, inside the fishnet structure, we observed backward wave propagation in the simulations. The video of this backward wave propagation simulation can be seen in the electronic copy of our paper [104, 105]. The EM wave is guided through channels as shown with a dashed rectangular box in Figure 4.7.a. There is no transmission through the wire pairs as expected. The wave propagation inside the metamaterial at 17.00 GHz is along the +z direction [104, 106], since this frequency corresponds to the right-handed transmission regime where ε and μ are both positive. Therefore, numerical simulations verified the backward wave propagation within the fishnet metamaterial at left-handed transmission band.

4.5 Parametric study of the Fishnet Structures

In this section, we performed a parametric study of fishnet structures which is important for optimization issues. We need to characterize fishnet structures to fully understand the physical mechanisms of them. Kafesaki *et al.* suggested LC description of the fishnet structure for a

qualitative analysis [87]. The L and C parameters of fishnet are suggested to be $\frac{1}{C} \sim \frac{t}{w_s l_s}$ and $\frac{1}{L} \sim \frac{w_n}{l_n t} + \frac{w_s}{l_s t}$ leading to a magnetic resonance of the form $f_m \sim \sqrt{\frac{1}{t^2} + \frac{w_n}{l_s l_n w_s}}$ where w_s is the slab width, w_n is the neck width, l_s is the slab length, l_n is the neck length and t is the thickness of the slab. This resonance frequency is able to account for the influence of all the geometrical parameters on the magnetic resonance frequency [87].

Since w_x and w_y parameters (see Figure 4.1) are enough to characterize the behavior of fishnet structure, we varied w_x and w_y values our parametric study. Firstly, we investigated the effect of the effect of w_x (neck width, w_n) on the left-handed transmission band of fishnet structure while keeping the other parameters w_y, a_x (w_s) and a_y ($2l_n + l_s$) constant ($a_x = a_y$ = 14 mm, w_y = 7 mm). Neck width (w_x) is varied ranging from 6 to 8 mm with 1 mm steps while keeping w_y (slab length, l_s) constant. Figure 4.8 is the transmission results for different neck widths (w_n = 6, 7, 8 mm).

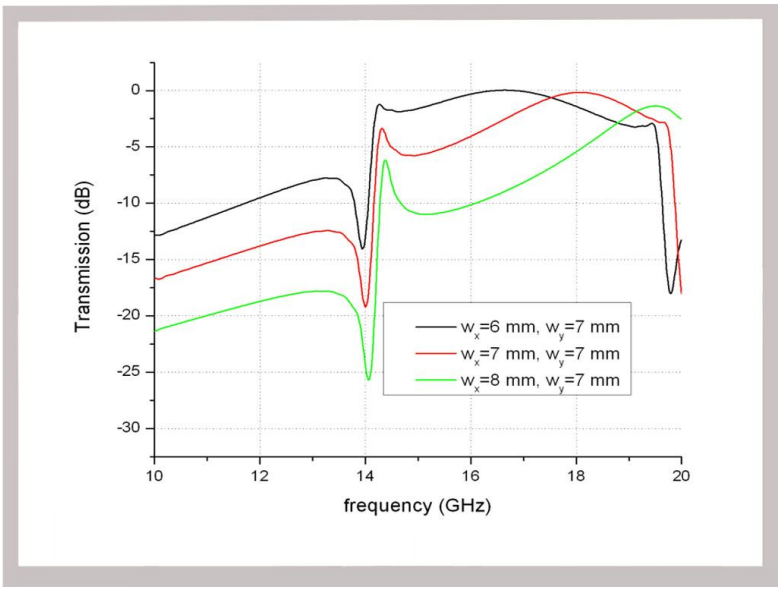

Figure 4.8: Calculated transmission spectrum of fishnet structure with varying w_x while w_y is constant.

As can be seen from Figure 4.8, the left-handed transmission frequency band increases with the increasing neck width. Moreover, the distance between left-handed transmission peak and the neighboring right-handed transmission peak increases with increasing neck width. The inductance of the system decreases with increasing neck width and the decrease in the neck inductance increase the left-handed frequency band. Moreover, the plasma frequency of the system increases with increasing neck width which causes the increase in the distance between the left-handed and right-handed transmission peaks; because, the necks in the fishnet serves as continuous wires and determine the plasma frequency of the system [87].

After observing the effect of neck width, we investigated the effect of the effect of l_s (slab length, w_y) on the left-handed transmission band of fishnet structure. Slab length (l_s) is varied ranging from 6 to 8 mm with 1 mm steps while keeping w_x (neck width, w_n) constant. Figure 4.9 is the transmission results for different slab lengths (l_s = 6, 7, 8 mm).

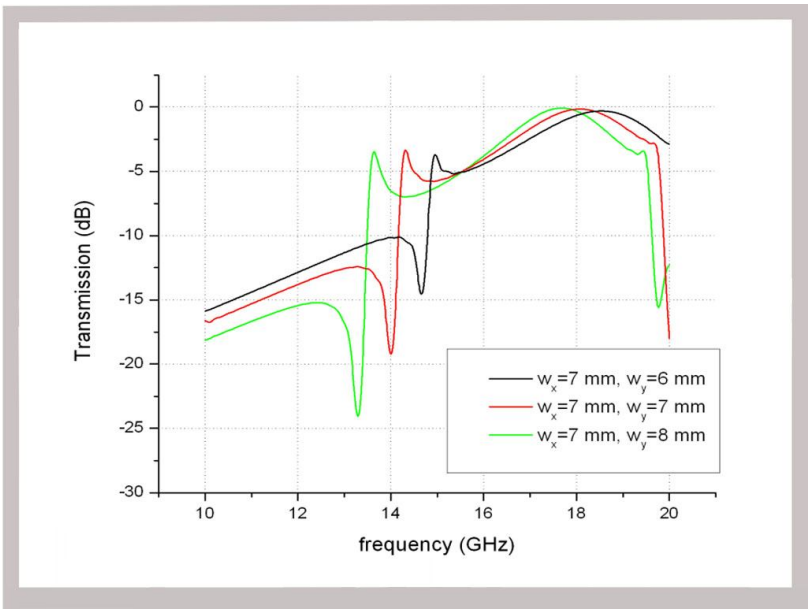

Figure 4.9: Calculated transmission spectrum of fishnet structure with varying w_y while w_x is constant.

Simulation results indicate that the left-handed transmission frequency decreases with the increasing slab length. The effective lengthening of the current flow in the slab increases both the capacitance and the inductance of the system [87]. Since both of the capacitance and inductance of the system increases with increasing slab length, the left-handed transmission band decreases.

In this chapter, we investigated fishnet-type metamaterial structure operating at microwave frequencies. Transmission measurements and simulations confirmed a left-handed transmission band with negative permittivity and negative permeability over a common frequency range. In addition, negative-index is verified by using the retrieval procedure and also by observing the phase shift of structure while adding additional structure layers in the propagation direction. Finally, we examined the effect of several geometrical parameters on the left-handed behavior of the fishnet structure which is important for optimization issues.

CHAPTER 5

ENHANCED TRANSMISSION THROUGH A SUB-WAVELENGTH APERTURE

5.1 Introduction

The simplest structure of scientific study is probably a simple hole in a screen. However, the study and debates on the characterization of a hole in a screen have been ongoing for centuries. In the middle of the 17th century, Grimaldi described diffraction form circular aperture, which contributed the foundation of classical optics [107, 108]. As classical optics suggests, the description of Grimaldi was valid only for a circular apertures having diameters much larger than the excitation wavelength.

Since interest in the microwave regime (longer wavelengths compared to the optical the wavelengths) increased in the 1940s as a result of World War II, the interest in the electromagnetic characterization of small (sub-wavelength) holes also increased. In 1944, Bethe gave a theoretical analysis of electromagnetic wave transmission through a sub-wavelength circular hole (aperture) in a perfectly conducting metal screen of zero thickness and suggested that the amplitude of the transmitted wave is proportional to the square of the area of sub-wavelength aperture with

$k \cdot (r/\lambda)^4$ where the radius (r) of the aperture is much smaller than the wavelength (λ) of incident electromagnetic wave ($r \ll \lambda$) [109]. In other words, the transmitted wave is proportional to the square of the aperture area and is inversely proportional to the fourth power of the excitation signal's wavelength.

According to Bethe's ideal theoretical structure, the transmission spectra for an aperture of radius $r \ll \lambda$ has a rapidly decreasing transmission with the increased wavelength of incident field by the power of four. We have simulated and confirmed the Bethe's expectation by simulating the transmission spectra of a circular hole in a Perfect Electric Conductor (PEC) as shown in Figure 5.1 where the CST Microwave Studio is used for simulations and k is an arbitrary constant to overlap the simulation results and $k \cdot (r/\lambda)^4$ curve for comparison.

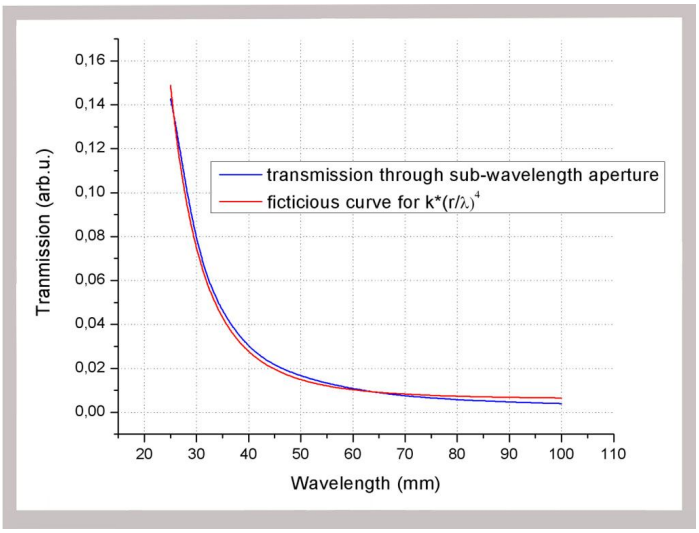

Figure 5.1: Theoretical suggestion of Bethe (λ^{-4} decrease) and the simulation results of transmission through a sub-wavelength aperture where $r < \lambda/10$.

As can be seen from the simulation results in Figure 5.1, the theoretical expectation of Bethe and our simulation results agree well. However, there is a slight difference between the simulation curve and $k \cdot (r/\lambda)^4$ curve; because an aperture in real life has a lateral dimension, which makes an aperture a waveguide-like structure. This waveguide structure modifies the dispersion relation of the incident field and the monotonic increase of transmission becomes distorted between a frequency band: There exists a specific frequency (wavelength) at which an incident wave in a given mode cannot be maintained (cut-off frequency/wavelength) as shown in Figure 5.2 [108].

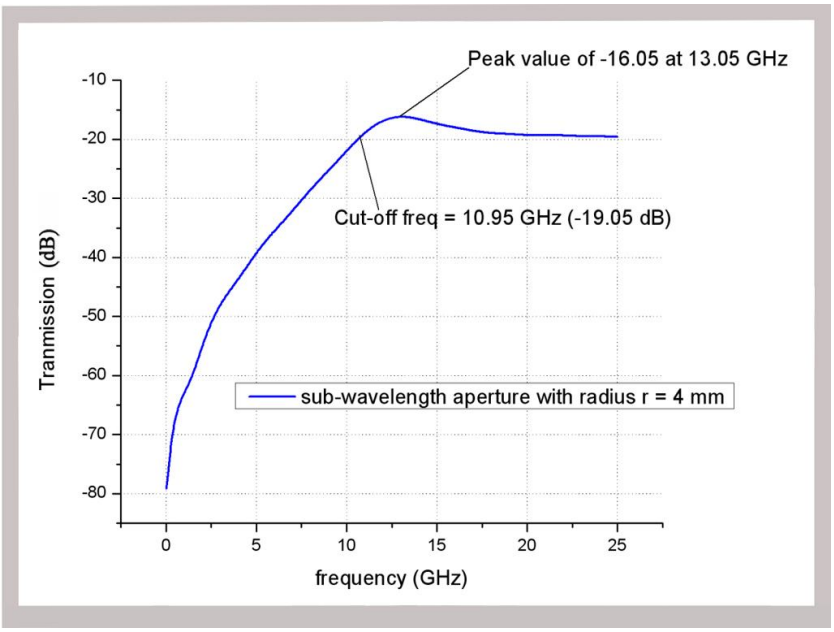

Figure 5.2: Transmission through a sub-wavelength aperture.

Annular apertures that resemble coaxial waveguides are supposed to have a TEM_0 mode without a cut-off [110, 135]. However, there exists a cut-off frequency and also an extraordinary transmission peak: Several

studies have shown that single sub-wavelength apertures have peaks (Figure 5.2) in their transmission spectrum as a result of the constructive excitation of propagating, surface and evanescent modes [108, 127]. In addition, the cut-off frequency cannot be sharply defined while considering real metals (with finite conductivity); because the transmission regime goes continuously from the propagative to evanescent regime as the wavelength increases [108].

When the finite conductivity of the metal is taken into account, the cut-off wavelength of the aperture is larger compared to an aperture in a perfectly conducting plane [115]. Also, transmission through a sub-wavelength aperture further decreases due to the non-zero depth of the aperture [116]. All of these studies reveal that Bethe's theory holds for idealized situations, in which the enhancement of electromagnetic wave propagation beyond the limit of Bethe's suggestion could be obtained by utilizing novel methods to improve the coupling of incident wave and aperture [111-114].

Advances in the characterization and fabrication techniques enable researchers to reduce severe effects of extremely high transmission losses and diffraction of electromagnetic waves through sub-wavelength aperture transmission. In 1998, "extraordinary optical transmission (EOT) through a sub-wavelength hole array in a metal screen" phenomena was reported by the seminal work of Ebbesen *et al.* [118]. It has been shown that the coupling of light with the Surface Plasmons (SP) of a two

dimensional array of sub-wavelength holes in turn causes a strong enhancement of transmitted light, which is above the limit of Bethe's prediction. This new era has attracted the interest of researchers on the enhancement of "light/electromagnetic wave" transmission through sub-wavelength apertures. Various studies on the characterization of EOT phenomenon approved the involvement of Surface Plasmons; and also showed that the interplay between light and the resonant excitation of SPs, which are induced by a periodic array of holes, causes the EOT [119-122].

The EOT phenomenon and new fabrication techniques opened up significant opportunities to new research areas and applications such as new probes for the scanning near-field optical microscope (SNOM) [123, 124], near-field optical recording [125, 126], nano-scale lithography [127-129] tracking single molecule (fluorescence spectroscopy) [124, 130], ultrafast miniature photodetector [131].

Surface Plasmons are propagating resonant modes confined to metallic surfaces that is caused by the coupling between the free surface charges of metal and the incident electromagnetic field at the interface separating a dielectric media and a metal. Since metals have very high conductivities at microwave frequencies (i.e. they behave similar to PECs in the microwave spectrum); surface plasmons are not supposed to exist at the microwave frequency regime. Therefore, there has been a debate on the existence of EOT phenomena at microwave frequencies [132, 133]. As a

matter of fact, SPs are not considered to exist in the microwave region; but the "Spoof Surface Plasmons", that are very similar to SPs, are formed between a dielectric substrate and a metal layer at microwave frequencies [132]. SPs and Spoof SPs serve similarly to guide the electromagnetic wave to the aperture in order to obtain an enhanced transmission. In our work, we obtained enhanced transmission at microwave frequencies in which the metals behave like perfect conductors. Therefore, localized surface plasmons do not contribute to the enhancement process. In addition, since grating structures are not used in our approach, there is no significant contribution of surface waves to the enhanced transmission. As we will show in the following sections, the strong localized fields around SRR-based novel structures couple to the incident electromagnetic field through a resonant process, causing a strong extraordinary transmission.

5.2 Enhanced Transmission through SRR-coupled apertures

In this section, we will discuss the enhanced transmission of an electromagnetic wave through a single sub-wavelength aperture by effective coupling of the incident wave to sub-wavelength aperture. The effective coupling is achieved by placing a Split Ring Resonator (SRR) structure in the near field of an aperture in parallel and perpendicular configurations. Figure 5.3 shows the proposed SRR structures in front of the aperture.

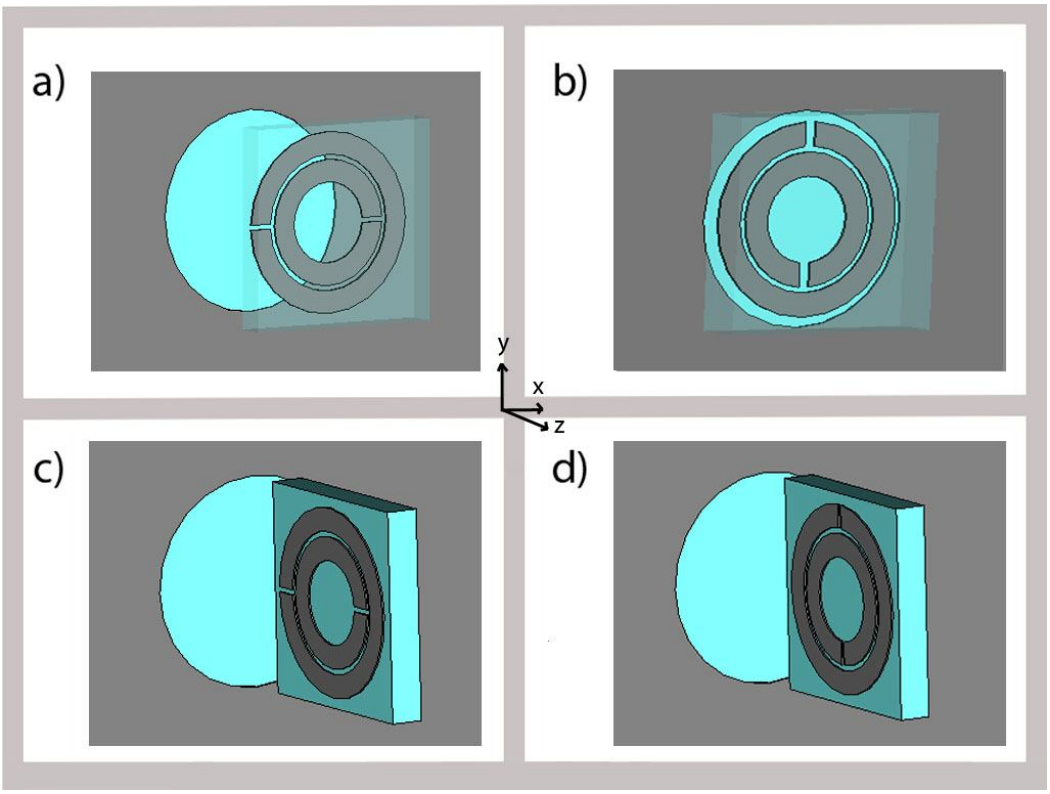

Figure 5.3: Schematic drawings of a) SRR_A type configuration, b) SRR_B type configuration, c) SRR_C type configuration, d) SRR_D type configuration.

The SRR structure that we used is a type of electromagnetic resonator that gives rise to strong resonance and a high intensity of electromagnetic waves in between splits of the SRR [55]. A detailed analysis of SRRs is provided in Chapter 3. In this work, we use a well-known SRR structure that has been used in a variety of research studies [41, 55, 63].

Split-ring resonator structures are composed of two concentric copper rings with splits oriented at opposite sides. Figure 5.4 shows a schematic representation of the SRR that we used. The gap between the inner and outer rings (t); and the width of the splits (d) are 0.2 mm, the metal width (w) is 0.9 mm, and the outer radius of the SRR structure is 3.6 mm. SRR is

deposited on a commercial FR4 dielectric board with a thickness of 1.6 mm [61].

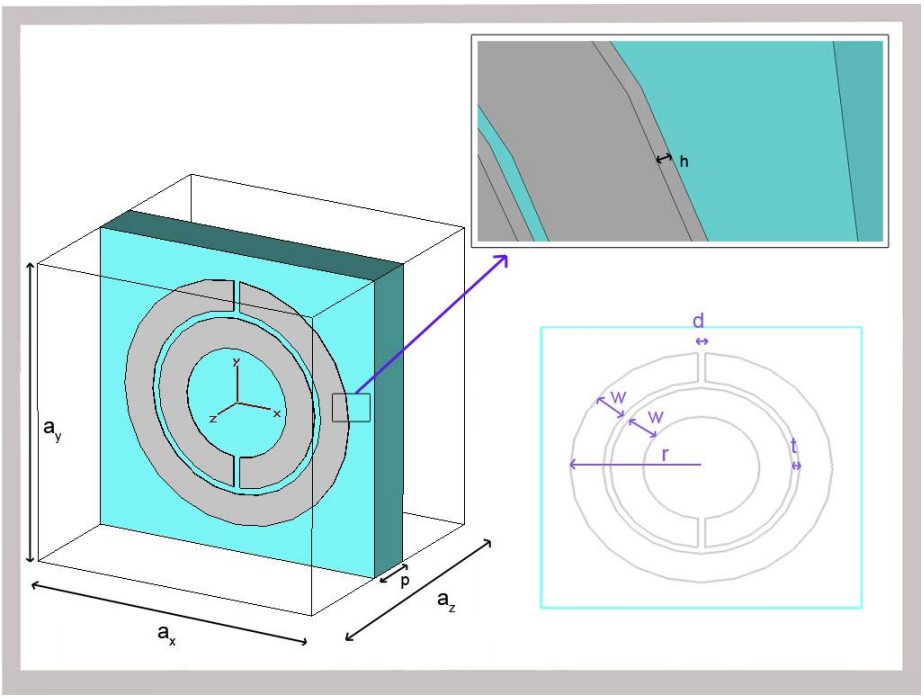

Figure 5.4: Schematic drawing of a Split Ring Resonator structure.

We also employed a square plate with a size of L x L (L = 200 mm), which is composed of a copper metal with a thickness of 30 μm and 1.6 mm thick commercial FR-4 PCB substrate. The deposited metal on the FR-4 substrate has an aperture that has a radius of 4 mm at the center of the substrate (Figure 5.3). The radius of the aperture is 4 mm, which is comparable with the largest size of the SRR (outer diameter = 3.6 mm).

In Chapter 3, the SRR structures are analyzed in detail. We also showed that the electromagnetic behavior of SRRs is bianisotropic. Furthermore, the dissimilar response of an SRR to electromagnetic waves for four

different configurations of SRR (Figure 3.21) was demonstrated and the results are plotted in Figure 3.22. For the sake of clarity, we will briefly explain these structures in this section too. We grouped four SRR orientations two by two according to the propagation direction of incident plane. The first group is called "perpendicular oriented SRRs" (SRR_A and SRR_B), in which the propagation direction is perpendicular to the plane of SRR; and the second group is called "parallel oriented SRRs" (SRR_C and SRR_D), in which the propagation direction is parallel to the plane of SRR. As we know from previous studies [63, 70], there are two types of resonance mechanisms (electrical and magnetic resonance) for SRRs and the magnetic resonance can only be excited for the parallel-oriented-SRR structures where the magnetic component of the incident field ($\overline{H}$) is perpendicular to the SRR plane. Thus, there is magnetic resonance for SRR_C and SRR_D structures. On the other hand, there exists electrical resonance for SRR_A and SRR_C structures due to the asymmetry of these SRR structures with respect to the incident electromagnetic field's electric component ($\overline{E}$) [70]. To sum up, SRR_A only excites an electrical resonance at 3.4 GHz with a dip value of -11 dB (Figure 3.22). SRR_B excites no resonance type; therefore, there is no transmission for SRR_B (see Figure 3.22). SRR_C excites both electrical resonance and magnetic resonance with a dip value of -19 dB at 3.3 GHz (Figure 3.22). SRR_D only excites magnetic resonance with a dip value of -27 dB at 3.25 GHz (see Figure 3.22). Since different resonance mechanisms play a role for different orientations of an SRR, the response of the SRR strongly depends on its orientation. Therefore, we used these

results outlined above to obtain the best enhancement from our proposed structure.

In this work, we proposed; and both experimentally and numerically verified an approach that utilizes the resonance of split ring resonator structures, which are placed in the close vicinity of a sub-wavelength aperture. The work presented in this section was appeared as a journal article in Physical Review Letters [100].

Firstly, we performed numerical simulations to observe the theoretical results of our novel approach. The numerical simulations, which are performed by the commercially available software (CST Microwave Studio), confirmed enhanced transmission through a sub-wavelength aperture via placing an SRR in the front of the aperture.

In the simulations, we modeled the complete scene of the electromagnetic measurement setup in order to decrease the deviations from the experimental results (see Figure 5.5). Namely, two waveguide antennas including the waveguide feed structures are modeled together with the device under test (DUT). The metallic plate with a sub-wavelength aperture is placed 0.1 mm away from the transmitter antenna and the receiver antenna is located at 5 cm away from the transmitter antenna.

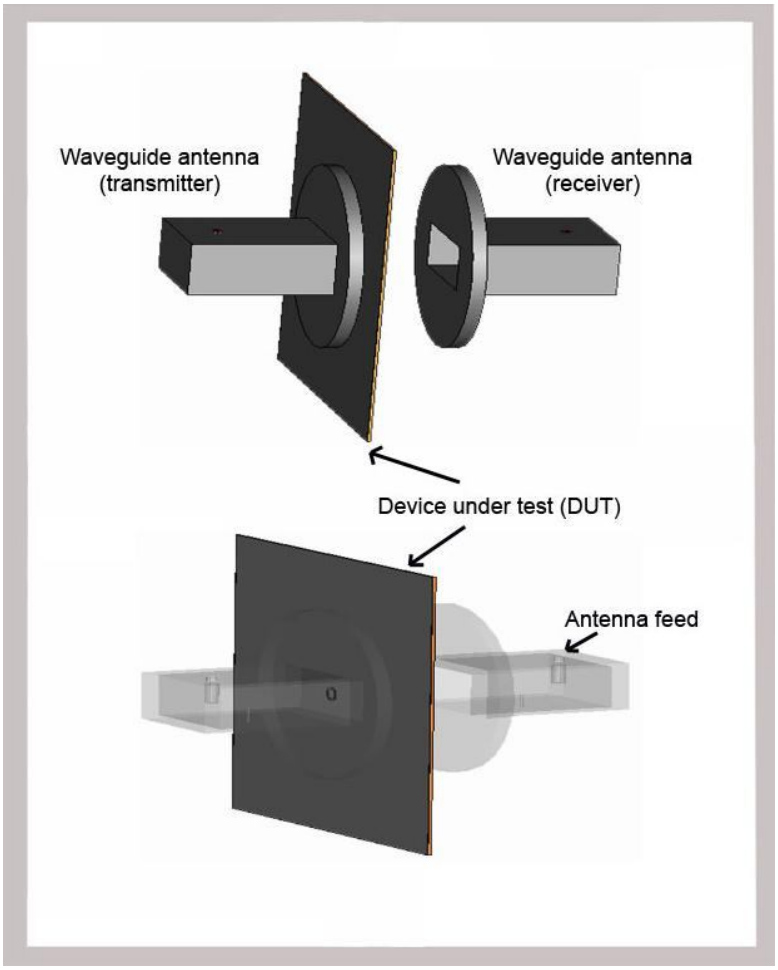

Figure 5.5: Schematics of two waveguide antennas, including the waveguide feed structures and the device under test (DUT).

Open boundary conditions are applied along all directions, in which perfect electric conductor (PEC) approximation for the metal structures is introduced as approximations for simulations. Since the metals are very good conductors at the microwave spectrum and the open boundary conditions can be obtained by using enough absorbers around the measurement setup; the approximations that are used in the simulations are reasonable and acceptable.

The dielectric constant of the FR-4 dielectric substrate is taken as $\varepsilon = 3.6$ with a tangent loss of $\delta = 0.01$. We started with the simulation of a single aperture with a 4 mm radius; and obtained the transmission result as shown in Figure 5.6.

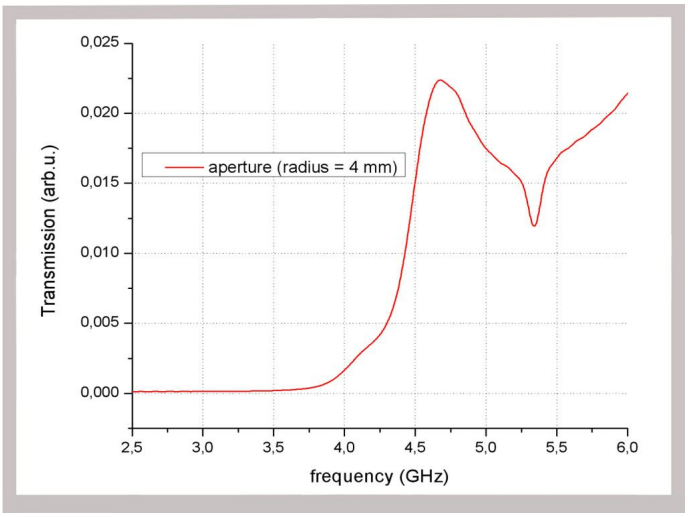

Figure 5.6: Calculated transmission spectrum of a single aperture.

This result indicates the lack of transmission through the hole up to 4 GHz. Moreover, an exponential increase in the transmission is observed after 4 GHz. The reason behind that increase in the transmission can be explained by the increasing electrical length of the aperture in terms of wavelength. As the electrical length of the aperture increases, the transmission also increases as described in Bethe's work [109]. We explained the details of Bethe's diffraction theory previously.

Afterwards, we placed an SRR in front of the transmitter side of the antenna as shown in Figure 5.7.

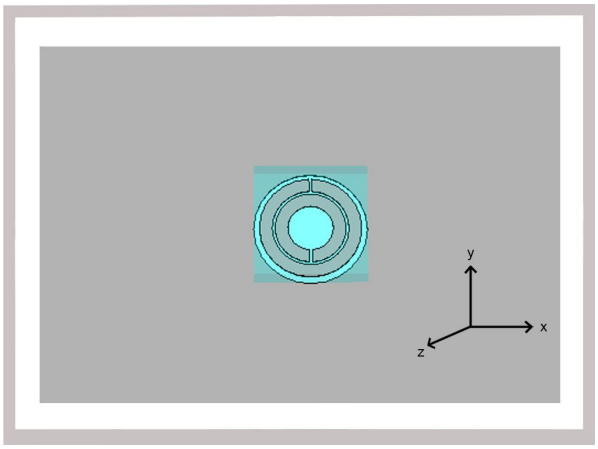

Figure 5.7: Schematics of proposed structure: SRR placed in front of the aperture (SRR_B type configuration).

However, no significant transmission enhancement (see Figure 5.8) is obtained in this configuration as expected; because the configuration of SRR structure in Figure 5.7 does not excite any resonances as discussed in detail at Chapter 3.

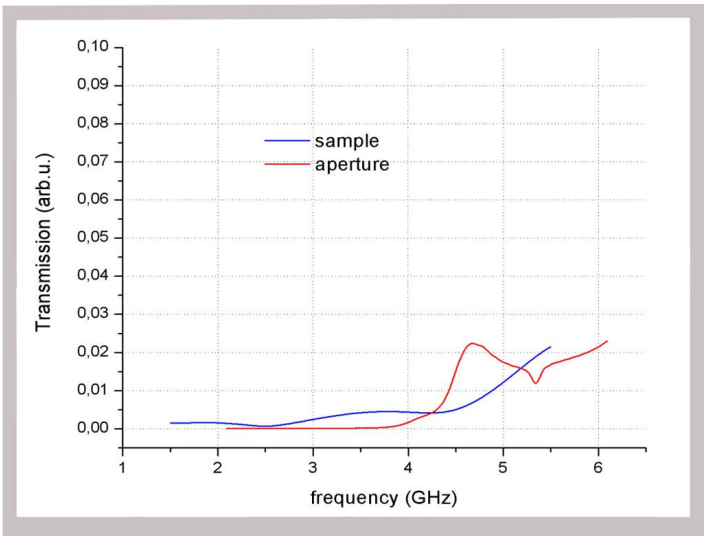

Figure 5.8: Transmission spectrum of proposed structure (SRR_B type configuration), which is shown in Figure 5.7.

Since we need to excite the resonance of SRR, we rotated the structure 90 degrees as seen in Figure 5.9. However, we also did not obtain any significant transmission enhancement as shown in Figure 5.10.

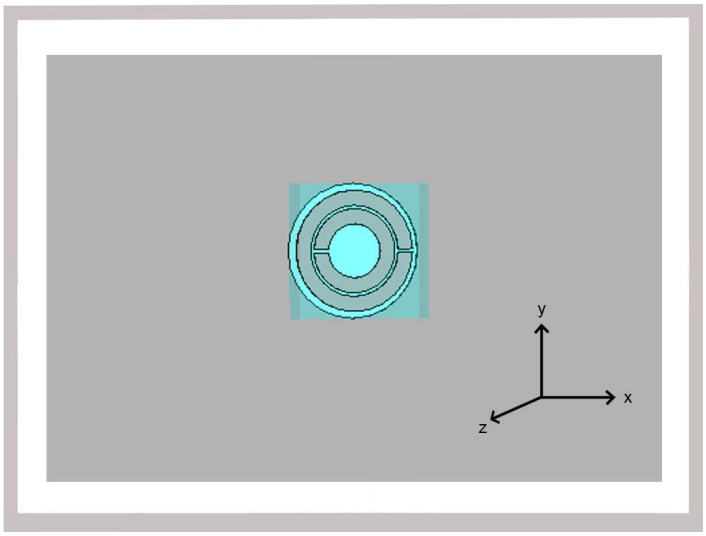

Figure 5.9: Schematics of proposed structure: SRR placed in front of the aperture (90 degrees rotated version of the structure in Figure 5.7).

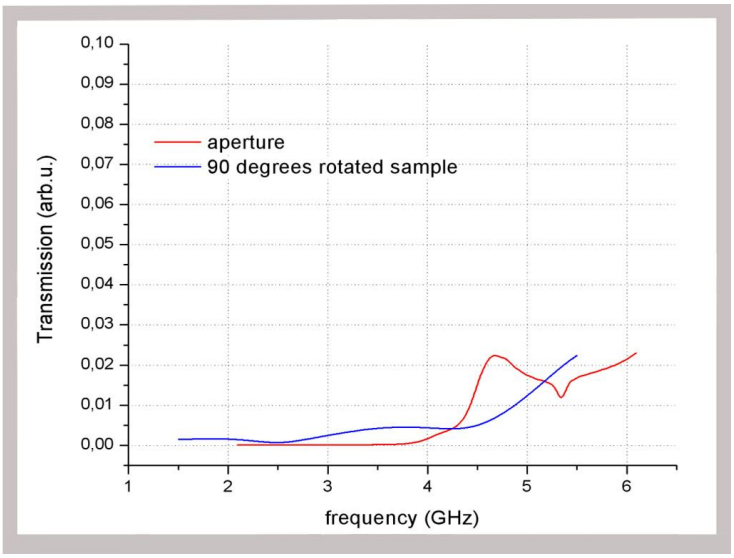

Figure 5.10: Transmission spectrum of proposed structure shown in Figure 5.9.

We checked different combinations of the SRR structure and the circular aperture in Figure 5.9 by changing the coordinates of the center of the SRR. We obtained enhancement in the transmission spectrum as we shifted the SRR along the x-axis. The transmission enhancement of the SRR structure is found maximum when the SRR is placed 0.1 mm away from the aperture and the outer split of the SRR is placed at the centerline of aperture (see Figure 5.3.a, Figure 5.11).

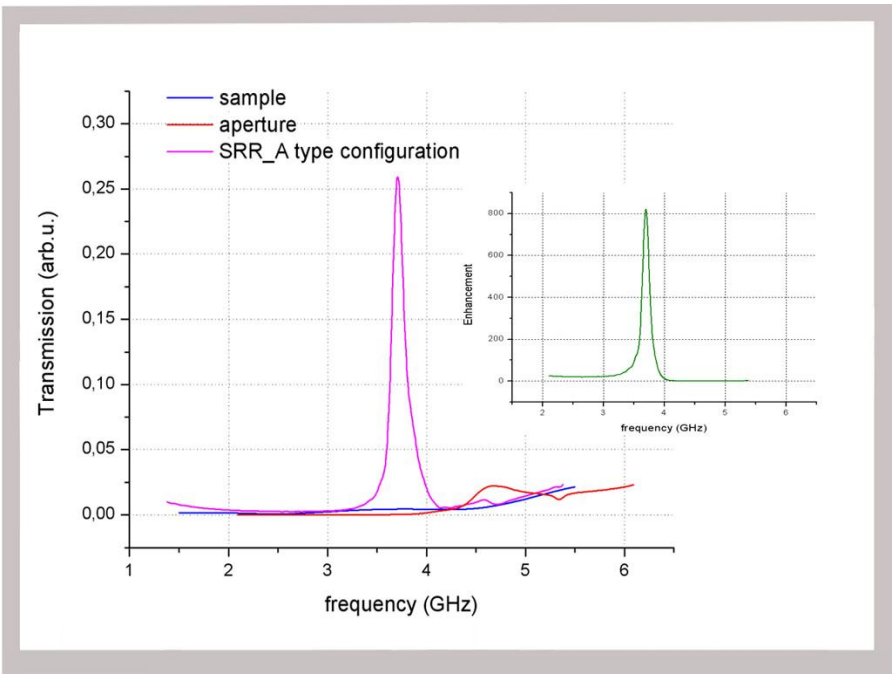

Figure 5.11: Transmission spectrum of optimized version of proposed structure, which is shown in Figure 5.9 (SRR_A type configuration). The inset shows the enhancement spectrum.

The transmission is significantly increased by utilizing a single SRR in the optimum orientation and location (see Figure 5.3.a). 820-fold transmission enhancement, which is defined as the ratio of transmitted electromagnetic wave intensity through SRR and aperture to transmitted electromagnetic

wave intensity through only aperture, is realized at 3.71 GHz (see the inset of Figure 5.11). Note that the enhanced transmission through aperture is obtained at the resonance frequency of SRR (SRR_A, Figure 3.22). The wavelength at 3.71 GHz is ($\lambda = \frac{c}{f}$) approximately 80 mm and the aperture radius (r = 4 mm) is approximately 0.05λ, which is quite small ratio for an aperture to be considered as sub-wavelength. This is the smallest aperture size to wavelength ratio in the contemporary literature according to our knowledge.

We performed additional numerical simulations in order to understand the enhancement phenomena. We utilized the field monitoring feature of CST Microwave Studio. We performed simulations at the frequency where the maximum enhancement is obtained (3.71 GHz). The electric field profile was calculated by placing electric field monitors at the y=0 plane at 3.71 GHz (Figure 5.12).

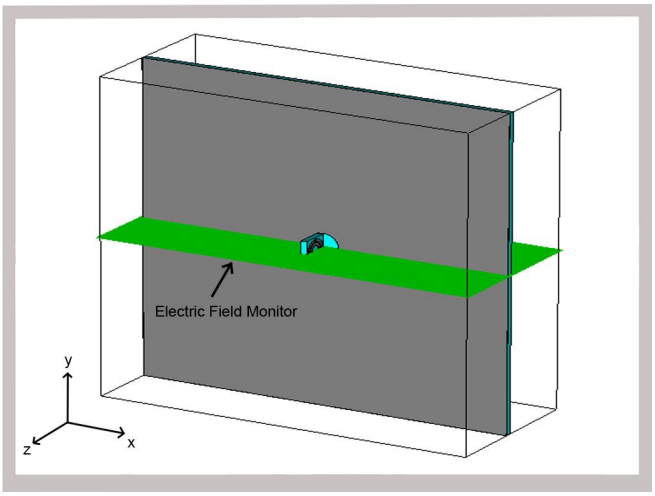

Figure 5.12: Simulation setup introduced for calculating the electric field profile by placing electric field monitors at the y=0 plane.

We introduced an incident plane wave sent by a transmitting antenna and a probe as a receiving antenna. The propagation of electromagnetic wave is from +z to -z; and the center of the aperture is placed at z=0. The electric field is localized at the splits of the SRR (see Figure 5.13). The results of the field monitors demonstrated that the electrical resonance of SRR structure gives rise to strong localization and high intensity of electromagnetic waves in the splits and the gap between the two rings of SRR. As can be seen in Figure 5.13, the incident electromagnetic field is coupled to aperture by utilizing the strong localization of electromagnetic field by SRR.

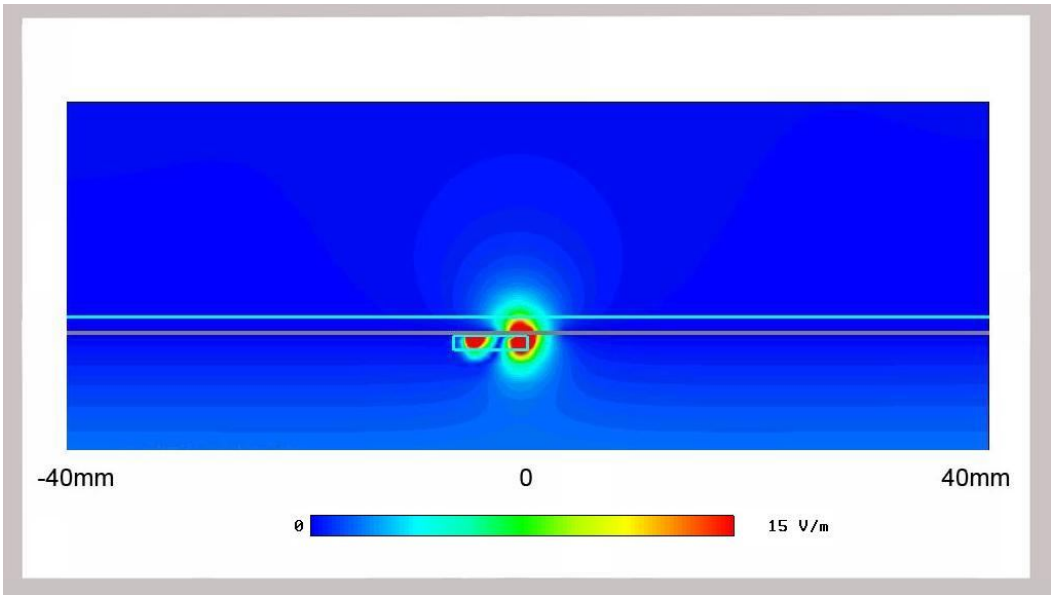

Figure 5.13: The electric field distribution of SRR_A type configuration by placing an electric field monitor at y=0 plane (top view), at the peak transmission frequency (3.71 GHz).

As was aforementioned, four possible orientations of SRR are available, and we have already tired using the SRR_A and SRR_B types of SRR.

Enhancement is achieved with SRR_A type configuration; and no significant enhancement is obtained with SRR_B type configuration, as expected. SRR_A structure excites only electrical resonance and SRR_B does not excite any resonance as a result of its symmetric structure [122]. On the other hand, SRR_D excites magnetic resonance and SRR_C excites both electric and magnetic resonance. Therefore, we expect transmission enhancement with SRR_C and SRR_D structures where a different resonance mechanism (magnetic resonance) contributes to the enhanced transmission.

Accordingly, the SRR_C structure is placed in front of the aperture as demonstrated in Figure 5.14; and its location is optimized for the highest enhancement: The SRR structure is again 0.1 mm away from the aperture and the metallic rings of the SRR_C is along the centerline of the aperture for the strongest electric and magnetic resonance.

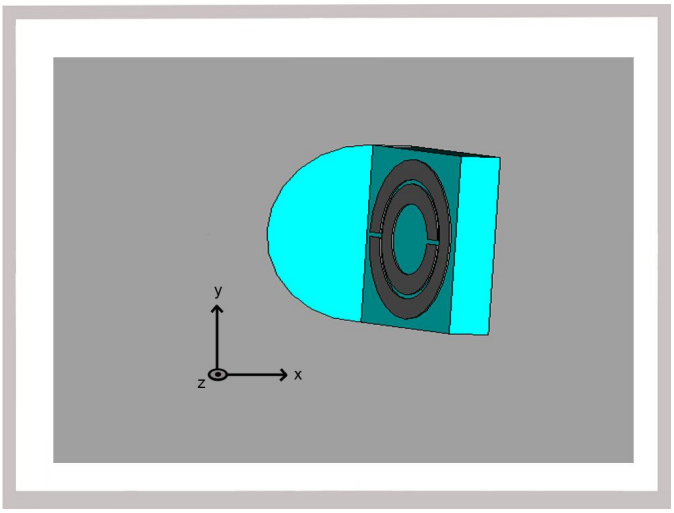

Figure 5.14: Schematics of proposed structure: SRR_C placed in front of the aperture.

Under these conditions, 7.8- fold enhancement is obtained at 3.76 GHz in the simulations as seen in the inset of Figure 5.15.

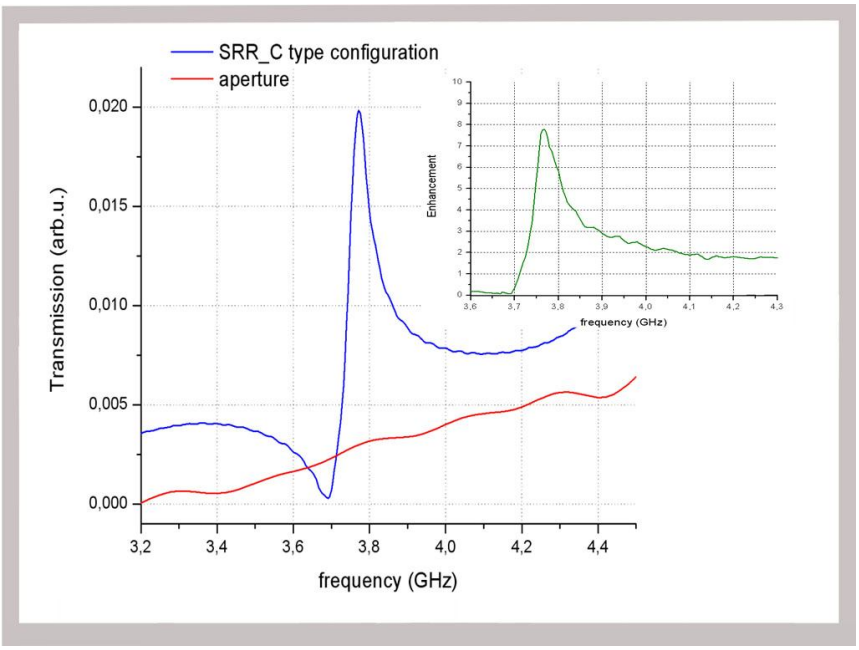

Figure 5.15: Transmission spectrum of proposed SRR_C type configuration. The inset shows the enhancement spectrum.

The field monitor results (Figure 5.16) for both SRR_A and SRR_C configurations demonstrated that both electrical and magnetic resonances of SRR_C structure give rise to more stronger localization and higher intensity of electromagnetic waves in the splits of SRR_C than SRR_A.

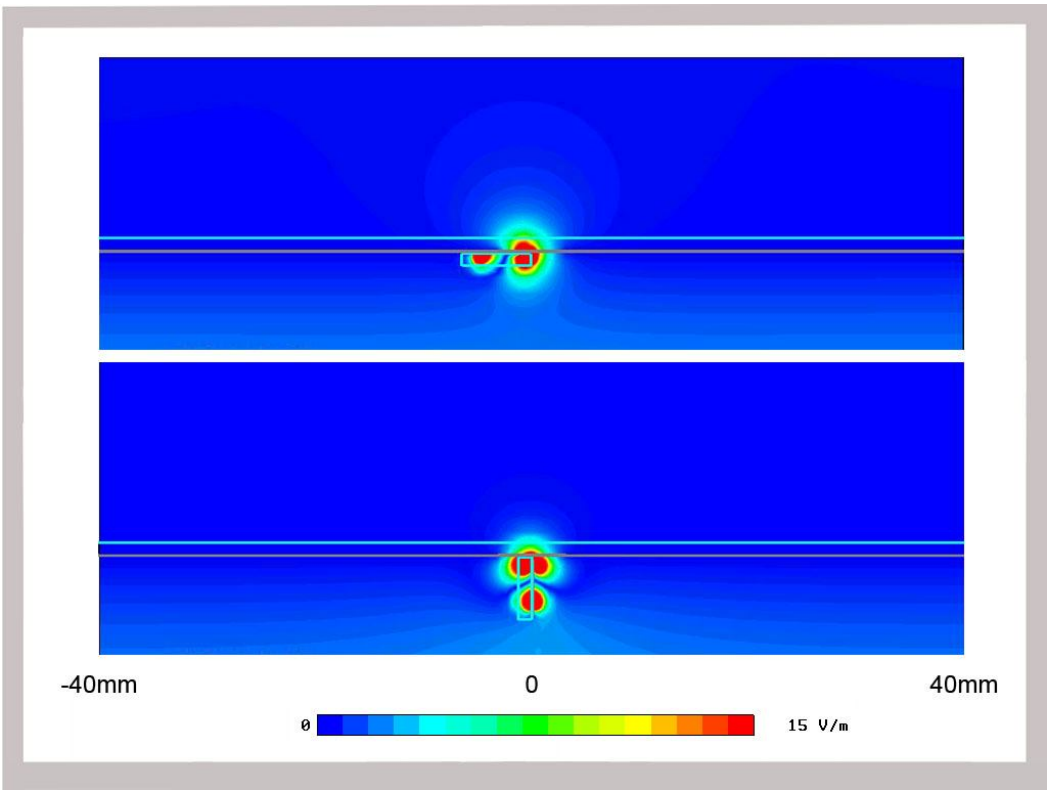

Figure 5.16:.The electric field distribution of SRR_A type configuration (top view) and SRR_C type configuration (bottom view), at the peak transmission frequencies of the structures.

We also attempted SRR_D structure for transmission enhancement. The optimum placement for the SRR_D is found the same as that for the SRR_C structure. The SRR structure is again 0.1 mm away from aperture and the metallic rings of the SRR_C is along the centerline of the aperture for the strongest electric and magnetic resonance (see Figure 5.17).

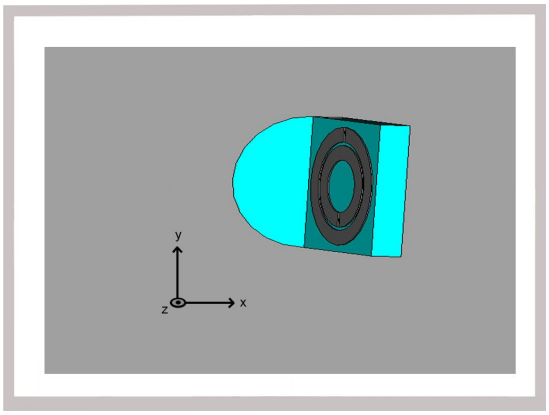

Figure 5.17: Schematics of proposed structure: SRR_D placed in front of the aperture.

For this configuration, 37-fold enhancement is obtained at 3.84 GHz in the simulations as shown in the inset of Figure 5.18.

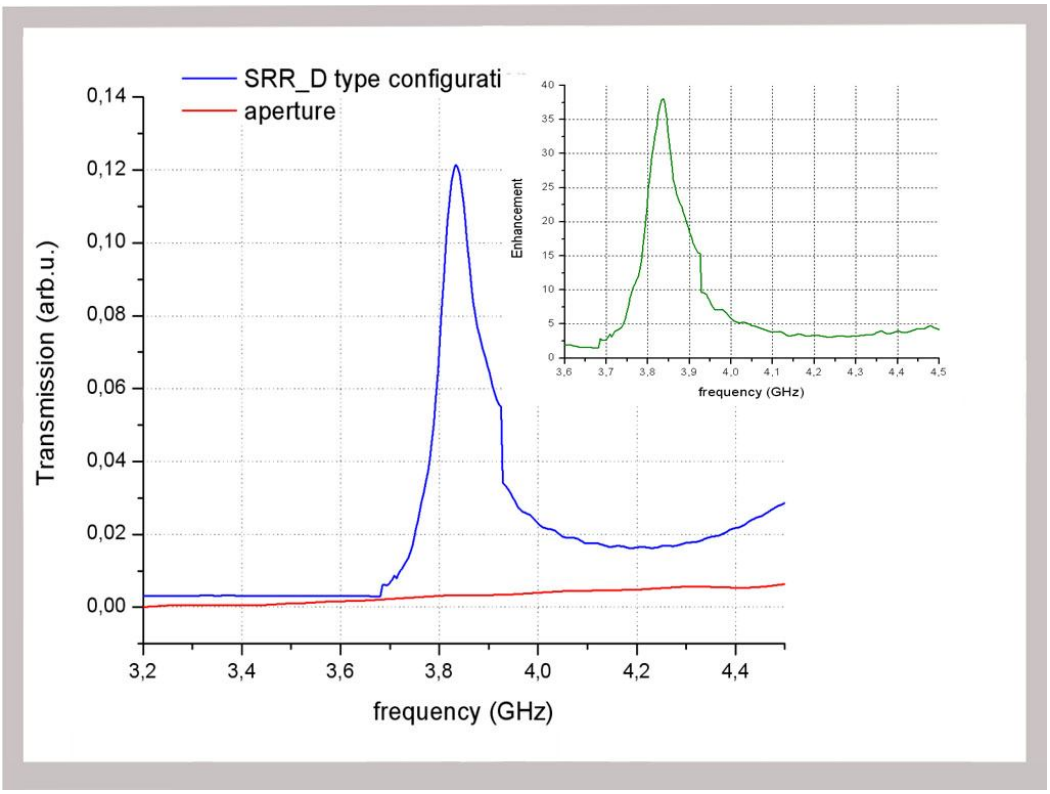

Figure 5.18: Transmission spectrum of proposed SRR_D type configuration. The inset shows the enhancement spectrum.

The combined field monitor results for SRR_A, SRR_C and SRR_D configurations demonstrated that the magnetic resonance of SRR_D structure give rise stronger localization and higher intensity of electromagnetic waves in the splits of SRR_D as compared to the SRR_A structure (Figure 5.19). However, the localization of electromagnetic wave in the splits of SRR_C is the highest.

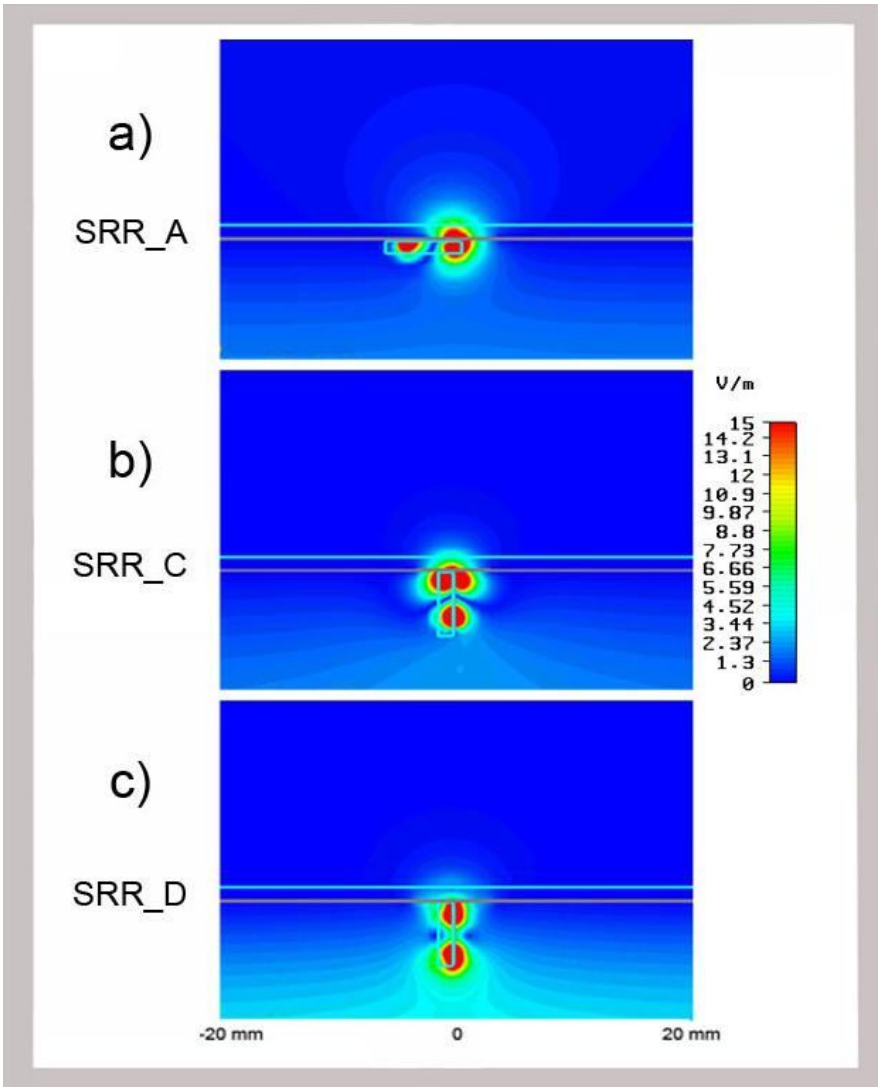

Figure 5.19: The electric field distributions of SRR_A, SRR_C and SRR_D type configurations.

The enhancement results of all the SRR configurations (Figure 5.20) revealed that the highest enhancement is achieved when the SRR is placed 0.1 mm away from the aperture and the outer split of the SRR is placed at the centerline of the aperture (SRR_A type configuration). The propagation direction of the incident wave is perpendicular to the SRR plane for SRR_A configuration. Therefore, the magnetic component of the incident field ($\overline{H}$) is parallel to the SRR plane. Thus, there is no magnetic resonance that indicates that the enhancement stems from electric resonance of SRR only. On the other hand, the transmission enhancement via magnetic resonance of the SRR_C type structure and SRR_D type structure are both less than the enhancement from SRR_A type structure configuration. Both the electric and magnetic resonance play a role in the resonance of SRR_C. Therefore, the resonance and localization of electromagnetic field is largest for the SRR_C configuration; and the SRR_A configuration shows the lowest localization in comparison with SRR_C and SRR_D (see Figure 5.19). However, the SRR_D configuration yields higher transmission than SRR_C; and the SRR_A yields the highest transmission (Figure 5.10). Since electric coupling to magnetic resonance for SRR_C occurs as a result of asymmetric structure with respect to incident E-field that is not present in SRR_D, we would expect to have higher transmission. However, additional electric resonance disrupts the performance of enhanced transmission for the SRR_C type configuration; because the electrical and magnetic resonances of SRR_C structure work destructively in terms of sub-wavelength aperture transmission [100].

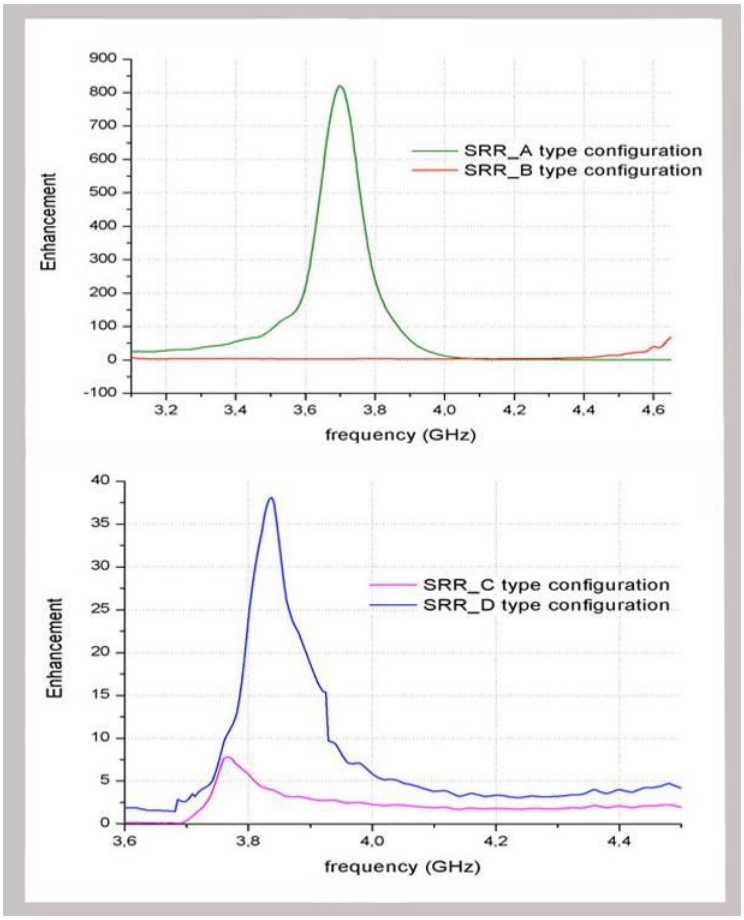

Figure 5.20: The calculated enhancement results of SRR_A, SRR_B, SRR_C and SRR_D type configurations.

The numerical simulation results presented so far confirmed the usefulness of our proposed structures for SRR-coupled transmission enhancement through sub-wavelength aperture. Therefore, we shall continue to make further progress by conducting experiments. The structures are fabricated with a process resolution of 0.1 mm, which is the smallest length of our proposed structures.

We used an experimental setup that is composed of an Agilent N5230A portable network analyzer, two waveguide ports and proper SMA cables.

The waveguide ports are used as transmitter and receiver and they are connected to the network analyzer with SMA cables. Figure 5.21 shows the setup used for transmission experiments.

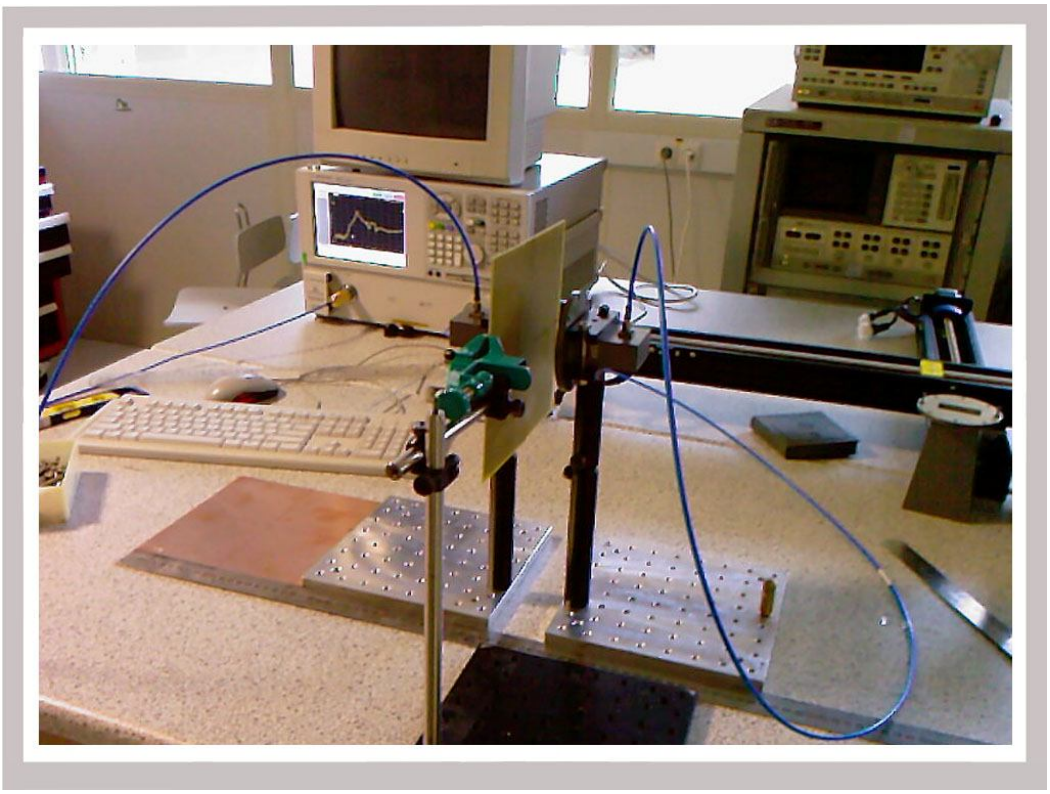

Figure 5.21: Experimental setup used in measurements.

In the measurements, the metallic plate with a single circular aperture is placed 0.1 mm away from the transmitter antenna and the receiver antenna is located 5 cm away from the transmitter antenna, as we modeled in numerical simulations. Waveguide ports are employed as transmitter and receiver antennas. The propagation of wave is along the z-axis, E-field is along the y direction and H-field is along the x direction (see Figures 5.5, 5.12 and 5.21).

We started with the transmission measurement of a single aperture that has radius of 4 mm. There is no enhancement in transmission, as we expected. The experimental results and simulation results are shown together in Figure 5.22.

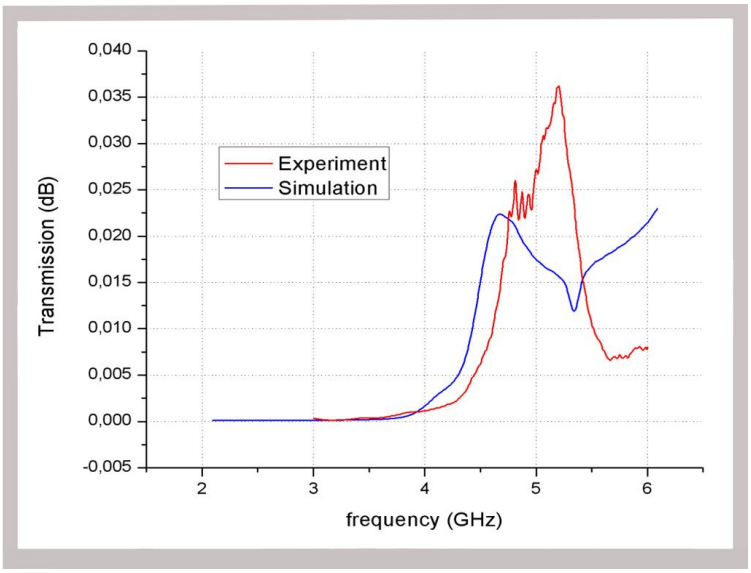

Figure 5.22: Calculated and measured transmission spectrum of single aperture.

Afterwards, we placed a single SRR very close to the aperture (0.1 mm) as SRR_A type configuration (Figure 5.3.a). As we expected, very high transmission enhancement is achieved, when SRR is placed 0.1 mm away from the aperture and the outer split of the SRR is placed at the centerline of the aperture.

The experimental and numerical transmission results are in good agreement and transmission through sub-wavelength aperture is significantly increased as shown in Figure 5.23. 820-fold enhancement with numerical simulation and 740-fold enhancement with experimental

results is observed by utilizing a single SRR only, in the near field of a sub-wavelength aperture (see the inset of Figure 5.23).

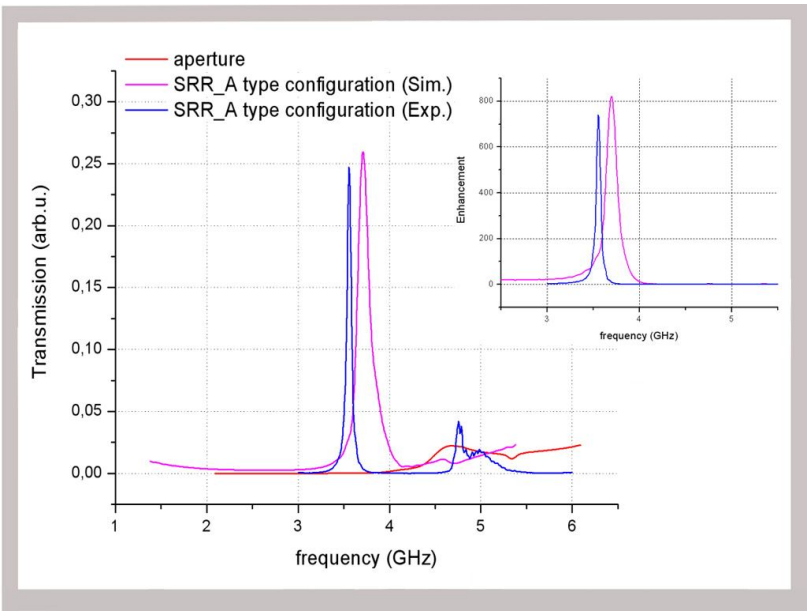

Figure 5.23: Calculated and measured transmission spectrum of SRR_A type configuration. The inset shows the enhancement spectrum obtained.

Figure 5.23 indicates that, the strong localization of electromagnetic field, caused by electrical resonance of SRR, enabled a significant enhancement of transmission (740-fold at 3.55 GHz) through sub-wavelength aperture, which is the highest value reported in literature to our knowledge.

We also checked the SRR_B configuration with aperture. Since no resonance is excited for this configuration; we did not observe any enhanced transmission (see Figure 5.24).

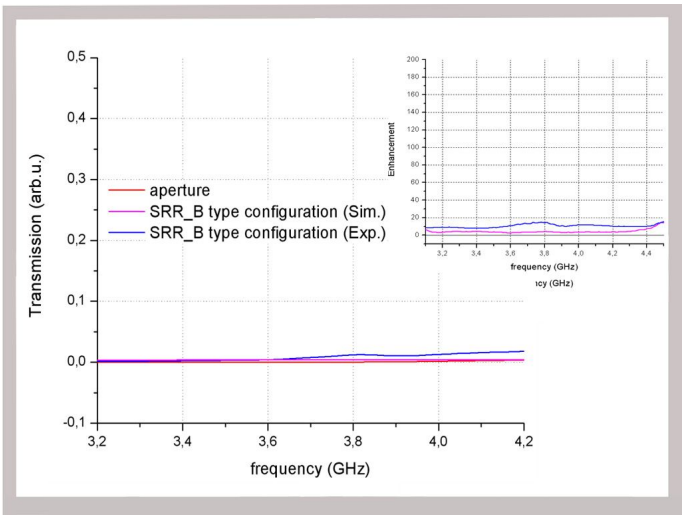

Figure 5.24: Calculated and measured transmission spectrum of SRR_B type configuration. The inset shows the enhancement spectrum.

Next, the SRR_C type configuration is also fabricated and measured. Transmission measurements of configuration SRR_C demonstrated less of a transmission enhancement than the SRR_A configuration enhancement, as we expected from the simulation results (see Figure 5.25). We obtained a 7.5-fold enhancement at 3.76 GHz, which agrees well with the numerical simulation results.

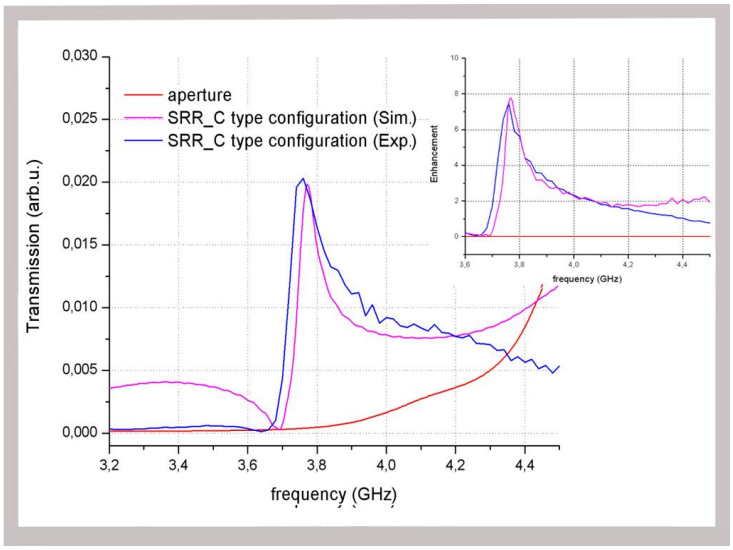

Figure 5.25: Calculated and measured transmission spectrum of SRR_C type configuration. The inset shows the enhancement spectrum.

Finally, we measured the transmission spectra of the SRR_D configuration, in which we obtained a 38-fold enhancement at 3.84 GHz, which agrees well with the numerical simulation results as shown in Figure 5.26.

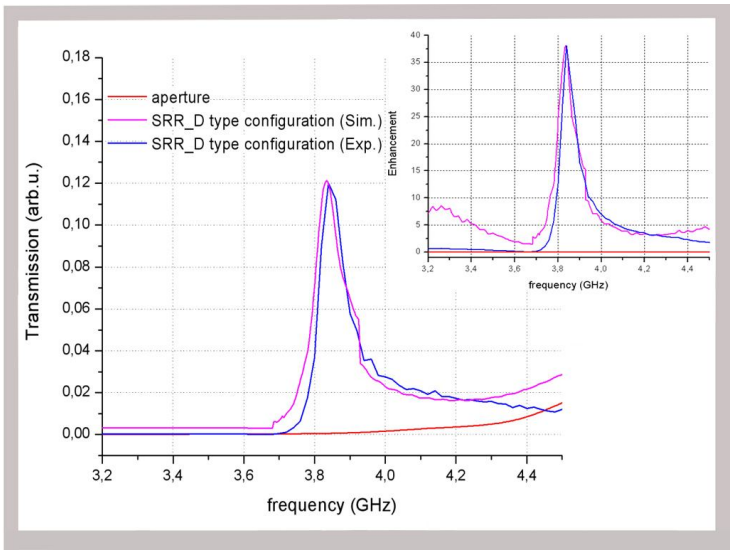

Figure 5.26: Calculated and measured transmission spectrum of SRR_D type configuration. The inset show the enhancement spectrum.

The experimental results are found in very good agreement with the numerical simulations. However, slight differences between the simulations and experimental results are observed such as small shifts in the peak frequencies. Such differences between the experimental results and simulation results could be attributed to the misalignment of the SRR in the experiments and the deviation of the electrical parameters of the materials from their ideal values used in the simulations.

As demonstrated so far in this chapter, enhanced transmission via SRR structure is polarization dependent. Other possible SRR geometries such as single ring with single cut resonators [63], rectangular SRR structures [65, 66] and elliptical SRRs [60] are also possible options to obtain enhanced transmission for specific polarizations of the incident wave. In this work, we successfully demonstrated a novel approach that utilizes the resonance of a circular bianisotropic split ring resonator that is placed in the close vicinity of a sub-wavelength aperture.

5.3 Enhanced Transmission through SRR-shaped apertures

In this section, we investigate a novel structure which is utilized for the enhanced transmission of electromagnetic wave through a single sub-wavelength aperture. Previous studies have shown that aperture with rectangular [117, 134] and elliptical [115] shapes in turn yield enhanced transmission for the specific polarization of an incident electromagnetic wave. The manipulation of the aperture shapes is a promising approach

for enhanced transmission through sub-wavelength apertures. In this work, we utilized SRR-shaped apertures in order to increase the transmission through a sub-wavelength aperture by using the strong localization characteristics of SRR structures.

The idea of SRR-shaped aperture stems from the Babinet's principle. By using the Babinet's principle, we can anticipate that the reflected fields of the SRR structure for a given incident polarization are supposed to be similar to the transmittance spectra of the SRR-shaped aperture (complementary SRR) for the orthogonal polarization. Since the SRR is a strong resonator structure, there exists a dip in the transmittance spectra at the resonance frequency. The dip in the transmission spectrum of the SRR corresponds to a peak in the reflection spectrum. Therefore, we can utilize this peak in order to obtain enhanced transmission through sub-wavelength apertures according to Babinet's principle.

We started with the simulation of SRR structure that corresponds to the complementary of a 90 degrees rotated version of SRR-shaped sub-wavelength aperture (see Figure 5.27.a). The geometrical parameters of SRR are the same as those of the SRR_A structure described in Chapter 3.

Figure 5.27.b represents the calculated transmission and reflection spectrum of SRR structure. There is a peak in the reflection spectrum. Therefore, we expect to have a peak in the transmission spectrum of SRR-

shaped aperture for the orthogonal polarization of incident wave (in accordance with the Babinet's Principle).

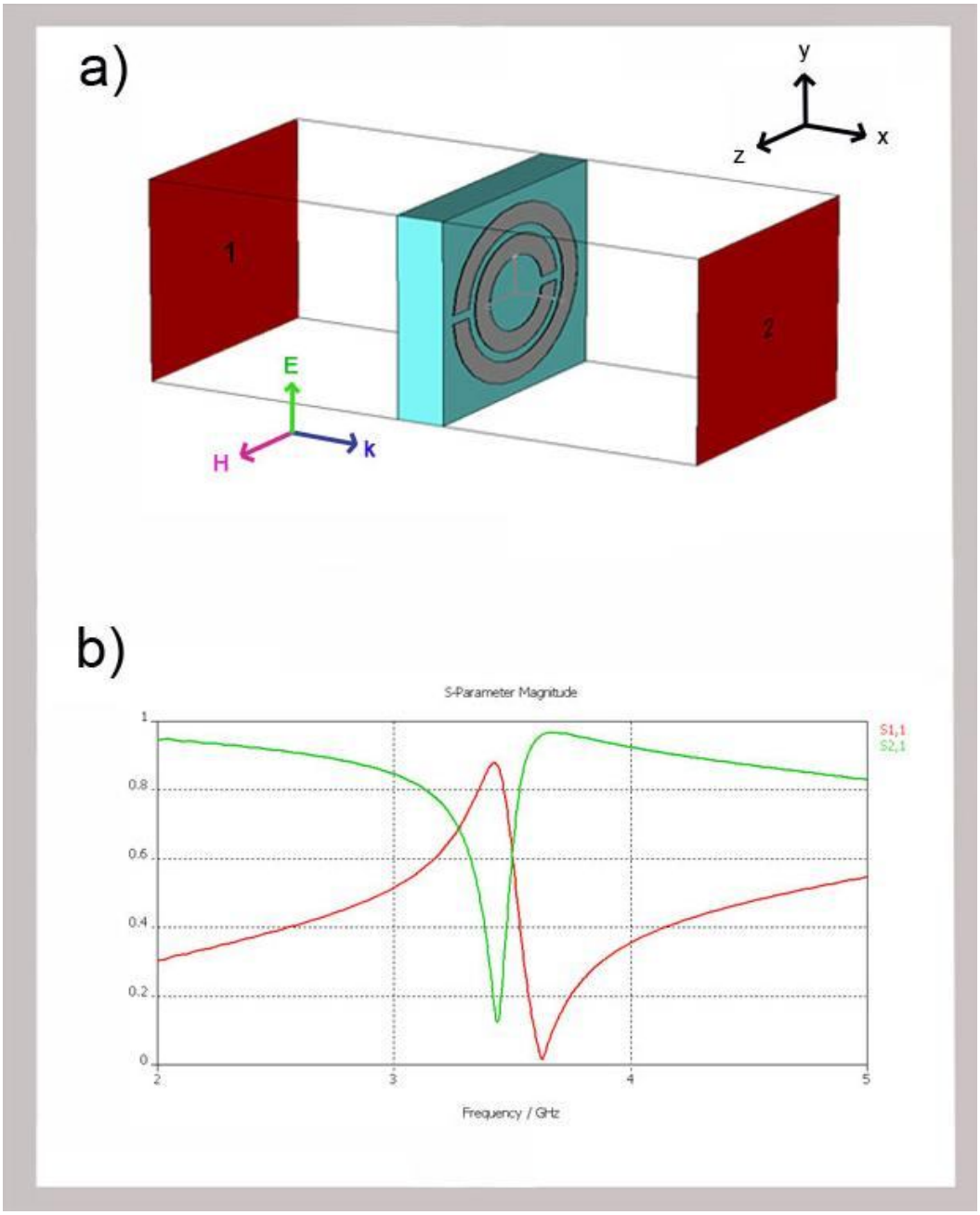

Figure 5.27: a) Schematic representation of SRR_A structure given in Chapter 3. b) Transmission (S21) and reflection (S11) spectrum of the SRR_A structure.

Firstly, we performed numerical simulations to confirm our expectation. The numerical simulations are performed by the commercially available software, CST Microwave Studio. As we did in Section 5.2, we modeled the complete scene in a realistic electromagnetic measurement setup in order to minimize the deviations from the experimental results. Namely, two waveguide antennas including the waveguide feed structures and the device under test (DUT) are modeled (Figure 5.5). Open boundary conditions are applied along all directions and perfect electric conductor (PEC) approximation for metal structures is introduced as approximations for simulations. Since metals are very good conductors at the microwave frequencies and the open boundary conditions can be realized by using enough absorbers around the measurement setup, the approximations that are used in the simulations are reasonable and acceptable.

The metallic plate with an aperture is placed 0.1 mm away from the transmitter antenna and the receiver antenna is located 5 cm away from the transmitter antenna. The SRR-shaped aperture is complementary to an exact replica of the SRR_A structure. Namely, the SRR-shaped aperture is modeled by subtracting the SRR_A structure from a square metal plate with a size of L x L (L = 200 mm). The metal plate is made of copper with a thickness of 30 μm over a 1.6 mm thick commercial FR-4 PCB substrate. Figure 5.28 shows a schematic representation of the SRR-shaped aperture that we used. The gap between the inner and outer rings (t) and the width of the splits (d) are 0.2 mm, the ring width (w) is 0.9

mm, and the outer radius of the SRR structure is 3.6 mm (SRR_A type configuration). The dielectric constant of the FR-4 dielectric substrate is taken as ε=3.6 with a tangent loss of δ=0.01.

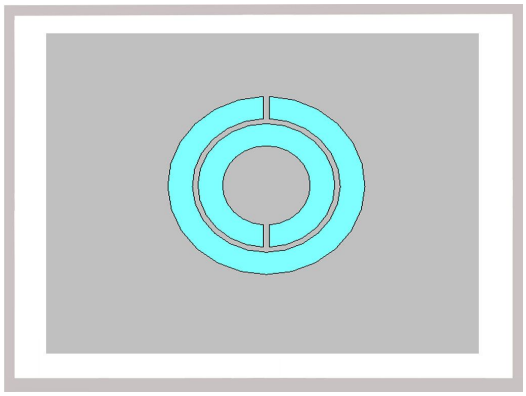

Figure 5.28: Schematic representation of the SRR-shaped aperture (Gray parts are metal plate and blue parts are the gaps).

Figure 5.29 represents the calculated transmission curve for the SRR-shaped aperture, which demonstrated an extraordinary transmission peak.

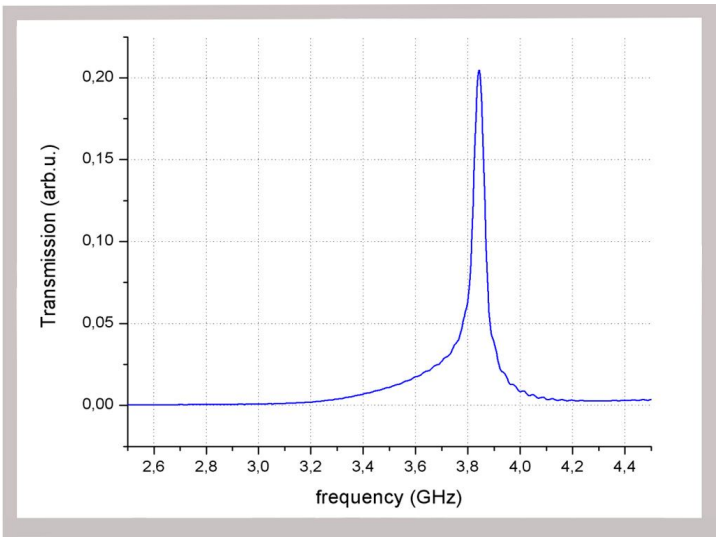

Figure 5.29: Calculated transmission spectrum of SRR-shaped aperture.

The extraordinary transmission result observed in the response of SRR-shaped aperture confirms that our expectation, which is based on Babinet's Principle, holds. This novel approach opens up significant opportunities to utilize several resonator structures for obtaining extraordinary transmission through sub-wavelength apertures. In the present work, we investigate SRR-shaped apertures for increasing the transmission through a sub-wavelength aperture; but it is also possible to utilize other types of resonators which will be a future work for us.

The simulation results for the SRR-shaped structure (Figure 5.29) and for the single aperture confirm the presence of a significant enhancement in the transmission of a single sub-wavelength aperture as shown in Figure 5.30.

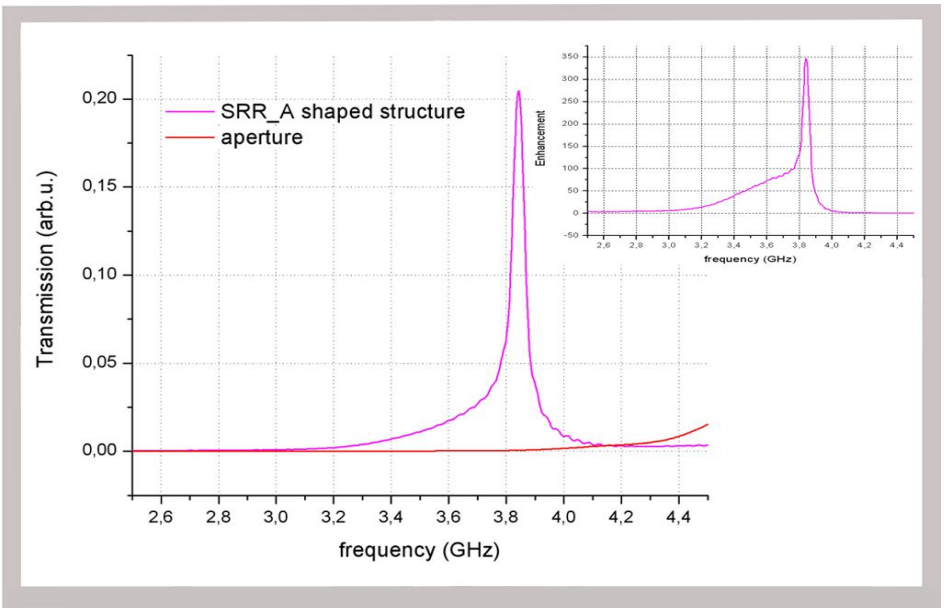

Figure 5.30: The calculated transmission spectrum of the SRR-shaped structure and a single aperture. The enhancement spectrum obtained by employing SRR-shaped structure is given in the inset.

The enhancement in the transmission through an aperture is defined as; the ratio of the field intensity of transmitted electromagnetic wave through SRR-shaped aperture to that through the aperture only. The inset of Figure 5.30 shows the enhancement that was obtained by manipulating the shape of the aperture as SRR-shaped aperture. We obtained a 346-fold transmission enhancement at 3.84 GHz by using this SRR-shaped aperture instead of simple circular aperture. Note that; the enhancement peak is very close to the resonance frequency of SRR_A structure. The resonance coupling of incident electromagnetic wave to the SRR-shaped aperture causes the strong localization of the electric field at the splits and gaps of the SRR-shaped aperture. Therefore, we can state that the resonator characteristic of SRR is responsible for the confined electromagnetic waves in the SRR-shaped aperture. We checked the role of the SRR characteristics on the enhanced transmission through an SRR-shaped aperture by closing the split regions of the structure, in which the structure becomes a CRR (closed ring resonator)-shaped aperture (Figure 5.31.a). Since the resonant behavior of SRR diminishes by closing the splits, the role of resonant structure of SRR on the enhancement mechanism of SRR-shaped aperture is evident (Figure 5.31.b).

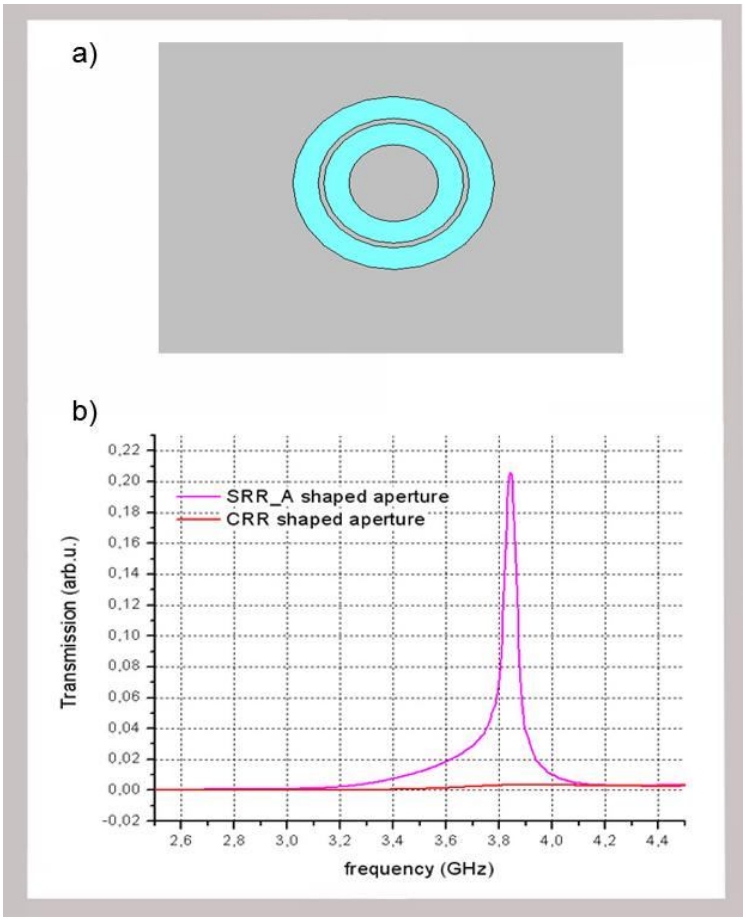

Figure 5.31: a) Schematic representation of Closed Ring Resonator (CRR) shaped aperture. b) Transmission spectrum of CRR-shaped aperture and SRR-shaped aperture.

After the successful demonstration of enhanced transmission through SRR-shaped aperture, we simulated, manufactured and measured several other types of split ring resonator structures in order to better characterize the novel approach/structure that we proposed. We performed a parametric study of SRR-shaped aperture and we also investigated single-ring SRR-shaped apertures. We mostly used square shaped structures because of its easier fabrication for the applications at

optical frequencies. The schematic representations of proposed structures are provided in Figure 5.32.

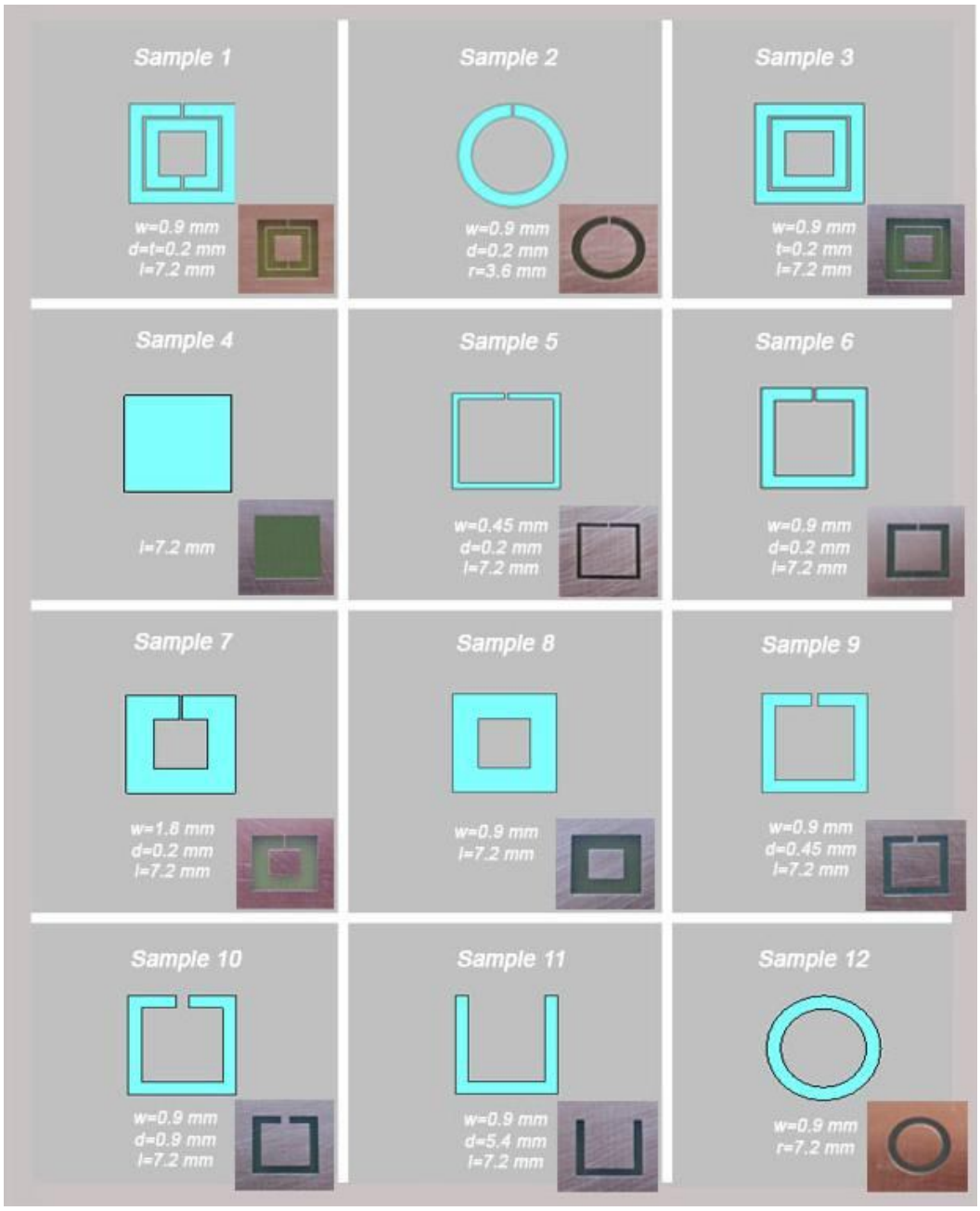

Figure 5.32: The schematics of proposed SRR-shaped aperture structures (Gray parts are metal plate and blue parts are the gaps). The insets demonstrate the fabricated samples.

We investigated the enhanced microwave transmission through sub-wavelength apertures for 12 different samples. The maximum length of all the samples is 7.2 mm, which corresponds to approximately 0.1λ at the resonance frequency of these SRR structures (~ 3-4 GHz).

Figure 5.33 presents the numerical simulation results of the transmission intensity of electromagnetic wave that propagates through the proposed SRR-shaped apertures.

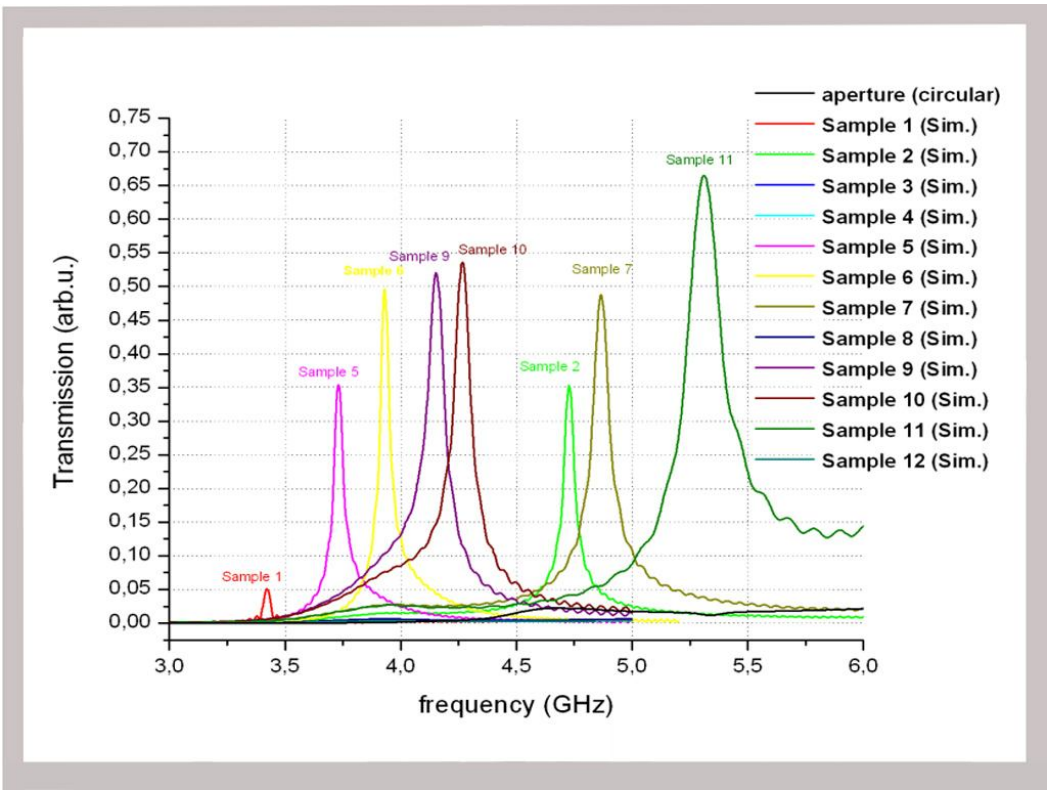

Figure 5.33: Calculated transmission results of proposed SRR-shaped apertures that are shown in Figure 5.32.

As can be seen in Figure 5.33, the transmission through the sub-wavelength aperture is significantly increased when SRR-shaped

apertures are placed instead of the single aperture. Moreover, we observed that the annular apertures (Samples 3, 8 and 12) transmit electromagnetic waves very close to the single aperture sample (Sample 4), which indicates that SRR-shaped apertures show superior performance versus annular apertures in terms of sub-wavelength aperture transmission. This also shows the effect of resonant coupling mechanism via SRR-shaped apertures. The resonance of SRR enables the coupling of incident wave to transmitted wave. Figure 5.34 represents the enhancement values of the simulated structures.

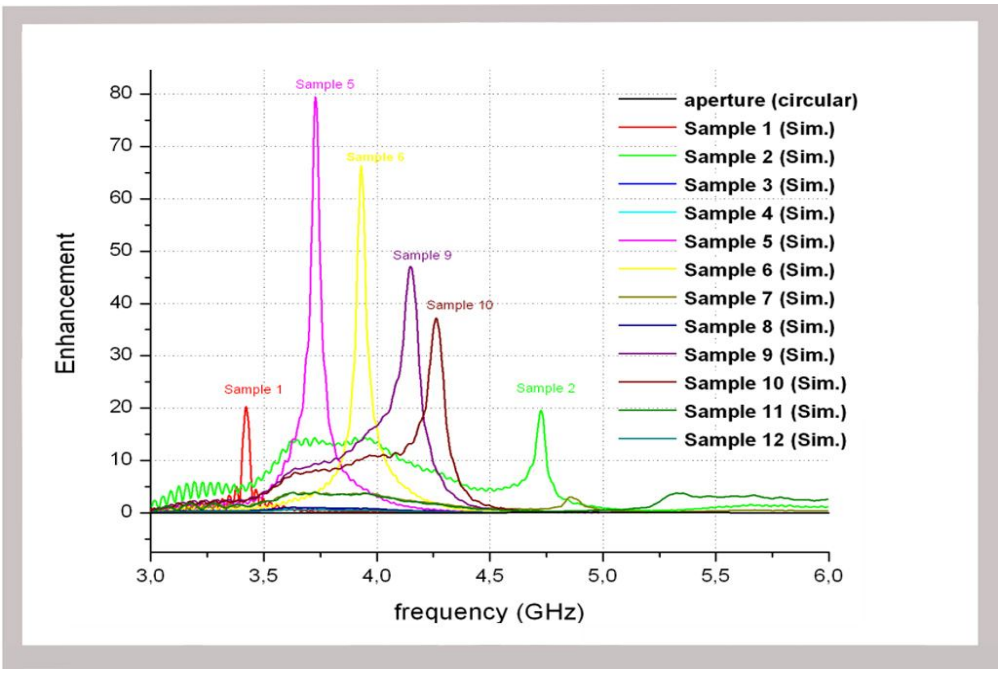

Figure 5.34: Calculated enhancement spectrum of proposed SRR-shaped apertures shown in Figure 5.32.

As can be seen in Figure 5.34, some of the peaks shown in Figure 5.33 are not available; because, transmission through a sub-wavelength aperture

(Sample 4 and circular aperture) increases with the fourth power of frequency. Therefore, certain transmission peaks occurring at higher frequencies become very small and hence disappear in the enhancement plot (Figure 5.34) as a result of an increase in transmission through aperture at higher frequencies.

After demonstrating the significant enhancement provided by the proposed structures, we fabricated and experimentally measured the samples in order to confirm the performance of these novel structures. The insets of Figure 5.32 represent the fabricated structures. Theses samples are fabricated by using a CNC machine with a process resolution of 0.1 mm. Figure 5.35 is the measured transmission spectra of the proposed 12 samples.

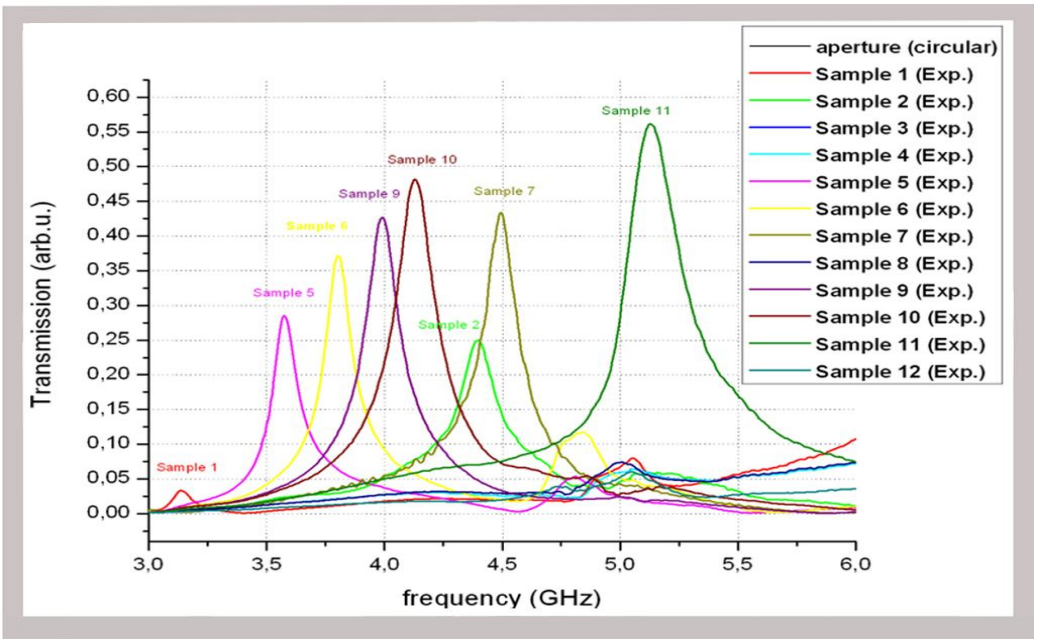

Figure 5.35: Measured transmission spectrum of proposed SRR-shaped apertures.

The experimental results for the enhancement values of the proposed SRR-shaped apertures are given in Figure 5.36:

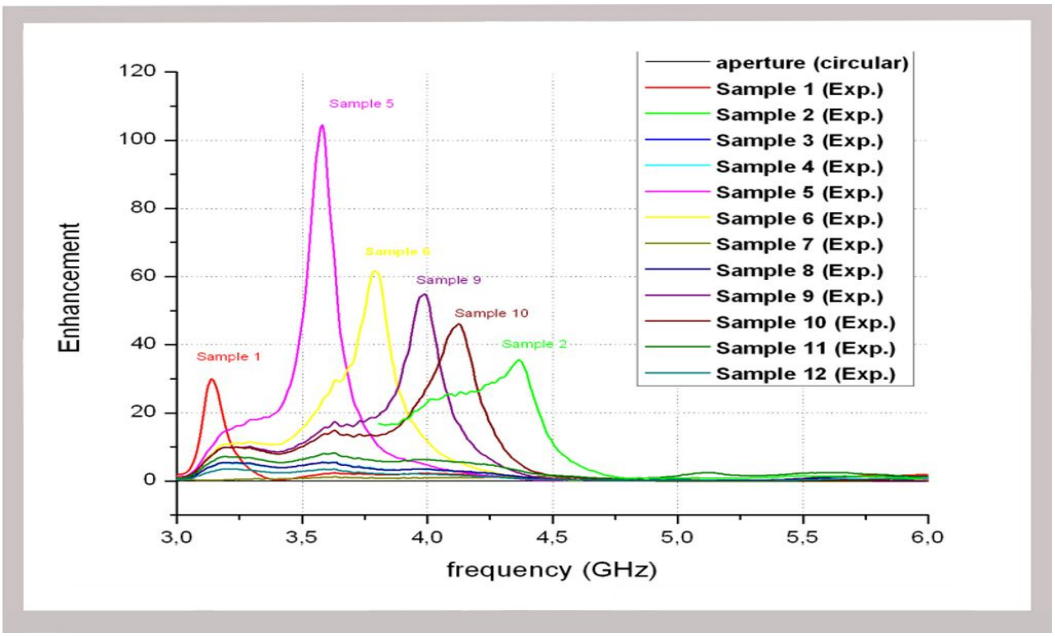

Figure 5.36: Measured enhancement spectrum of the proposed SRR-shaped apertures.

The experimental and numerical transmission results are in good agreement, which indicates that a significant enhancement is achieved by using the SRR-shaped apertures we proposed. The following table presents the summary of transmission and enhancement values for the proposed structures.

Table 5.1: Measured transmission and enhancement values of proposed structures.

	w (mm)	d / t (mm)	r / l (mm)	peak frequency (GHz)		Transmission peak (arb. u.)		Enhancement peak (arb. u.)	
				Sim.	*Exp.*	*Sim.*	*Exp.*	*Sim.*	*Exp.*
Sample 1	0.9	0.2 / 0.2	7.2	3.42	3.13	0.051	0.033	20	30
Sample 2	0.9	0.2	3.6	4.73	4.41	0.35	0.25	20	36
Sample 3	0.9	- / 0.2	7.2	N/A	N/A	N/A	N/A	N/A	N/A
Sample 4	-	-	7.2	N/A	N/A	N/A	N/A	N/A	N/A
Sample 5	0.45	0.2	7.2	3.73	3.58	0.35	0.29	80	104
Sample 6	0.9	0.2	7.2	3.93	3.79	0.49	0.37	66	62
Sample 7	1.8	0.2	7.2	4.87	4.49	0.49	0.43	N/A	N/A
Sample 8	0.9	-	7.2	N/A	N/A	N/A	N/A	N/A	N/A
Sample 9	0.9	0.45	7.2	4.15	3.99	0.52	0.43	47	55
Sample 10	0.9	0.9	7.2	4.26	4.13	0.54	0.48	37	46
Sample 11	0.9	5.4	7.2	5.31	5.13	0.66	0.56	N/A	N/A
Sample 12	0.9	-	7.2	N/A	N/A	N/A	N/A	N/A	N/A

Sample-4 is the reference sample for our measurements. As we stated above, the sub-wavelength apertures transmit very poorly and diffract electromagnetic radiation in all directions. Therefore, all of the samples are designed on a 20 cm x 20 cm metal plate in order to better collect the transmitted wave and better isolate the incident wave and transmitted wave.

Sample-1 has the highest transmission wavelength (lowest radius to wavelength ratio) as a result of the additional splits and rings compared to the other samples. Also, we observed that as the ring width decreases the transmission enhancement and transmission peak frequency increases; this is because the decreased width of the SRR-shaped apertures increases the coupling between the plate at the center and the surrounding large plane, which increases the resonant coupling.

We also investigated the effect of split width on the enhancement peak. The enhancement value of the samples decreases as we increase the split width. Furthermore, the resonance peak frequency increases with increasing split width. The split width is very crucial for the resonance of SRR, as we stated in Chapter 3. The effect of increasing split width is also very important for application of our proposed structures at optical frequencies. Since the fabrication of the sample-11 is the easiest among all the others, it will be the best choice for higher frequencies. As we can see from the results, we obtained a significant transmission peak which is very promising for higher frequency applications. This will be future work for us to carry out.

Finally, we investigated the effect of the shape of SRR structures (SRR-shaped apertures) on the enhancement. We fabricated sample-2 and sample-12 for observing the effect of the SRR-type. The transmission of sample-12 is as we expected, very low. However, we obtained a significant enhancement (36-fold) by only utilizing a small wire that

makes the structure an SRR-shaped structure (Sample-2). We used a circular aperture (radius 3.6 mm) as the reference sample for circular SRR-shaped aperture structures and square aperture (l = 7.2 mm) as the reference sample for square SRR-shaped apertures, for a fair comparison.

The metal that we used in our structures is very close to a perfect conductor at the microwave frequencies. Therefore, localized surface plasmons do not contribute to the enhanced transmission. Moreover, we did not use a grating structure and, therefore, there is no contribution of surface waves to the enhancement. The enhancement stems from the strongly localized fields that are caused by the resonant process of SRR-shaped aperture to the sub-wavelength aperture.

In this chapter, we demonstrated several novel structures to increase the transmission through a sub-wavelength aperture. The enhanced transmission through a sub-wavelength aperture has become a current subject of intense research; because the enhanced transmission phenomenon has a wide range of application in many fields [136-140]. We obtained enhanced transmission at microwave frequencies by utilizing novel structures. It is possible to use these structures at optical frequencies by making several modifications. SRRs are already being realized at optical frequencies [75, 141]. Therefore, these structures are promising candidates for novel applications. The research for novel applications will be future work for us to conduct.

CHAPTER 6

CONCLUSION

In this thesis, the transmission and propagation characteristics of novel metamaterial structures are investigated; and new approaches for the design of novel devices are proposed. This chapter includes a concise summary of the results that are achieved in this thesis. In addition, any possible future work that our results have led us to will also be mentioned.

In the second chapter, a detailed analysis on the theoretical background of metamaterials is provided. We have given an analytical description of the constitutive parameters of metamaterials. In addition, we analyzed negative permittivity, negative permeability and negative index metamaterials. We successfully demonstrated the electromagnetic characteristic of metamaterials by numerical simulations. Negative refraction of electromagnetic waves is demonstrated by numerical simulations.

Chapter 3 studied one of the main building blocks of metamaterials, namely the split ring resonator (SRR) structures. The resonance characteristic of SRR is successfully demonstrated by the numerical simulations of transmission through SRR structures. The magnetic resonance of SRR is verified by comparing the SRR structure with a CRR structure, in which the splits are removed. Since removing the splits annihilates the magnetic resonance effects in the resulting CRR structure, the magnetic resonance characteristics of the SRR becomes proven. Also, the effect of geometrical parameters on the magnetic resonance of SRR is discussed. Furthermore, we analyzed several different types of SRR in order to observe their electromagnetic characteristics. Finally, the effect of SRR orientations on the electromagnetic resonance mechanism of SRR is discussed.

In the fourth chapter, a fishnet-type metamaterial structure operating at microwave frequencies is proposed and investigated. Transmission measurements and simulations confirmed a left-handed transmission band for fishnet structures over a narrow frequency range. In addition, negative-index of refraction is verified by using an effective parameter retrieval procedure. The phase shift introduced by this structure, while adding additional structure layers in the propagation direction, is investigated. The left-handed behavior of the fishnet structure is revealed as negative phase advance occurs at the left-handed frequency band of the fishnet structure. Additionally, we examined the effect of several geometrical parameters on the left-handed behavior of the fishnet

structure, which is important for optimization issues. The major advantages of our proposed fishnet design are demonstrated: Firstly, fishnet structures provide high transmission due to concentration of the feeds in the low-loss substrate. Secondly, this planar fishnet structure shows negative index behavior, which is independent of the incident electromagnetic wave polarization due to the symmetric configuration of wire and slab pairs. We will search for the possibilities of adding capacitive and inductive elements in order to optimize the transmission peak of the fishnet structure in future work. Moreover, we will attempt to manually tune the left-handed peak of a fishnet structure by utilizing active elements.

Finally in Chapter 5, novel approaches to increase the transmission through a sub-wavelength aperture are proposed. Firstly, enhanced transmission through a sub-wavelength aperture by placing a SRR structure in the near field of the aperture is achieved at microwave frequencies. A 740-fold enhancement is obtained by experimental measurements. Subsequently, we manipulated the shape of sub-wavelength aperture. We utilized SRR-shaped apertures in order to increase the transmission though a sub-wavelength aperture by using the strong localization property of SRR structures. We obtained a 104-fold enhancement by utilizing SRR-shaped apertures. The enhancement stems from the strongly localized fields caused by SRR-shaped apertures. The strongly localized fields are a result of the resonant process of SRR-shaped aperture to the sub-wavelength aperture. It is possible to use

these proposed structures at optical frequencies by making several modifications. SRRs are already realized at optical frequencies [75, 141]. Thus, these structures are promising candidates for novel applications. The research for novel applications will be future work for us to conduct. We will investigate the possibility of utilizing sub-wavelength dipole-like antennas in order to increase the transmission through sub-wavelength apertures. The results that we obtained in this section confirm the suitableness of our structure for enhanced transmission through sub-wavelength apertures. Therefore, our proposed structures can be utilized in new research areas and applications such as new probes for the scanning near-field optical microscope (SNOM) [123, 124], near-field optical recording [125, 126], nano-scale lithography [127-129] tracking single molecule (fluorescence spectroscopy) [124, 130] and ultrafast miniature photodetector [131].

REFERENCES

[1] B. Edwards, A. Andrea, E. Michael, M.S. Young, N. Engheta, *Experimental verification of epsilon-near-zero metamaterial coupling and energy squeezing using a microwave waveguide*, Phys. Rev. Lett., 100, 033903, 2008.

[2] W.J. Padilla, A.J. Taylor, C. Highstrete, M. Lee, R.D. Averitt *Dynamical electric and magnetic metamaterial response at terahertz frequencies,* Phys. Rev. Lett., 96, 107401, 2006.

[3] R. Liu, Q. Cheng, T. Hand, J.J. Mock, T.J. Cui, S.A. Cummer, D.R. Smith, *Experimental Demonstration of Electromagnetic Tunneling Through an Epsilon-Near-Zero Metamaterial at Microwave Frequencies*, Phys. Rev. Lett., 100, 023903, 2008.

[4] S. Feng, K. Halterman, *Parametrically Shielding Electromagnetic Fields by Nonlinear Metamaterials*, Phys. Rev. Lett., 100, 063901, 2008.

[5] Y. Cheng, J.Y. Xu, X.J. Liu, *One-dimensional structured ultrasonic metamaterials with simultaneously negative dynamic density and modulus,* Phys. Rev. B 77, 045134, 2008.

[6] X.Q. Lin, T.J. Cui, J.Y Chin, X.M. Yang, Q. Cheng, R. Liu, *Controlling electromagnetic waves using tunable gradient dielectric metamaterial lens*, Applied Physics Letters, 92, 131904, 2008.

[7] K.L. Tsakmakidis, A.D. Boardman, O. Hess, *'Trapped rainbow' storage of light in metamaterials,* Nature 450, 397–401, 2007.

[8] J. Valentine, S. Zhang, T. Zentgraf, E. Ulin-Avila, D.A. Genov, G. Bartal, X. Zhang, *Three-dimensional optical metamaterial with a negative refractive index*, Vol. 455, 376-379, 2008.

[9] H.T. Chen, W.J. Padilla, J.M.O. Zide, A.C. Gossard, A. J. Taylor, R.D. Averitt, *Active terahertz metamaterial devices*, Nature 444, 597-600, 2006.

[10] N.C. Panoiu, R.M. Osgood, *Numerical investigations of negative refractive index metamaterials at infrared and optical frequencies,* Opt. Comm. 223, 331–337, 2003.

[11] C.M. Soukoulis, S. Linden, M. Wegener, *Negative refractive index at optical frequencies,* Science 315, 47-49, 2007.

[12] T. Li, H. Liu, F.M. Wang, Z.G. Dong, S.N. Zhu, X. Zhang, *Coupling effect of magnetic polariton in perforated metal/dielectric layered metamaterials and its influence on negative refraction transmission,* Opt. Express 14, 11155–11163, 2006.

[13] A. Alu, N. Engheta, *Three-dimensional nanotransmission lines at optical frequencies: A recipe for broad band negative-refraction optical metamaterials,* Phys. Rev. B 75, 024304, 2007.

[14] M.C.K. Wiltshire, J.B. Pendry, I.R. Young, D.J. Larkman, D.J. Gilderdale, J.V. Hajnal, *Microstructured Magnetic Materials for RF Flux Guides in Magnetic Resonance Imaging*, Science, Vol. 291, 2001.

[15] Z.W. Liu, H. Lee, Y. Xiong, C. Sun, X. Zhang, *Far field optical hyperlens magnifying sub-diffraction-limited objects*, Science, 315, 1686, 2007.

[16] Z. Jacob, L.V. Alekseyev, E. Narimanov, *Optical hyperlens: Far-field imaging beyond the diffraction limit*, Opt. Exp., 14, 8247-8256, 2006.

[17] I.I. Smolyaninov, Y.J. Hung, C.C. Davis, *Magnifying superlens in the visible frequency range*, Science, 315, 1699-1701, 2007.

[18] K. Aydin, I. Bulu, E. Ozbay, *Subwavelength resolution with a negative-index metamaterial superlens*, Appl. Phys. Lett., 90, 254102, 2007.

[19] M. Gokkavas, K. Guven, I. Bulu, K. Aydin, M. Kafesaki, R. Penciu, C. M. Soukoulis, E. Ozbay, *Experimental demonstration of a left-handed metamaterial operating at 100 GHz*, Phys. Rev. B 73, 193103, 2006.

[20] V.M. Shalaev, *Optical negative-index metamaterials*, Nature Photonics 1, 41, 2007.

[21] J.B. Pendry, A.J. Holden, W.J. Stewart, I. Youngs, *Extremely Low Frequency Plasmons in Metallic Mesostructures*, Phys. Rev. Lett, Vol.76, Number 25 1996.

[22] J.B. Pendry, A.J. Holden, D.J. Robbins, W.J. Stewart, *Low frequency Plasmons in thin-wire structures*, J.Phys.: Condens. Matter, Vol.10, 4785-4809, 1998.

[23] D.R. Smith, D.C. Vier, W.J. Padilla, S. C. Nemat-Nasser, S.Schultz, *Loop-wire medium for investigating Plasmons at microwave frequencies*, Appl. Phys. Lett., Vol. 75, p1425, 1999.

[24] V.G. Veselago, *The electrodynamics of substances with simultaneously negative values of permittivity and permeability*, Sov. Phys. Uspekhi, Vol.10, p.509, 1968.

[25] J.B. Pendry, A.J. Holden, D.J. Robbins, W.J. Stewart, *Magnetism from Conductors and Enhanced Nonlinear Phenomena*, IEEE Trans. Microwave Theory Tech., Vol.47, p.2075, 1999.

[26] D.R. Smith, W.J. Padilla, D.C. Vier, S.C. Nemat-Nasser, S. Schultz, *Composite medium with simultaneously negative permeability and permittivity*, Phys. Rev. Lett, Vol. 84, p.4184, 2000.

[27] R.A. Shelby, D.R. Smith, S.C. Nemat-Nasser, S. Schultz, *Microwave transmission through a two-dimensional, isotropic, left-handed metamaterial*, Appl. Phys. Lett., Vol. 78, p489, 2001.

[28] D.R. Smith, N. Kroll, *Negative Refractive Index in Left-Handed Materials*, Phys. Rev. Lett., Vol.85, Number 14, 2000.

[29] R.A. Shelby, D.R. Smith, S. Schultz, *Experimental verification of a negative index of refraction*, Science, Vol.292, p.77, 2001.

[30] C.G. Parazolli, R.B. Greegor, K. Li, B.E.C. Koltenbah, M. Tanielian, *Experimental verification and simulation of negative index of refraction using Snell's Law*, Phys. Rev. Lett., Vol.90. Number 10, 2003.

[31] A.A. Houck, J.B. Brock, I.L. Chuang, *Experimental observations of a left-handed material that obeys Snell's Law*, Phys. Rev. Lett., Vol.90, Number 10, 2003.

[32] K. Aydin, K. Guven, C. M. Soukoulis, E. Ozbay, *Observation of negative refraction and negative phase velocity in left-handed metamaterials*, Appl. Phys. Lett. 86, 124102, 2005.

[33] N. Seddon, T. Bearpark, *Observation of the inverse Doppler effect*, Science, Vol.302, 1537-1540, 2003.

[34] J. Lu, T. Grzegorczyk, Y. Zhang, J. Pacheco Jr., B. Wu, J. Kong, M. Chen , *Čerenkov radiation in materials with negative permittivity and permeability*, Optics Express, 2003.

[35] D.R. Smith, J.B. Pendry, M.C.K. Wiltshire, *Metamaterials and negative refractive index*, Science, 305, 788, 2004.

[36] S.I. Maslowski, S.A. Tretyakov, P.A. Belov, *Wire media with negative effective permittivity: a quasi-static model*, Microwave Opt. Technol. Lett., 35:47, 2002.

[37] IEEE, *Research on the macro effect of the thin wire array in metamaterial by equivalent circuit method*, IEEE AP-S International Symposium and USNC/URSI National Radio Science Meeting, Washington D.C., USA, 2005.

[38] M. Bayindir, K. Aydin, E. Ozbay, P. Marko, C.M. Soukoulis, *Transmission properties of composite metamaterials in free space*, Appl. Phys. Lett., 81:120, 2002.

[39] R. Marques, J. Martel, F. Mesa, F. Medina, *Left-handed-media simulation and transmission of electromagnetic waves in subwavelength split-ring resonator-loaded metallic waveguides*, Phys. Rev. Lett., 89:183901, 2002.

[40] P. Markos, C.M. Soukoulis, *Transmission studies of left-handed materials*, Phys. Rev. B., 65:033401, 2001.

[41] K. Aydin, K. Guven, M. Kafesaki, L. Zhang, C.M. Soukoulis, E. Ozbay, *Experimental observation of true left-handed transmission peak in metamaterials*, Opt. Lett., 29, 2623, 2004.

[42] P. Gay-Balmaz, O.J.F. Martin, *Electromagnetic Resonances in individual and coupled split-ring resonators*, J. Appl. Phys., 92:2929, 2002.

[43] C.R. Simovski, B. Sauviac, *Role of wave interaction of wires and split-ring resonators for the loss in a left handed composite*, Phys. Rev. E, 70:046607, 2004.

[44] M. Shamonin, E. Shamonina, V. Kalinin, L. Solymar, *Properties of a metamaterial element: Analytical solutions and numerical simulations for a singly split double ring*, J. Appl. Phys., 95:3778, 2004.

[45] J. Zhou, T. Koschny, M. Kafesaki, E.N. Economou, J.B. Pendry, C.M. Soukoulis, *Saturation of magnetic response of split-ring resonators at optical frequencies*, Phys. Rev. Lett., 95, 223902, 2005.

[46] N. Katsarakis, M. Kafesaki, I. Tsiapa, E.N. Economou, C.M. Soukoulis, *High transmittance left-handed materials involving symmetric split-ring resonators,* Photon. Nanostruct: Fundam. Appl. 5, 149, 2007.

[47] M. Born, E. Wolf, *Principles of Optics: Electromagnetic Theory of Propagation, Interference and Diffraction of Light*, Cambridge University Press, The Edinburgh Building, Cambridge CB2 2RU, UK, 7. Edition, 1999.

[48] D.R. Smith, D. Schurig, J.B. Pendry, *Negative Refraction of modulated electromagnetic waves*, Appl. Phys. Lett., Vol.81, p.2713, 2002.

[49] J.B. Pendry, *Negative Refraction makes a perfect lens*, Phys. Rev. Lett. Vol.85, p.3966, 2000.

[50] X. Zhang, Z. Liu, *Superlenses to overcome the diffraction limit*, Nature Mater, 7, 435-441, 2008.

[51] J.B. Pendry, D. Schurig, D.R. Smith, *Controlling electromagnetic fields*, Science 312, 1780-1782, 2006.

[52] A.J. Hoffman, L. Alekseyev, S.S. Howard, K.J. Franz, D. Wasserman, V.A. Podolskiy, E.E. Narimanov, D.L. Sivco, C Gmachl, *Negative refraction in semiconductor metamaterials*, Nature Mater 6, 946-950, 2007.

[53] D.D. Stancil, B.E. Henty, A.G. Cepni, J.P. Van't Hof, *Observation of an inverse Doppler shift from left-handed dipolar spin waves*, Physical Review B (Condensed Matter and Materials Physics), 74(6):060404, Aug. 2006.

[54] Y.O. Averkov, V.M. Yakovenko, *Cherenkov radiation by an electron bunch that moves in a vacuum above a left-handed material*, Phys. Rev. B, 72:205110, 2005.

[55] K. Aydin, E.Ozbay, *Experimental and numerical analyses of the resonances of split-ring resonators*, Phys. Stat. Sol. (b) 244, No.4, 1197-1201, 2007.

[56] K. Li, S.J. McLean, R.B. Greegor, C.G. Parazolli, M.H Tanielian, *Free-space focused-beam characterization of left-handed materials,* Appl. Phys. Lett, 82, 2535, 2003.

[57] F. Martin, F. Falcone, J. Bonache, R. Marques, M. Sorolla, *Miniaturized Coplanar Waveguide Stop Band Filters Based on Multiple Tuned Split Ring Resonators,* IEEE Microwave Wireless Comp., 13, 511, 2003.

[58] J. Martel, R. Marques, F. Falcone, J.D. Baena, F. Medina, F. Martin, M. Sorolla, *A New LC Series Element for Compact Bandpass Filter Design,* IEEE Microwave Wireless Comp., 14, No.5, 2004.

[59] K. Aydin, E. Ozbay, *Identifying the magnetic response of split-ring resonators at microwave frequencies*, Opto-Electron Rev 14, 193-199, 2006.

[60] B. Sauviac, C.R Simovski, S.A. Tretyakov, *Double split-ring resonators: Analytical modeling and numerical simulations*, Electromagnetics 24, 317-338, 2004.

[61] E. Ozbay, K. Aydin, K. Guven, *Metamaterials with negative permeability and negative refractive index: experiments and simulations*, J. Opt. A: Pure and Appl. Opt. 9, 301, 2007.

[62] J. Gomez Rivas, C. Schotsch, P. Haring Bolivar, H. Kurz *Enhanced transmission of THz radiation through subwavelength holes*, Physical Review B 68, 201306, 2003.

[63] K. Aydin, I. Bulu, K. Guven, M. Kafesaki, C.M. Soukoulis, E. Ozbay, *Investigation of magnetic resonances for different split-ring resonator parameters and designs*, New Journal of Physics 7, 168, 2005.

[64] User Manual, Version 5.0, CST GmbH, Darmstadt, Germany, 2005, http://www.cst.de.

[65] C.M. Soukoulis, M. Kafesaki, E.N. Economou, *Negative index materials: New frontiers in optics,* Adv. Mater. 18, 1941, 2006.

[66] E. Ozbay, I. Bulu, H. Caglayan, *Transmission, refraction, and focusing properties of labyrinth based left-handed metamaterials,* Phys. Stat. Sol. (b) 244, No. 4, 1202–1210, 2007.

[67] P. Markos, C.M. Soukoulis, *Numerical studies of left-handed materials and arrays of split ring resonators*, Physical Review E, Vol.65, 036622, 2002

[68] T. Weiland, R. Schuhmann, R.B. Greegor, C.G. Parazzoli, A.M. Vetter, D.R. Smith, D.C. Vier, S. Schultz, *Ab initio numerical simulation of left-handed metamaterials: Comparison of calculations and experiments* , J. Appl. Phys. 90 No.10, 2001.

[69] P. Markos, C.M. Soukoulis, *Transmission properties and effective electromagnetic parameters of double negative metamaterials*, Opt. Exp. 11 649, 2003.

[70] N. Katsarakis, T. Koschny, M. Kafesaki E.N. Economou C.M. Soukoulis, *Electric coupling to the magnetic resonance of split ring resonators,* Applied Physics Letters, Vol.84, No.15, 2004.

[71] B. Sauivac, C.R. Simovski, S. Tretyakov, *Double Split-Ring Resonators: Analytical Modeling and Numerical Simulations,* Electromagnetics, 24, 317, 2004.

[72] J.D. Baena, R. Marques, F. Medina, J. Martel, *Artificial magnetic metamaterial design by using spiral resonators,* Phys. Rev. B 69 014402, 2004.

[73] A.B. Movchan, S. Guenneau, *Split-ring resonators and localized modes*, Phys. Rev. B 70 125116, 2004.

[74] S. Linden, C. Enkrich, M. Wegener, J. Zhou, T. Koschny, C.M. Soukoulis, *Magnetic Response of Metamaterials at 100 Terahertz,* Science, 306, 1351, 2004.

[75] T. J. Yen, W. J. Padilla, N. Fang, D. C. Vier, D. R. Smith, J. B. Pendry, D. N. Basov, and X. Zhang, *Terahertz magnetic response from artificial materials*, Science 303,1494, 2004.

[76] H.O. Moser, B.D.F. Casse, O. Wilhelmi, B.T. Saw, *Terahertz Response of a Microfabricated Rod–Split-Ring-Resonator Electromagnetic Metamaterial,* Phys. Rev. Lett., 94, 063901, 2005.

[77] N. Wongkasem, A. Akyurtlu J. Li, A. Tibolt, Z. Kang, W.D. Goodhue, *Novel Broadband Terahertz Negative Refractive Index Metamaterials: Analysis And Experiment,* Progress In Electromagnetics Research, PIER 64, 205–218, 2006.

[78] V.M. Shalaev, W. Cai, U.K. Chettiar, H. Yuan, A.K. Sarychev, V P. Drachev, A.V. Kildishev, *Negative index of refraction in optical metamaterials*, Opt. Lett. 30, 3356, 2005.

[79] G. Dolling, C. Enkrich, M. Wegener, J.F. Zhou, C.M. Soukoulis, S. Linden, *Cut-wire pairs and plate pairs as magnetic atoms for optical metamaterials*, Opt. Lett. 30, 3198, 2005.

[80] J. Zhou, L. Zhang, G. Tuttle, T. Koschny, C.M. Soukoulis, *Negative index materials using simple short wire pairs*, Phys. Rev. B 73, 041101, 2006.

[81] J. Zhou, E.N. Economou, T. Koschny, C.M. Soukoulis, *Unifying approach to left-handed material design*, Opt. Lett. 31, 3620, 2006.

[82] K. Guven, M.D. Caliskan, E. Ozbay, E*xperimental observation of left-handed transmission in a bilayer metamaterial under normal-to-plane propagation*, Opt. Express 14, 8685, 2006.

[83] S. Zhang, W. Fan, K.J. Malloy, S.R. J. Brueck, N.C. Panoiu, R.M. Osgood, *Near-infrared double negative metamaterials*, Opt. Express 13, 4922, 2005.

[84] S. Zhang, W. Fan, N.C. Panoiu, K.J. Malloy, R.M. Osgood, S.R.J. Brueck, *Experimental demonstration of near-infrared negative-index metamaterials*, Phys. Rev. Lett. 95, 137404, 2005.

[85] G. Dolling, C. Enkrich, M. Wegener, C.M. Soukoulis, S. Linden, *Simultaneous negative phase and group velocity of light in a metamaterial*, Science 12, 892, 2006.

[86] G. Dolling, M. Wegener, C.M. Soukoulis, S. Linden, *Negative-index metamaterial at 780 nm wavelength*, Opt. Lett. 32, 53, 2007.

[87] M. Kafesaki, I. Tsiapa, N. Katsarakis, T. Koschny, C.M. Soukoulis, E.N. Economou, *Left-handed metamaterials: The fishnet structure and its variations*, Phys. Rev. B 75, 235114, 2007.

[88] V.D. Lam, J.B. Kim, S.J. Lee, Y.P. Lee, *Left-handed behavior of combined and fishnet structures*, J. Appl. Phys. 103, 033107, 2008.

[89] J. Zhou, T. Koschny, M. Kafesaki, C.M. Soukoulis, *Size dependence and convergence of the retrieval parameters of metamaterials*, Photon. Nanostruct: Fundam. Appl. 6, 96, 2008.

[90] G. Dolling, M. Wegener, S. Linden, *Realization of a three-functional-layer negative-index photonic metamaterial*, Opt. Lett. 32, 551, 2007.

[91] N. Liu, H. Guo, L. Fu, S. Kaiser, H. Schweizer, H. Giessen, *Three-dimensional photonic metamaterials at optical frequencies*, Nature Materials 7, 31, 2008.

[92] D.R. Smith, S. Schultz, P. Markos, C.M. Soukoulis, *Determination of effective permittivity and permeability of metamaterials from reflection and transmission coefficients*, Phys. Rev. B. 65, 195104, 2002.

[93] X. Chen, T.M. Grzegorczyk, B.I. Wu, J. Pacheco Jr., J.A. Kong, *Robust method to retrieve the constitutive effective parameters of metamaterials*, Phys. Rev. E 70, 016608, 2004.

[94] T. Koschny, P. Markoš, E.N. Economou, D.R. Smith, D.C. Vier, C.M. Soukoulis, *Impact of the inherent periodic structure on the effective medium description of left-handed and related meta-materials*, Phys. Rev. B 71, 245105, 2005.

[95] R.S. Penciu, M. Kafesaki, T.F. Gundogdu, E.N. Economou, C.M. Soukoulis, *Theoretical study of left-handed behavior of composite metamaterials*, Photon. Nanostruct: Fund. Appl. 4, 12, 2006.

[96] N. Katsarakis, M. Kafesaki, I. Tsiapa, E.N. Economou, C.M. Soukoulis, *High transmittance left-handed materials involving symmetric split-ring resonators*, Photon. Nanostruct: Fundam. Appl. 5, 149, 2007.

[97] V.D. Lam, J.B. Kim, S.J. Lee, Y.P. Lee, *Left-handed behavior of combined and fishnet structures*, Journal of Applied Physics 103, 033107, 2008.

[98] J. Zhou, T. Koschny, C.M. Soukoulis, *An efficient way to reduce losses of left-handed metamaterials,* Vol.16, No.15, Optics Express 11147, 2008.

[99] C. M Soukoulis, J. Zhou, T. Koschny, M. Kafesaki, E.N Economou, *The science of negative index materials* J. Phys.: Condens. Matter 20, 304217, 2008.

[100] K. Aydin, A.O. Cakmak, L. Sahin, Z. Li, F. Bilotti, L. Vegni, E. Ozbay, *Split-ring-resonator-coupled enhanced transmission through a single subwavelength aperture*, Phys. Rev. Lett. 102, 013904, 2009.

[101] H. Chen, L. Ran, J. Huangfu, X. Zhang, K. Chen, T.M. Grzegorczyk, J.A. Kong, *Left-handed materials composed of only S-shaped resonators*, Phys. Rev. E 70, 057605, 2004.

[102] J. Huangfu, L. Ran, H. Chen, X.M. Zhang, K. Chen, T.M. Grzegorczyk, J.A. Kong, *Experimental confirmation of negative refractive index of a metamaterial composed of Ω-like metallic patterns*, Appl. Phys. Lett. 84, 1537, 2004.

[103] Z.G. Dong, S.Y. Lei, Q. Li, M.X. Xu, H. Liu, T. Li, F.M. Wang, S.N. Zhu, *Non-left-handed transmission and bianisotropic effect in a Π-shaped metallic metamaterial*, Phys. Rev. B 75, 075117, 2007.

[104] K. Aydin, Z. Li, L. Sahin, E. Ozbay, *Negative phase advance in polarization independent, multi-layer negative-index metamaterials*, Optics Express, Vol.16, No.12, 8835, 2008.

[105] Optics Info Base - *Multimedia Page;* http://www.opticsinfobase.org/viewmedia.cfm?uri=oe-16-12-8835&seq=1, *Last Accessed Date: 30 November 2008.*

[106] Optics Info Base - *Multimedia Page;* http://www.opticsinfobase.org/viewmedia.cfm?uri=oe-16-12-8835&seq=2, Last Accessed Date: 30 November 2008.

[107] F.M. Grimaldi, *Physico-mathesis de Lumine, Coloribus, et Iride, Aliisque Sequenti Pagina Indicatis 9* , Bologna, 1665.

[108] C. Genet, T.W. Ebbesen, *Light in tiny holes*, Nature, Vol. 445, 39-46, January 2007.

[109] H.A Bethe, *Theory of diffraction by small holes*, Phys. Rev. 66, 163-182, 1994.

[110] H. Çağlayan, *Enhanced Confined Microwave Transmission by Single Subwavelength Apertures*, Page 29, M.Sc. Thesis, Bilkent Univ., August 2005.

[111] X. Shi, L. Hesselink, R. Thornton, *Ultrahigh light transmission through a C-shaped nanoaperture*, Optics Letters, Vol. 28, No. 15, August 2003.

[112] X. Shi, L. Hesselink, *Design of a C aperture to achieve λ/10 resolution and resonant transmission*, Optical Society of America, Vol. 21, No. 7, July 2004.

[113] L. Tang, D.A.B. Miller, A.K. Okyay, J.A. Matteo, Y. Yuen, K.C. Saraswat, L. Hesselink, *C-shaped nanoaperture-enhanced germanium photodetector*, Optics Letters, Vol. 31, No. 10, May 2006.

[114] P. Hansen, L. Hesselink, B. Leen, *Design of a subwavelength bent C-aperture waveguide*, Optics Letters, Vol.32, No.12, June 2007.

[115] R. Gordon, A. Brolo, *Increased cut-off wavelength for a sub-wavelength hole in a real metal*, Optics Express 13, 1933-1938, 2005.

[116] A. Roberts, *Electromagnetic theory of diffraction by a circular aperture in a thick, perfectly conducting screen*, J. Opt. Soc. Am., A 4, 1970-1983, 1987.

[117] F.J. Garcia-Vidal, E. Moreno, J.A. Porto, L. Martin-Moreno, *Transmission of Light through a single rectangular hole*, Phys. Rev. Lett. 95, 103901, 2005.

[118] T.W. Ebbesen, H.J. Lezec, H.F. Ghaemi, T. Thio, P.A. Wolff, *Extraordinary optical transmission through sub-wavelength hole arrays*, Nature 391, 667–669, 1998.

[119] T.D. Visser, *Plasmonics: Surface Plasmons at work?*, Nature Physics, Vol2, August 2006.

[120] P. Lalanne, J.P Hugonin, I*nteraction between optical nano-objects at metallo-dielectric interfaces*, Nature Physics, Vol.2, 551-556, 2006.

[121] H.F. Schouten, N. Kuzmin, G. Dubois, T.D. Visser, G. Gbur, P.F.A. Alkemade, H. Blok, G.W. Hooft, D. Lenstra, E.R. Eliel, *Plasmon-assisted Two-Slit Transmission: Young's Experiment Revisited*, Phys. Rev. Lett. 94, 053901, 2005.

[122] K.L. Klein Koerkamp, S. Enoch, F.B. Segerink, N.F. van Hulst, L. Kuipers, *Strong Influence of Hole Shape on Extraordinary Transmission through Periodic Arrays of Subwavelength Holes*, Phys. Rev. Lett. 92, 183901, 2004.

[123] M.J. Levene, J. Korlach, S.W. Turner, M. Foquet, H.G. Craighead, W.W. Webb, *Zero-mode waveguides for single molecule analysis at high concentrations*, Science 299, 682–686 2003.

[124] E. Betzig, J.K. Trautman, *Near-field optics: microscopy, spectroscopy, and surface modification beyond the diffraction limit*, Science 257, 189–194 1992.

[125] G. Gbur, H.F. Schouten, T.D. Visser, *Achieving super resolution in near-field optical data readout systems using surface plasmons*, Appl. Phys. Lett. 87, 191109, 2005.

[126] J. Fujikata, T. Ishi, H. Yokota, K. Kato, M. Yanagisawa, M. Nakada, K. Ishihara, K. Ohashi, T. Thio, *Surface plasmon enhancement effect and its application to nearfield optical recording*, Trans. Magn. Soc. Jpn 4, 255–259, 2004.

[127] W. Srituravanich, N. Fang, C. Sun, Q. Luo, X. Zhang, *Plasmonic nanolithography*, Nano Lett. 4, 1085–1088, 2004.

[128] X. Luo, T. Ishihara, *Sub-100nm photolithography based on plasmon resonance*, Jpn J. Appl. Phys. 43, 4017–4021, 2004.

[129] D.B. Shao, S.C. Che, *Surface-plasmon-assisted nanoscale photolithography by polarized light*, Appl. Phys. Lett. 86, 253107, 2005.

[130] H. Rigneault, J. Capoulade, J. Dintinger, J. Wenger, N. Bonod, E. Popov, T.W. Ebbesen, P. Lenne, *Enhancement of single-molecule fluorescence detection in subwavelength apertures*, Phys. Rev. Lett. 95, 117401, 2005.

[131] T. Ishi, J. Fujikata, K. Makita, T. Baba, K. Ohashi, *Si nano-photodiode with a surface plasmon antenna*, Jpn J. Appl. Phys. 44, L364–L366, 2005.

[132] J.B. Pendry, L. Martin-Moreno, F.J. Garcia-Vidal, *Mimicking surface Plasmons with structured surfaces*, Science 305, 847–848, 2004.

[133] F.J. Garcia-Vidal, L. Martin-Moreno, J.B. Pendry, *Surfaces with holes in them: new plasmonic metamaterials*, J. Opt. Pure Appl. Opt. 7, S97–S101, 2005.

[134] A. Degiron, H.J. Lezec, N. Yamamoto, T.W. Ebbesen, *Optical transmission properties of a single subwavelength aperture in a real metal*, Opt Comm. 239, 61-66, 2004.

[135] F.J. Garcia de Abajo, *Colloquium: Light scattering by particle and hole arrays*, Reviews of Modern Physics, volume 79, 1267-1290, 2007.

[136] J. Dintiger, S. Klein, T.W. Ebbessen, *Molecule-surface plasmon interactions in hole arrays: enhanced absorption, refractive index changes, and all optical switching*, Adv. Mater. (Wienheim, Ger.), 18, 1267-1270, 2006.

[137] I.I Smolyaninov, A.V. Zayats, A. Stanishevsky, C.C. Davis, *Optical control of photon tunneling through an array of nanometer-scale cylindrical channels*, Phys. Rev. B, 66, 205414, 2002.

[138] C. Janke, J. Gómez Rivas, P. Haring Bolivar, H. Kurz, 2005, *All-optical switching of the transmission of electromagnetic radiation through subwavelength apertures*, Opt. Lett. 30, 2357–2359.

[139] J. Dintinger, I. Robel, P.V. Kamat, C. Genet, T.W. Ebbesen, T*erahertz all-optical molecule-plasmon modulation*, Adv. Mater. (Weinheim, Ger.) 18, 1645–1648, 2006.

[140] E. Altewischer, M.P. van Exter, J.P. Woerdman, *Plasmon-assisted transmission of entangled photons*, Nature London, 418, 304-306, 2002.

[141] C. Enkrich, M. Wegener, S. Linden, S. Burger, L. Zschiedrich, F. Schmidt, J.F. Zhou, T. Koschny, C.M. Soukoulis, *Magnetic Metamaterials at Telecommunication and Visible Frequencies*, Phys. Rev. Lett., 95, 203901, 2005.